

PLACE IN RETURN BOX to remove this checkout from your record. TO AVOID FINES return on or before date due.

DATE DUE	DATE DUE	DATE DUE

MSU is An Affirmative Action/Equal Opportunity Institution attributed to provide the control of the control of

## **ABSTRACT**

# On Directional Reinforced Incompressible Nonlinearly Elastic Solids:

Simple Response and Correlation to the Linear Theory, and Failure of Ellipticity in Plane Deformation

By

#### YUE QIU

A model for finitely deformable incompressible elastic materials with fiber reinforcements is established. The engineering significance of this material model is verified since it fits well with real material data. The fully nonlinear responses of this material is discussed for a number of important deformations, and the loss of monotonicity of the material response is studied. The correlation to the linear theory is provided in terms of the elastic constants. The ellipticity of this anisotropic material and the plate bifurcation problem are further studied. It is revealed that the loss of ellipticity phenomena under planar deformation involve different patterns, depending on loading path. These patterns involve simple loss of ellipticity, loss-recovery-loss of ellipticity, and primary loss-secondary loss of ellipticity. The geometry of the ellipticity boundary is made clear. The discussion on the directions of the weak discontinuity surfaces is also presented. Finally, it is concluded that there is no explicit correlation between loss of ellipticity and loss of monotonicity of the stress response, and no explicit correlation between loss of ellipticity and bifurcation.

## **DEDICATE TO MY PARENTS**

## **ACKNOWLEDGMENTS**

I would like to express sincere appreciation to my advisor, professor Thomas J.

Pence, for his very helpful guidance and support throughout this work. The financial support for this work from the Research Excellence Fund for composite materials, administered by the Michigan State University Composite Materials and Structures Center, is also gratefully acknowledged.

# TABLE OF CONTENTS

1. Introduction	1
2. Material Model and Its Properties	10
2.1. Material Model with Fiber Reinforcements	
2.2. General Stress-Deformation Relation	
2.3. Homogeneous Deformations	19
2.4. Material Properties (Single Fiber Family)	23
2.4.1. Material Response to Homogeneous Deformations	
2.4.2. Material Properties at Infinitesimal Limit	
2.5. Material Properties (Two Balanced Fiber Families)	
3. Ordinary Ellipticity in Planar Deformation	60
3.1. The Ordinary Ellipticity Condition for Arbitrary Deformations	
3.2. Specialization of the Ordinary Ellipticity Condition to Planar Deformation	
3.3. Loss of Ellipticity in Local Plane Strain	
3.4. Basic Results for both Global and Local Plane Strain Ellipticity	
3.5. An Alternative Form of the Global Plane Strain Ellipticity Condition	
3.6. Loss of Ellipticity in Global Plane Strain	
3.7. Global Plane Strain Ellipticity Boundary: Cross-Sections at Constant C <sub>12</sub>	80
3.8. Projection of the Ellipticity Boundary onto the $(C_{12}, \gamma)$ -Plane	
3.9. Multiplicity and Orientation of the Discontinuity Surfaces for $C_{12} = 4$	
3.10. Orientation of the Discontinuity Surface at First Loss of Ellipticity	
3.11. Cross Sections of Sat Fixed y	
3.12. Asymptotic Properties of the Global Plane Strain Ellipticity Boundary	
3.13. Ellipticity under Special Deformations	
4. Summary and Conclusion	119
Appendix A: Algebraic Root Analysis of the Characteristic Polynomial	120
A.1 General Algebraic Procedures upon the Quartic Polynomial	
A.2 Criteria for Double Real Roots	
A.3 Criteria for Two Pairs of Double Real Roots	
A.4 Criteria for a Triple Roots and a Quadruple Roots	
Appendix B: Bifurcation from Homogeneous Deformation under End Thrust	125
B.1 Homogeneous Plane Deformation	
B.2 Incremental Formulation	
B.3 Inhomogeneous Bifurcation	
Appendix C: An Alternative Way to Obtain the Ellipticity Condition	
in the Buckling Problem	140
References	142

#### 1. Introduction

In nonlinear elasticity, important and closely related issues, which have obtained wide attention, are uniqueness, bifurcation and associated stability of the solution, as well as ellipticity and material stability. There are two kinds of bifurcations, namely homogeneous bifurcation and inhomogeneous bifurcation, from homogeneous equilibrium solutions have been discussed in the literature. The homogeneous bifurcation is a phenomenon in which more than one homogeneous deformation states correspond to one single stress state, and in which the shape of the material body is immaterial, as pointed out by Ball and Schaeffer [Ball and Schaeffer 1983]. It is, therefore, reasonable that the homogeneous bifurcation analysis be placed in the scope of material stability. The material stability analysis is a different aspect from the traditional (structural) stability analysis, since in the former there is no particular structure fabricated from the material involved. In the analysis of the inhomogeneous bifurcation, the shape or the structure of the material configuration must be addressed. We shall thus refer the inhomogeneous bifurcation as structural bifurcation, and the associated stability structural stability, in contrast to material bifurcation and material stability. It should be noted that the term material stability is placed on the overall material properties and is not at the microscopic level herein.

One famous example of the homogeneous bifurcation and stability is Rivlin's cube problem [Rivlin 1948b], where the deformation states of an incompressible, isotropic, neo-Hookean material point under equi-triaxial dead load traction were studied. Further discussion on this problem for a widened class of materials is given by Ball and Schaeffer [Ball and Schaeffer 1983]. The homogeneous bifurcation and stability of incompressible,

isotropic elastic material subject to in-plane equi-biaxial dead load traction was studied by Ogden under plane strain condition [Ogden 1985] and under plane stress condition [Ogden 1987]. Certain restrictions for material stability were then deduced from these studies.

Restrictions pertaining to material stability can be found in the literature. As Rivlin has summarized [Rivlin 1981], one condition for material stability is that the strain energy density function must be positive definite if expressed as a function of strain tensor. This condition is evident from the fact that if the strain energy is non-positive for some nonzero strain tensor, then the material will be unstable in its undeformed state. Another condition for material stability is Hadamard's condition, it requires that the speeds of all plane waves, propagated in the material body occupying a domain in three-dimensional space, must be positive [Beatty 1987]. Even in the case of infinitesimally small deformations, the above mentioned two conditions give different restrictions on material properties. In the cases where finite deformations are involved, the conditions for material stability can be that the strain energy density function, in terms of the deformation gradient tensor, be either positive semi-definite or locally convex [Truesdell and Noll 1965, Rivlin 1981]. Although the mechanisms that cause the material instability have not been made completely clear yet, we will adopt the condition that the strain energy density function must be positive semi-definite (and of value zero only for rigid body motions) in establishing our material model.

Another significant issue that concerns the regularity of the solutions in the theory of finite deformation is the ellipticity analysis of the governing field equations. Loss of ordinary ellipticity happens if, in the material body, there exists a surface across which

weak discontinuity of the solution field is capable of taking place. That is, singular equilibrium field exists in homogeneous material body. One such phenomenon observed in real world is localized shear band. Strong ellipticity, which concerns the material stability, is often correlated with bifurcation of equilibrium solutions. Conditions for ellipticity can be found in [Knowles and Sternberg 1975, 1977] for compressible materials, and [Abeyaratne 1980, Zee and Sternberg 1983] for incompressible materials, respectively. Conditions for ordinary ellipticity are usually expressed as the nonsingularity of acoustic tensor. In comparison, conditions for strong ellipticity, derived from Hadamard's condition, are usually expressed as the positive definiteness of the acoustic tensor. Further derivations of the ellipticity conditions to explicit inequalities for easy verification can also be found in these papers. Hill and Hutchinson have established the plane strain incremental governing equations for the tension problem of the class of time-independent piecewise linear or wholly linear materials [Hill and Hutchinson 1975, Hill 1979]. The governing equations change types among elliptic, strong elliptic, parabolic, hyperbolic types, depending on material and load parameters through the nature of the roots (real or complex) of the corresponding secular equations. [Rosakis 1990] has further discussed the derivation of ellipticity conditions and their mechanical interpretations for compressible materials. Together with a later paper, [Rosakis and Jiang 1993], they have analyzed the problem of existence of equilibrium deformations with discontinuous gradients. Recently, Horgan has analyzed the ellipticity problem for generalized Blatz-Ko material [Horgan 1996]. He has found the range of material parameter for possible loss of ellipticity, and further discussed the deformation parameter ranges which never fail ellipticity. A discussion on ordinary and strong ellipticity can also be found in [Ogden 1984].

A phenomenon that is associated with the structural instability is the structural (inhomogeneous) bifurcation (buckling) of equilibrium configuration. Among various types of inhomogeneous bifurcations, out-of-plane bifurcation is of special interest. Examples of this type of structural bifurcations can be found in [Sawyers and Rivlin 1974] for homogeneous material, and in [Pence and Song 1991, Qiu et. al. 1994] for composite material. The so called Euler's stability criterion [Beatty 1987] states, an equilibrium configuration of a structure is unstable for dead loading if there exists, for the same loading, another equilibrium configuration situated in the neighborhood of the assigned one. In the utilization of Euler's criterion, and in the scope of finite elasticity, the structural stability analysis is often carried out in the context of the theory of small deformation superposed on finite deformation [Biot 1965]. It has shown that the structural stability of equilibrium configuration can be affected by the material anisotropy [Polignone and Horgan 1993], and by the composite structure [Horgan and Pence 1989].

It has been shown that the out-of-plane inhomogeneous bifurcations under in-plane loading are possible to take place when the corresponding incremental governing equation is either elliptic or non-elliptic [Hill and Hutchinson 1975, Hill 1979, Kurashige 1981]. It is also found, however, that loss of ellipticity of the incremental governing equation and in-plane inhomogeneous bifurcation take place simultaneously, for incompressible isotropic elastic membranes under in-plane loading [Haughton 1987]. With the anisotropic material modeled by adding fiber stiffness to the Blatz-Ko material, Kurashige [1981] studied the bifurcation of a transversely isotropic slab under axial loads.

It is usual that the difficulty of solving the nonlinear partial differential equations

of finite elasticity largely confines the number of exact solutions to problems with a high degree of symmetry, or to problems with fewer dimensions. It is also usual in solving these problems that certain kinematic constraints and other simplification assumptions are introduced to restrict the variety of deformations. By the study of Ericksen and Rivlin, the total number of kinematic constraints can be as many as six [Ericksen and Rivlin 1954]. Among them, the incompressibility and inextensibility in assigned direction are frequently included in the research in finite elasticity. The incompressibility constraint is a good approximation for various real materials such as natural rubber, synthetic elastomers and biological tissues [Beatty 1987]. The inextensibility constraint is usually used to describe the effect of strong continuous fiber reinforcement [Adkins and Rivlin 1955].

Material models (constitutive relations) play an important role in the research in finite elasticity. These models enable one to analyze in deep the mechanical phenomena of a given system, and to predict the response of the material to specified traction and displacement boundary conditions, and thus provide convenient tools for engineering design. The material models can also provide guidelines for the design of material experiment and for the interpretation of experimental data. Two simple but widely-used isotropic materials models are the neo-Hookean type [Rivlin 1948a] for incompressible materials and Blatz-Ko type [Blatz and Ko 1962] for compressible materials. In finite elasticity, it is mathematically convenient to express the material model as a strain energy density function, while in the classical linear elasticity the material properties are usually described by a constant elasticity tensor.

The strain energy density is usually expressed as a function of a set of deformation parameters. These parameters are regularly independent, complete and irreducible strain

invariants under the symmetry transformation appropriate for the material. For compressible isotropic materials, the number of such strain invariants is three. For incompressible isotropic materials, this number becomes two. According to Green and Adkins [Green and Adkins 1960], the number of such strain invariants describing compressible transversely isotropic material is exactly five, while this number is four for the incompressible counterpart.

In engineering practice, material anisotropy is often introduced by fiber reinforcement. This provides unprecedented flexibility to economically meet performance setpoints by tailoring the directional response of the individual substructural constituents. For example, a material reinforced with one family of straight parallel fibers belongs to the class of transversely isotropic materials, and the corresponding strain energy density function involves five strain invariants or four strain invariants for compressible or incompressible materials, respectively. In linear elasticity this material is modeled by five elastic constants in the elasticity tensor [Christensen 1979]. For materials reinforced with multiple families of fibers, the number of such strain invariants depends on the number of families of the reinforcements and depends on the direction of each family of reinforcement. Besides, the anisotropic effects due to several fiber reinforcements will be coupled, since reinforcement in one direction may affect the material properties in other directions. The complete modeling of fiber reinforcements may proceed along the following line. Given a system of fiber reinforcements, first, derive the complete and irreducible set of strain invariants under the symmetry transformation group that is associated with the given system of fiber reinforcements. The material model is usually a polynomial of these strain invariants. Second, identify each term in this polynomial by its nature in deformation and attach each term with appropriate material parameter. The first step is within the theory of representations for tensor functions, which has obtained the efforts of a number of researchers and is presented pretty completely in [Zheng 1994].

In literature, there appear two straightforward ways of modeling the effect of fiber reinforcement. One way is to model the fiber reinforcement by the kinematical constraint of inextensibility in fiber direction, as can be seen in [Adkins and Rivlin 1955, Pipkin and Rogers 1971]. This modeling procedure may fail to yield sufficient deformability if the reinforcement consist of several families of fibers in different directions. Another way of modeling the fiber reinforcement, that has been used for the analysis of materials reinforced in single direction, is by adding extra stiffness in fiber direction. Referring to the works presented in [Kurashige 1981, Triantafyllidis and Abeyaratne 1983], the modeling of compressible material reinforced with a single family of fibers is gained by adding fiber stiffness to the Blatz-Ko material in the direction of reinforcement. In a recent paper [Polignone and Horgan 1993], a similar modeling is obtained in extending the incompressible neo-Hookean material by fetching in additional stiffness in the radial direction for the spherical problem considered.

In the early 1970s, Pipkin, Rogers and Spencer developed what is known as the *ideal continuum theory of fiber-reinforced material (ideal theory*, for abbreviation) [Pipkin and Rogers 1971, Rogers and Pipkin 1971b, Spencer 1972], its origin may date back to [Adkins and Rivlin 1955]. Here the term *ideal* has three aspects: (1) the fibers are continuously distributed so that they can be represented by a field of unit vectors and the material can be treated as continuum, (2) the material is inextensible in the fiber direction, and (3) the material is incompressible. A number of problems have been solved employing

the ideal theory [Rogers and Pipkin 1971a, 1971b, England et. al. 1992 and Bradford et. al. 1992]. Several interesting phenomena have been predicted by the ideal theory, such as: that stress is channeled, mainly due to the inextensibility, both parallel and normal to the fiber direction without attenuation; that there exist stress concentration layers; and that shear deformation can only take place along the fiber direction (see [Pipkin and Rogers 1971] as well as [Rogers 1975]). These phenomena can be expected for highly anisotropic materials (such as fiber-reinforced composites with stronger fibers and weaker matrices). For example, as we will see later, the shear modulus for shear normal to fiber direction will be significantly larger than that along fiber direction for anisotropic materials if the deformation is beyond infinitesimally small.

The standard mathematical approach for solving a boundary value problem is that one determines a physical field, often the deformation field, from the governing equation, the constitutive relations and the boundary conditions. In view of the nonlinearity of the differential equations of finite elasticity, the standard mathematical approach is usually not applicable. Instead, one adopts the semi-inverse approach. The semi-inverse approach can be summarized [Beatty 1987] as follows. First, a suitable class of deformations characterized by a number of parameters is chosen for study. Then the constitutive relations is used to determine the stress distribution that satisfies the differential equations of equilibrium. Finally, the surface loading necessary to maintain the deformation in its equilibrium configuration is determined. The deformation that can be produced in a material body by the application of surface traction alone is called the controllable deformation.

In the studies that follows, we will, in chapter 2, establish a material model for

materials reinforced, in general, with multiple families of fibers. The material reinforced with single family of fibers will be studied in detail. The nonlinear response of this material to certain important deformations will be addressed. The loss of monotonicity of the material response will be discussed. The elastic constants corresponding to the linear theory are then derived.

In chapter 3, we shall discuss the ordinary ellipticity of this material reinforced with single family of fibers. The phenomena of loss of ellipticity under planar deformation will be clarified. The generation of discontinuity surface in the material body, and the orientation of the discontinuity surface will be discussed. The loss of ellipticity is further studied in the context of certain special deformations introduced in chapter 2.

Two substantial appendices are also given. The first, Appendix A, develops the algebra associated with the polynomial root type changes. Criteria for double real roots, for two pairs of double real roots, as well as criteria for triple roots and quadruple roots are discussed. The second, Appendix B, correlates the results of this thesis with the out-of-plane inhomogeneous bifurcations of a thick plate consisting of the material reinforced with single family of fibers under end thrust. A short appendix, Appendix C, provides an alternative way to obtain the ellipticity condition in the buckling problem discussed in Appendix B.

### 2. Material Model and Its Properties

The description of nonlinear mechanical behaviors of anisotropic materials is still in its developing stage. In the present studies we do not attempt to model the fiber reinforcement in its complete nature. Instead, we take into account the effect of each family of fibers by including individually additional stiffness in specified directions given birth by each family of fiber reinforcements and omit any explicit coupling effect. It is evident that the most significant and direct effect introduced in material body by fiber reinforcement is the increased stiffness and strength in fiber direction. This modeling procedure allow us to isolate and investigate the most important effect of the fiber reinforcement and neglect any other effects at least at this stage. It is assumed that the material is incompressible, but we are not going to include the constraint of inextensibility in fiber direction. The fiber inextensibility can be simulated as the additional stiffnesses in the fiber directions become very large. It is assumed that fibers are continuously distributed throughout the material body and thus each family of fibers can be modeled by a field of unit vectors of which the trajectories are fibers. This makes it possible to employ continuum theory.

In this chapter, the material model is introduced and discussed, including the connection to material symmetry. Then the fully nonlinear response is discussed for a number of important deformations. The loss of monotonicity of the material response is studied, especially for simple shear deformation. Finally the correlation to the linear theory is provided in terms of the elastic constants that follow from the specialization to infinitesimal deformations.

#### 2.1. Material Model with Fiber Reinforcements

The mechanical responses of a nonlinearly elastic material that can sustain finite deformation are determined by two configurations, namely, original (or reference) configuration and current (or deformed) configuration, but do not depend on the time history from one configuration to the other. The deformation from original configuration to current configuration is then an invertible mapping between these two configurations and can be, in general, written as

$$\mathbf{x} = \mathbf{x}(\mathbf{X}), \tag{2.1.1}$$

or in component form as

$$x_1 = x_1(X_1, X_2, X_3), \qquad x_2 = x_2(X_1, X_2, X_3), \qquad x_3 = x_3(X_1, X_2, X_3), \quad (2.1.2)$$

which is not written as a function of time here since we are to deal with static processes only. The corresponding deformation gradient tensor that describes the configurational relation in between is defined as

$$\mathbf{F} = \frac{\partial \mathbf{x}}{\partial \mathbf{X}}.\tag{2.1.3}$$

The strain energy density function W, defined over the material body with respect to the original configuration, is important and convenient for determining the mechanical responses, such as the deformation and stress field, of an elastic material. This strain energy density function W, in general, is a function of deformation gradient tensor

$$W = W(F, X) \qquad \text{or} \qquad W = W(F) \tag{2.1.4}$$

for an elastic material that is initially inhomogeneous or initially homogeneous, respectively, in its original configuration.

Among the various strain energy density functions for finite elastic materials, the neo-Hookean type is the simplest for the purpose of analysis and gives reasonable description for incompressible isotropic finite elastic materials. Here, we consider an incompressible anisotropic finite elastic material model that is extended from the neo-Hookean material by taking into account the effects of reinforcements of M families of fibers by adding extra stiffnesses in the fiber directions. This material model given by the strain energy density function is expressed as

$$W = \frac{\mu}{2}(I_1 - 3) + \sum_{m=1}^{M} \frac{\beta^{(m)}}{2} (K^{(m)} - 1)^{\alpha^{(m)}}, \qquad (2.1.5)$$

where

$$I_1 = tr(C), K^{(m)} = A^{(m)} \cdot CA^{(m)}, C = F^TF.$$
 (2.1.6)

Here  $I_1$  is the first invariant of the right Cauchy-Green strain tensor C given by  $(2.1.6)_3$ . The incompressibility constraint requires

$$\det \mathbf{F} = 1. \tag{2.1.7}$$

For the material reinforced with M families of fibers, quantities with the superscript (m) (m = 1,2,...,M) are associated with the m<sup>th</sup> family of fibers. For the case where materials are reinforced with only one family of fibers, we will omit the superscript (1). The fiber reinforcements are assumed to be continuously distributed. Thus, vector  $\mathbf{A}^{(m)}$  is the m<sup>th</sup> unit vector field modeling the m<sup>th</sup> family of fibers in the undeformed configuration and is determined by the orientation of the fiber of the m<sup>th</sup> family at a specified point in a given coordinate system. Now, it is clear that  $\mathbf{K}^{(m)}$ -1 is the elongation in the direction of the m<sup>th</sup> family of fibers. Note here that the unit vector field  $\mathbf{A}^{(m)}$  could in general be a function of

**X.** If so, the strain energy density W, in view of (2.1.5), takes the form of (2.1.4)<sub>1</sub>. If the material is uniformly reinforced with only straight parallel fibers, then  $A^{(m)}$  is independent of the position vector **X** and the strain energy density function W takes the form of (2.1.4)<sub>2</sub>. We shall say that the fiber reinforcement is *in-plane fiber reinforcement* if all of the fibers lie in parallel planes. This is the common case for fiber-reinforced composite materials. For in-plane fiber reinforcement, we shall set the rectangular Cartesian coordinate system in the way that the planes determined by the in-plane fibers are normal to the  $X_2$ -axis. We can, therefore, determine the fiber orientation of the  $m^{th}$  family of fibers at a specified point by an angle  $\theta^{(m)}$  in planes parallel to the  $(X_1, X_3)$ -plane. This angle  $\theta^{(m)}$  is measured from the positive direction of the  $X_1$  coordinate to the tangent direction of the fiber at that point by a rotation about the  $X_2$ -axis, and  $\theta^{(m)}$  is positive for rotations that obey right hand rule, and vice versa (refer to Figure 1). Thus, for straight parallel in-plane fiber reinforcement, the unit vector

$$\mathbf{A}^{(m)} = \{\cos\theta^{(m)}, 0, \sin\theta^{(m)}\}. \tag{2.1.8}$$

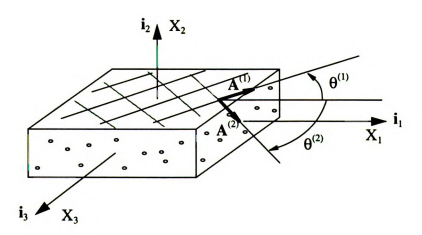


Figure 1. The graphical description of a composite thick plate reinforced with multiple families of fibers. The strain energy density function of this type of composite material is modeled in expressions (2.1.5).

The fibers in the deformed configuration will in general change their orientation. The counterpart of  $A^{(m)}$  in the deformed configuration is  $a^{(m)}$  (m = 1,2,...M), given by

$$\mathbf{a}^{(m)} = \frac{\mathbf{F}\mathbf{A}^{(m)}}{\sqrt{\mathbf{K}^{(m)}}}.$$
 (2.1.9)

In the material model (2.1.5)  $\mu>0$  is the shear modulus of the neo-Hookean material. The parameter  $\beta^{(m)} \ge 0$  characterizes the increased stiffness contributed by the m<sup>th</sup> family of fibers in the fiber direction. This in turn will depend on the stiffness and the fiber volume fraction of the m<sup>th</sup> family of fibers. The neo-Hookean behavior is retrieved if  $\beta^{(m)} = 0$  for all m. It is evident that W is symmetric in C. In its undeformed state,  $I_1 = 3$  and  $K^{(m)} = 1$ , in which case the strain energy density function W given by (2.1.5) is zero.

Anisotropy introduced by the fiber reinforcement is characterized analytically by the symmetry transformations that do not affect mechanical response. For M=1 the material is locally transversely isotropic, and we may let  $\theta^{(1)}=0$ , so that  $A^{(1)}=\mathbf{i}_1$ . Under transverse isotropy, arbitrary rotations about the  $\mathbf{i}_1$ -axis, and reflections about the plane with normal  $\mathbf{i}_1$ , do not affect the local mechanical response. For M=2 if either  $A^{(1)} \cdot A^{(2)}=0$ , or  $\beta^{(1)}=\beta^{(2)}$  and  $\alpha^{(1)}=\alpha^{(2)}$ , then the material is locally orthotropic. If  $A^{(1)} \cdot A^{(2)}=0$ , let  $\theta^{(1)}=0$  and  $\theta^{(2)}=-\pi/2$ , then  $A^{(1)}=\mathbf{i}_1$  and  $A^{(2)}=\mathbf{i}_3$ . This situation describes perpendicular reinforcing fibers which need not provide identical reinforcing. If, on the other hand,  $\beta^{(1)}=\beta^{(2)}$  and  $\alpha^{(1)}=\alpha^{(2)}$ , let  $\theta^{(1)}=-\theta^{(2)}=\theta$ , then  $\mathbf{i}_1$  and  $\mathbf{i}_3$  are the perpendicular bisectors of the fiber axes in this plane. That is,  $\mathbf{i}_1=(A^{(1)}+A^{(2)})/(2\cos\theta)$ ,  $\mathbf{i}_3=(A^{(2)}-A^{(1)})/(2\sin\theta)$ . This situation describes biassed reinforcing fibers with balanced reinforcing. Note in both cases that reflections with respect to planes that are normal to  $\mathbf{i}_1$ ,  $\mathbf{i}_2$  or  $\mathbf{i}_3$ , respectively, do not affect mechanical

1

response. For M = 2 with  $A^{(1)} \cdot A^{(2)} \neq 0$  and either  $\beta^{(1)} \neq \beta^{(2)}$  or  $\alpha^{(1)} \neq \alpha^{(2)}$ , the material is said to be locally *clinotropic* (see [Zheng 1994]). This situation describes biassed reinforcing fibers with different reinforcing. Under clinotropy,  $\pi$ -rotation about  $\mathbf{i}_2$  and reflection with respect to a plane normal to  $\mathbf{i}_2$  have no effect on mechanical response.

In the linear theory, transversely isotropic materials are characterized by 5 elastic constants, orthotropic materials are characterized by 9 elastic constants, and clinotropic materials are characterized by 13 elastic constants. In sections 2.4 and 2.5 we give these elastic constants derived from material (2.1.5) for the transversely isotropic and biassed orthotropic cases respectively. In this regard it is necessary to take  $\alpha^{(m)} = 2$  (m = 1,2,...,M) for the material (2.1.5) to have finite additional stiffness in the fiber directions under infinitesimal deformations, since  $\alpha^{(m)}>2$  involves no detectable strengthening in the infinitesimal limit and  $\alpha^{(m)}<2$  gives no extension along the  $A^{(m)}$ -axis in the infinitesimal limit. In other words, the exponent  $\alpha^{(m)}=2$  gives a nontrivial consistency with the familiar linear elasticity theory. It is worthwhile noting that, in the similar material models [Kurashige 1981, Triantafyllidis and Abeyaratne 1983, Polignone and Horgan 1993], this exponent of the additional stiffness, though not mentioned, is taken to be 2. Henceforth we take  $\alpha^{(m)}=2$  (m = 1,2,...,M) so that (2.1.5) is rewritten as

$$W = \frac{\mu}{2}(I_1 - 3) + \sum_{m=1}^{M} \frac{\beta^{(m)}}{2} (K^{(m)} - 1)^2.$$
 (2.1.10)

It is clear that the specific augmentation applied to the neo-Hookean form is only one particular model for fiber reinforcement. In the present study we consider only materials reinforced with families of *straight parallel fibers*, hence from now on we will say fibers instead of straight parallel fibers for abbreviation.

The generality of the material model (2.1.10) within the symmetry classes corresponding to transverse isotropy and to orthotropy is clarified by referring to the work of Zheng [1994] specialized to incompressible materials, and hence isochoric deformations. For transversely isotropic incompressible materials, it follows that the most general form for the strain energy density function is given by ([Zheng 1994])

$$W = W(tr(C), tr(C^2), A \cdot CA, A \cdot C^2A). \tag{2.1.11}$$

In our case  $A = \{1,0,0\}$  and so gives a dependence on the four scalar arguments:

$$tr(\mathbf{C}) = \mathbf{C}_{11} + \mathbf{C}_{22} + \mathbf{C}_{33}$$
,  $tr(\mathbf{C}^2) = \mathbf{C}_{11}^2 + \mathbf{C}_{22}^2 + \mathbf{C}_{33}^2 + 2(\mathbf{C}_{12}^2 + \mathbf{C}_{13}^2 + \mathbf{C}_{23}^2)$ , (2.1.12)  
 $\mathbf{A} \cdot \mathbf{C} \mathbf{A} = \mathbf{C}_{11}$ ,  $\mathbf{A} \cdot \mathbf{C}^2 \mathbf{A} = \mathbf{C}_{11}^2 + \mathbf{C}_{12}^2 + \mathbf{C}_{13}^2$ .

In particular, (2.1.10) with M = 1 gives

$$W = \frac{\mu}{2}(C_{11} + C_{22} + C_{33} - 3) + \frac{\beta}{2}(C_{11} - 1)^2$$
 (2.1.13)

and so represents only one particular model for the finite elastic response of a transversely isotropic incompressible material. Nevertheless, just as the utility of the neo-Hookean model for isotropic incompressible materials is widely acknowledged, the form (2.1.13) provides an idealized form for investigating the effects of transverse isotropy in finite deformation.

In a similar fashion, the general form of the strain energy density function in an orthotropic incompressible material is given by ([Zheng 1994])

$$W = W(tr(C), tr(C^2), tr(MC), tr(MCM), tr(CMC), tr(MC^2M)), \qquad (2.1.14)$$

where

$$\mathbf{M} = \mathbf{i}_1 \otimes \mathbf{i}_1 - \mathbf{i}_3 \otimes \mathbf{i}_3. \tag{2.1.15}$$

It can be shown that the dependence upon the six scalar trace variables appearing in the argument list of (2.1.14) is equivalent to dependence upon the six quantities:  $C_{11}$ ,  $C_{22}$ ,  $C_{33}$ ,  $C_{12}^2$ ,  $C_{13}^2$ ,  $C_{23}^2$ . This is because, in addition to the first two equations in (2.1.12),

$$tr(\mathbf{MC}) = C_{11} - C_{33}, tr(\mathbf{CMC}) = C_{11}^2 + C_{12}^2 - C_{23}^2 - C_{33}^2, tr(\mathbf{MCM}) = C_{11} + C_{33}, tr(\mathbf{MC}^2\mathbf{M}) = C_{11}^2 + C_{12}^2 + 2C_{13}^2 + C_{23}^2 + C_{33}^2,$$
 (2.1.16)

which, in turn, gives

$$C_{11} = \frac{1}{2}(tr(MC) + tr(MCM)),$$

$$C_{22} = tr(C) - tr(MCM),$$

$$C_{33} = \frac{1}{2}(-tr(MC) + tr(MCM)),$$

$$C_{12}^{2} = \frac{1}{2}(-tr(C)^{2} + tr(C^{2}) + 2tr(C)tr(MCM) - tr(MC)tr(MCM)$$

$$-tr(MCM)^{2} + tr(CMC) - tr(MC^{2}M)),$$

$$C_{13}^{2} = \frac{1}{4}(2tr(C)^{2} - 2tr(C^{2}) - tr(MC)^{2} - 4tr(C)tr(MCM)$$

$$+ tr(MCM)^{2} + 4tr(MC^{2}M)),$$

$$C_{23}^{2} = \frac{1}{2}(-tr(C)^{2} + tr(C^{2}) + 2tr(C)tr(MCM) + tr(MC)tr(MCM)$$

$$- tr(MCM)^{2} - tr(CMC) - tr(MC^{2}M)).$$

For the orthotropic case arising from perpendicular reinforcing fibers, (2.1.10) with  $K^{(1)} = C_{11}$ ,  $K^{(2)} = C_{33}$  provides the strain energy density representation

$$W = \frac{\mu}{2}(C_{11} + C_{22} + C_{33} - 3) + \frac{\beta^{(1)}}{2}(C_{11} - 1)^2 + \frac{\beta^{(2)}}{2}(C_{33} - 1)^2. \tag{2.1.18}$$

For the orthotropic case arising from biassed, balanced reinforcing fibers, (2.1.10) with

$$\begin{split} \mathbf{K}^{(1)} &= (\cos\theta)^2 \mathbf{C}_{11} + 2\cos\theta\sin\theta \mathbf{C}_{13} + (\sin\theta)^2 \mathbf{C}_{33} ,\\ \mathbf{K}^{(2)} &= (\cos\theta)^2 \mathbf{C}_{11} - 2\cos\theta\sin\theta \mathbf{C}_{13} + (\sin\theta)^2 \mathbf{C}_{33} , \end{split} \tag{2.1.19}$$

provides the strain energy density representation

$$W = \frac{\mu}{2} (C_{11} + C_{22} + C_{33} - 3)$$

$$+ \beta (((\cos\theta)^2 C_{11} + (\sin\theta)^2 C_{33} - 1)^2 + 4(\cos\theta\sin\theta)^2 C_{13}^2).$$
(2.1.20)

As required, C<sub>13</sub> enters into this last strain energy density expression only through its square.

#### 2.2. General Stress-Deformation Relation

The Cauchy stress tensor for the incompressible anisotropic finite elastic material (2.1.10) is

$$\mathbf{T} = 2\mathbf{F}\frac{\partial \mathbf{W}}{\partial \mathbf{C}}\mathbf{F}^{\mathrm{T}} - p\mathbf{I} = 2\mathbf{F}\left\{\frac{\partial \mathbf{W}}{\partial \mathbf{I}_{1}}\frac{\partial \mathbf{I}_{1}}{\partial \mathbf{C}} + \sum_{m=1}^{M} \frac{\partial \mathbf{W}}{\partial \mathbf{K}^{(m)}}\frac{\partial \mathbf{K}^{(m)}}{\partial \mathbf{C}}\right\}\mathbf{F}^{\mathrm{T}} - p\mathbf{I}.$$
 (2.2.1)

Here we have the following response functions

$$\frac{\partial W}{\partial I_1} = \frac{\mu}{2} , \qquad \frac{\partial W}{\partial K^{(m)}} = \beta^{(m)} (K^{(m)} - 1) , \qquad (2.2.2)$$

and the derivatives of these strain invariants with respect to the right Cauchy-Green strain tensor

$$\frac{\partial \mathbf{I}_1}{\partial \mathbf{C}} = \mathbf{I} , \qquad \frac{\partial \mathbf{K}^{(m)}}{\partial \mathbf{C}} = \mathbf{A}^{(m)} \otimes \mathbf{A}^{(m)} . \tag{2.2.3}$$

The hydrostatic pressure field p = p(X) in (2.2.1) is a scaler (undetermined by the deformation alone) that is due to the incompressibility constraint that is given in (2.1.7). It

is usually determined by boundary conditions. The Cauchy stress tensor is

$$\mathbf{T} = \mu \mathbf{F} \mathbf{F}^{T} - p \mathbf{I} + \sum_{m=1}^{M} 2\beta^{(m)} (\mathbf{F} \mathbf{A}^{(m)} \cdot \mathbf{F} \mathbf{A}^{(m)} - 1) \mathbf{F} \mathbf{A}^{(m)} \otimes \mathbf{F} \mathbf{A}^{(m)}.$$
 (2.2.4)

This is the stress-deformation relation (constitutive law) established from material model (2.1.10) with M families of fibers arranged in orientations indexed by the vectors  $\mathbf{A}^{(m)}$ . The Piola-kirchhoff stress tensor S is then given by  $\mathbf{S} = \mathbf{F}^{-1}\mathbf{T}$ .

In the context of this research, consideration will be placed on the material whose constitutive law is given by expression (2.2.4). It is evident that the strain energy density W, given in (2.1.10), regarded as a function of deformation gradient F, is positive semi-definite. The strain energy density W takes the value of zero only if the material modeled is in its undeformed state or undergoes a rigid body motion.

#### 2.3. Homogeneous Deformations

When a material body undergoes a homogeneous deformation, the size and shape of the material body have no effect on the pointwise mechanical responses. In other words, when we consider the material mechanical properties pointwisely under deformation, it is equivalent to consider a material body of certain size and shape (usually a unit cube) under the same but homogeneous deformation. For this purpose, the deformation is best described by the deformation gradient tensor **F**. We set-forth here the homogeneous deformations that will be applied in the following sections.

The deformation gradient has the right polar decomposition

$$\mathbf{F} = \mathbf{R}\mathbf{U},\tag{2.3.1}$$

where  $\mathbf{R}$  is proper orthogonal ( $\mathbf{R}\mathbf{R}^{T} = \mathbf{R}^{T}\mathbf{R} = \mathbf{I}$ ) and characterizes a rigid body rotation,

while U is symmetric and positive-definite and thus has three real eigenvalues and the associated three mutually orthogonal eigen-directions. Thus, a deformation can be observed as, first a pure deformation U, then a post rigid body rotation R. It is worthwhile noting that the mechanical responses of a material is only affected by U, not affected by R. It is clear from  $(2.1.6)_3$  that the right Cauchy-Green strain tensor

$$\mathbf{C} = \mathbf{F}^{\mathsf{T}}\mathbf{F} = \mathbf{U}\mathbf{R}^{\mathsf{T}}\mathbf{R}\mathbf{U} = \mathbf{U}^{2} \tag{2.3.2}$$

is not affected by rigid body rotation.

We consider first the homogeneous triaxial deformation described by the deformation gradient tensor

$$\mathbf{F} = \begin{bmatrix} \lambda_1 & 0 & 0 \\ 0 & \lambda_2 & 0 \\ 0 & 0 & \lambda_3 \end{bmatrix}. \tag{2.3.3}$$

Here, the principal stretches

$$\lambda_i > 0, \qquad i = 1, 2, 3.$$
 (2.3.4)

In the literature, this deformation is often referred to as homogeneous pure deformation. We shall call it homogeneous triaxial deformation to reflect the directional feature shared with the anisotropic material that will be studied. The constraint of incompressibility (2.1.7) now becomes

$$\lambda_1 \lambda_2 \lambda_3 = 1. \tag{2.3.5}$$

Secondly, a general plane deformation taking place in the  $(X_1, X_2)$ -plane can be written, in the deformation gradient tensor, as

-

$$\mathbf{F} = \begin{bmatrix} \mathbf{F}_{11} & \mathbf{F}_{12} & \mathbf{0} \\ \mathbf{F}_{21} & \mathbf{F}_{22} & \mathbf{0} \\ \mathbf{0} & \mathbf{0} & 1 \end{bmatrix}, \tag{2.3.6}$$

and  $F_{12} \neq F_{21}$  in general. For this plane deformation, the left Cauchy-Green strain tensor is

$$\mathbf{C} = \mathbf{C}^{\mathrm{T}} = \begin{bmatrix} \mathbf{C}_{11} & \mathbf{C}_{12} & 0 \\ \mathbf{C}_{12} & \mathbf{C}_{22} & 0 \\ 0 & 0 & 1 \end{bmatrix}, \tag{2.3.7}$$

with  $C_{ij} = F_{ki}F_{kj}$  so that

$$C_{11} > 0, C_{22} > 0.$$
 (2.3.8)

The corresponding incompressibility constraint is

$$C_{11}C_{22} - C_{12}^2 = 1. (2.3.9)$$

An important specialization of (2.3.6) is generated by requiring  $F_{12} = F_{21} = 0$ . This gives the *biaxial deformation* described by the deformation gradient tensor

$$\mathbf{F} = \begin{bmatrix} \lambda_1 & 0 & 0 \\ 0 & \lambda_2 & 0 \\ 0 & 0 & 1 \end{bmatrix} = \begin{bmatrix} \lambda_1 & 0 & 0 \\ 0 & \lambda_1^{-1} & 0 \\ 0 & 0 & 1 \end{bmatrix}, \tag{2.3.10}$$

where  $\lambda_3=1$ , and

$$\lambda_2 = \lambda_1^{-1} \tag{2.3.11}$$

is the incompressibility constraint directly obtained from (2.3.5). Here the deformation is described by the principal stretch  $\lambda_1$  alone. Biaxial deformations taking place in other

coordinate planes can be similarly defined.

Consider now the simple shear deformation with respect to coordinate planes. There are in total six different canonical cases of simple shear deformations regarding the direction of shear and the coordinate plane, in which the deformation take place. For a simple shear of amount k in  $X_p$ -direction taking place in the  $(X_p, X_q)$ -plane, the deformation gradient tensor has the components

$$F_{ij} = \delta_{ij} + k \delta_{ip} \delta_{jq}. \qquad (2.3.12)$$

The incompressibility constraint (2.1.7) is satisfied by the simple shear deformation.

Finally we set here more general simple shear deformation in the  $(X_1, X_2)$ -plane. Consider a unit vector  $\mathbf{e}_1$  lie in the  $(X_1, X_2)$ -plane and pass through the origin of the coordinate system set forth. This unit vector  $\mathbf{e}_1$  is apart from  $\mathbf{i}_1$  an angle  $\psi$  by right hand rotation about  $\mathbf{i}_3$ . Let  $\mathbf{e}_2 = \mathbf{i}_3 \times \mathbf{e}_1$  and  $\mathbf{e}_3 = \mathbf{i}_3$ . We define simple shear in the direction of  $\mathbf{e}_1$ , upon which line elements in the direction of  $\mathbf{e}_1$  in the planes normal to  $\mathbf{i}_3$  do not change their length and orientation, but have slides along  $\mathbf{e}_1$ -direction. Furthermore, the slide of a specific line element is proportional, by factor  $\mathbf{k}$ , to the distance measured along  $\mathbf{e}_2$  from  $\mathbf{e}_1$  to the line element. By this definition, the deformation gradient tensor with respect to the  $\{\mathbf{i}_1,\mathbf{i}_2,\mathbf{i}_3\}$  coordinate system is given by

$$\mathbf{F} = \begin{bmatrix} 1 - k\cos\psi\sin\psi & k\cos^2\psi & 0 \\ -k\sin^2\psi & 1 + k\cos\psi\sin\psi & 0 \\ 0 & 0 & 1 \end{bmatrix}.$$
 (2.3.13)

Simple shear defined in (2.3.12) with indices p = 1 and q = 2 is obtained by letting  $\psi = 0$  in (2.3.13). Simple shear in (2.3.12) with indices p = 2 and q = 1 is obtained from (2.3.13) by

setting  $\psi = \pi/2$  and replacing k with -k.

The stress state of a uniaxial load  $\tilde{T}$  in the  $X_p$ -direction is given, in components, by

$$T_{ij} = \tilde{T}\delta_{ip}\delta_{jp}. \tag{2.3.14}$$

#### 2.4. Material Properties (Single Fiber Family)

If the material expressed in (2.1.10) is reinforced with only one family of fibers (M = 1 in (2.1.10)), then it has three mutually orthogonal material principal directions and three mutually orthogonal planes of symmetry. Furthermore, one of these planes of symmetry is the plane of isotropy. This type of materials is the transversely isotropic material and is characterized by five independent elastic constants in linear elasticity. We now investigate the mechanical responses of this material model through prescribed simple homogeneous deformations in accordance with simple loading conditions, such as uniaxial load in fiber direction, uniaxial load transverse to fiber direction and simple shear. For this purpose, we arrange the rectangular Cartesian coordinate system so that the  $X_1$ -axis is in the direction of the family of fibers ( $\theta = 0$ ) and, therefore, the  $X_2$  and  $X_3$ -axes are in the material isotropic plane. Thus, the strain energy density function (2.1.10) becomes

$$W = \frac{\mu}{2}(I_1 - 3) + \frac{\beta}{2}(K - 1)^2. \tag{2.4.1}$$

The components of the Cauchy stress tensor, following from (2.2.4), are given by

$$T_{ii} = \mu F_{ik} F_{ik} - p \delta_{ii} + 2\beta (F_{rs} F_{rt} A_s A_t - 1) F_{ip} F_{iq} A_p A_q. \qquad (2.4.2)$$

The unit vector field A for the single family of fibers is simply given by

$$A = \{1, 0, 0\}^T$$
 or  $A_i = \delta_{i1}$  (2.4.3)

in the coordinate system set previously. This, for M = 1, reduces the Cauchy stress tensor (2.4.2) to as

$$T_{ij} = \mu F_{ik} F_{jk} - p \delta_{ij} + 2\beta (F_{r1} F_{r1} - 1) F_{i1} F_{j1}. \qquad (2.4.4)$$

In the case that the material is reinforced with single family of fibers (or families of fibers that only differ from orientation), we define a dimensionless material parameter (i.e. stiffness ratio) as

$$\gamma = \beta/\mu \ge 0. \tag{2.4.5}$$

#### 2.4.1. Material Response to Homogeneous Deformations

Here, we examine the mechanical responses and investigate the properties of the material (2.4.1) reinforced with one family of fibers through simple homogeneous deformations corresponding to some simple loading conditions.

#### (i) Uniaxial load in the $X_1$ -direction (fiber direction)

We seek the stress state of uniaxial traction in  $X_1$ -direction, given by (2.3.14) with index p = 1, corresponding to a homogeneous triaxial deformation (2.3.3). In view of the equivalence of the  $X_2$  and  $X_3$  material directions in this case, we seek solutions with the additional lateral symmetry  $\lambda_2 = \lambda_3$ . This, in connection with equation (2.3.5), yields

$$\lambda_2 = \lambda_3 = \lambda_1^{-1/2}. \tag{2.4.6}$$

The corresponding left Cauchy-Green strain tensor is diagonal and given by

$$\mathbf{C} = \begin{bmatrix} \lambda_1^2 & 0 & 0 \\ 0 & \lambda_1^{-1} & 0 \\ 0 & 0 & \lambda_1^{-1} \end{bmatrix}. \tag{2.4.7}$$

We now show that there is a single family of such solutions and that they can be parametrized by  $\lambda_1>0$ . That is, we obtain functions

$$T_{11} = \tilde{T}_{11}(\lambda_1), \qquad \lambda_2 = \tilde{\lambda}_2(\lambda_1), \qquad \lambda_3 = \tilde{\lambda}_3(\lambda_1), \qquad (2.4.8)$$

for each  $\lambda_1 > 0$ .

Substituting equations (2.3.3) with (2.4.6) into equation (2.4.4), the only possible nonzero components of the Cauchy stress tensor are

$$T_{11} = \mu \lambda_1^2 + 2\beta(\lambda_1^2 - 1)\lambda_1^2 - p, \qquad (2.4.9)$$

$$T_{22} = T_{33} = \mu \lambda_1^{-1} - p.$$
 (2.4.10)

The hydrostatic pressure p which makes  $T_{22} = T_{33} = 0$  is

$$p = \mu \lambda_1^{-1}. {(2.4.11)}$$

Therefore, the uniaxial load required to produce the deformation corresponding to deformation gradient (2.3.3) with (2.4.6) is

$$T_{11} = \mu(\lambda_1^2 - \lambda_1^{-1}) + 2\beta(\lambda_1^2 - 1)\lambda_1^2. \tag{2.4.12}$$

Equation (2.4.6) and (2.4.12) yield the following asymptotes:

$$\lambda_2 \to \infty$$
,  $\lambda_3 \to \infty$ ,  $T_{11} \sim -\mu \lambda_1^{-1} \to -\infty$ , as  $\lambda_1 \to 0$ , (2.4.13)

and

$$\lambda_2 \to 0$$
,  $\lambda_3 \to 0$ ,  $T_{11} \sim 2\beta \lambda_1^4 \to \infty$ , as  $\lambda_1 \to \infty$ . (2.4.14)

It can be seen from  $(2.4.13)_3$  that to compress the material body to a flattened state such as a deformation  $(2.4.13)_{1,2}$ , the dominant portion of load  $T_{11}$  is required to balance the hydrostatic pressure p which is generated for preserving volume. From  $(2.4.14)_3$  we see that if the material body is forced to extend very large, such as a deformation  $(2.4.14)_{1,2}$ , the dominant portion of load  $T_{11}$  is contributed to overcome the resistance generated by the additional stiffness in the fiber direction. Figure 2 and Figure 3 are the responses of material (2.4.1) in uniaxial load in fiber direction. In Figure 2,  $\lambda_2$  and  $\lambda_3$ , given by equation (2.4.6), is independent of the material properties and is determined by the incompressibility constraint only.

Noting (2.4.5) and (2.4.7), we derive from (2.4.1) the normalized strain energy density function for this deformation, expressed in terms of  $\lambda_1$  and  $\gamma$ , as well as its partial derivative with respect to  $\lambda_1$ :

$$\tilde{W}(\lambda_1, \gamma) = \frac{1}{\mu} W(C(\lambda_1), \mu, \beta) = \frac{1}{2} (\lambda_1^2 + 2\lambda_1^{-1} - 3) + \frac{1}{2} \gamma (\lambda_1^2 - 1)^2, \qquad (2.4.15)$$

$$\frac{\partial}{\partial \lambda_1} \tilde{W}(k, \psi, \gamma) = \lambda_1 - \lambda_1^{-2} + 2\gamma(\lambda_1^2 - 1)\lambda_1, \qquad (2.4.16)$$

respectively. Comparing (2.4.16) with (2.4.12) and noting (2.3.5), one verifies the well-known result

$$\frac{1}{\mu}T_{11}(\lambda_1, \gamma) = \frac{\lambda_1}{\lambda_1\lambda_2\lambda_3} \frac{\partial}{\partial \lambda_1} \tilde{W}(\lambda_1, \gamma), \qquad (2.4.17)$$

in the anisotropic problem studied here.

27

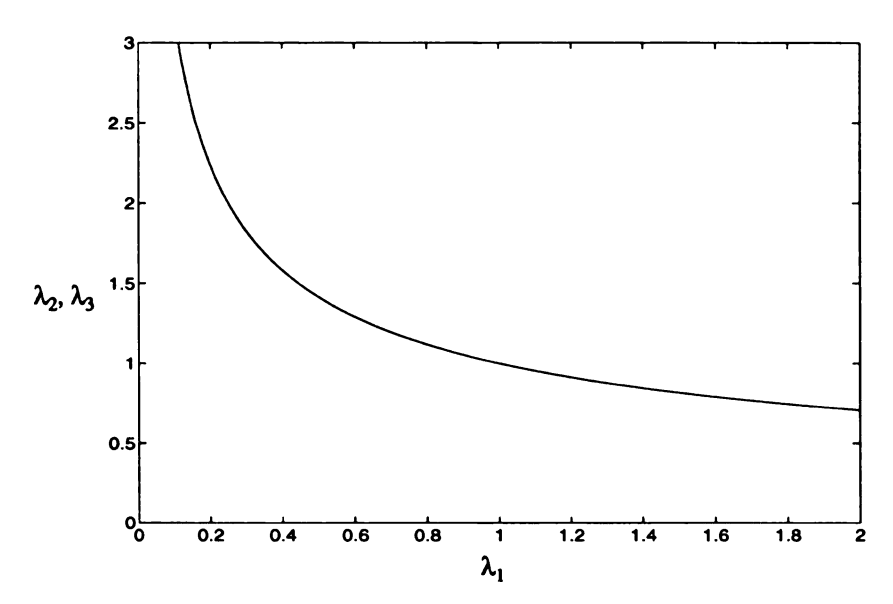


Figure 2. Lateral deformation vs. extension/contraction in the loading direction for the case of uniaxial load in the fiber direction. Here  $\lambda_2$  or  $\lambda_3$  is independent of the material properties and is determined by the incompressibility constraint only (2.4.6).  $\lambda_1 = 1$  represents to the undeformed configuration.

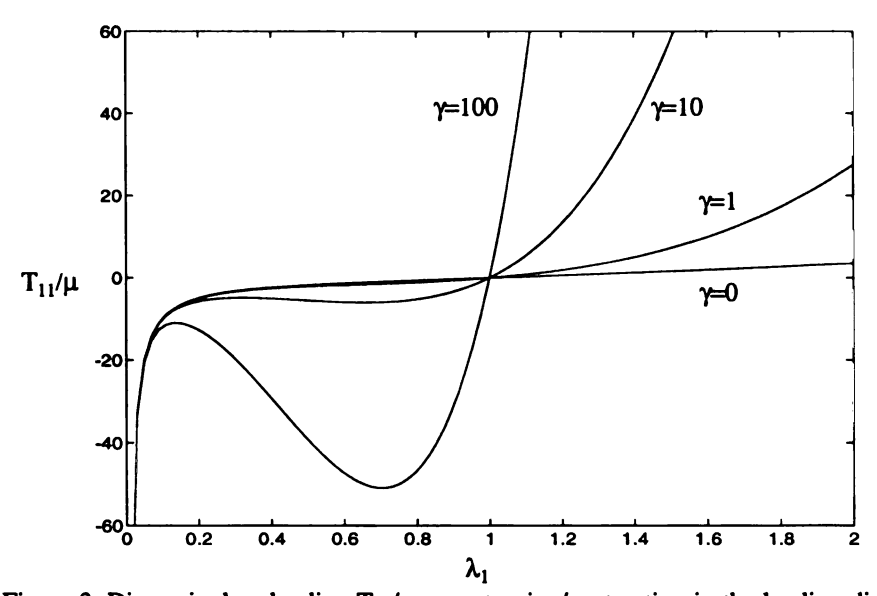


Figure 3. Dimensionless loading  $T_{11}/\mu$  vs. extension/contraction in the loading direction for the case of uniaxial load in the fiber direction (2.4.12). The stiffness ratio  $\gamma$  takes the value:  $\gamma = 0$ , 1, 10 and 100. For  $\gamma > 4.960745$ ,  $T_{11}$  behaves non-monotonically for  $\lambda_1 < 1$ . Loss of monotonicity first take place at  $\gamma = 4.960745$ ,  $\lambda_1 = 0.5194$ . This gives rise to the possibility that, in compression, three deformed configurations could correspond to one load level.  $\lambda_1 = 1$  represents the undeformed configuration.

In Figure 3, for larger stiffness ratio  $\gamma$ , the responses  $(T_{11})$  behave non-monotoni-

cally in compression ( $\lambda_1 < 1$ ) and give rise to the possibility that three deformed configurations correspond to one load level. The minimum  $\gamma$  at which  $T_{11}$  becomes non-monotonical is  $\gamma = 4.960745$ . The cases of  $\gamma = 0$ , 1, 10 and 100, are plotted in Figure 3. For the case that  $\gamma = 0$ , the response is simply that of the neo-Hookean material. Denoting the value of  $\lambda_1$  at which  $T_{11}/\mu$  takes its local maximum by  $\lambda_{1(\text{max})}^{\text{uni}}$ , and the value of  $\lambda_1$  at which  $T_{11}/\mu$  takes its local minimum by  $\lambda_{1(\text{min})}^{\text{uni}}$ , we now investigate the relation between these special values of  $\lambda_1$  and  $\gamma$ . For this purpose, we take the partial derivative of (2.4.17) with respect to  $\lambda_1$  and obtain the following equation

$$\frac{\partial}{\partial \lambda_1} \left( \frac{1}{\mu} T_{11}(\lambda_1, \gamma) \right) = 2\lambda_1 + \lambda_1^{-2} + 2\gamma (4\lambda_1^3 - 2\lambda_1) = 0, \qquad (2.4.18)$$

which, for every given  $\gamma$ , determines  $\lambda_{1(\max)}^{uni}$  and  $\lambda_{1(\min)}^{uni}$ . Since  $\lambda_1 > 0$ , the second equality in (2.4.18) is equivalent to

$$8\gamma\lambda_1^5 - (4\gamma - 2)\lambda_1^3 + 1 = 0. (2.4.19)$$

This is a fifth order polynomial equation and there is no standard solution procedure for it. However, the number of positive real roots may be determined by the Descarte's rule of sign, which states the number of positive real roots of a polynomial equals the number of sign variation of the polynomial, or less by an even number. The number of sign variation of the left hand side of (2.4.19) is 0 for  $\gamma \le 1/2$ , and is 2 for  $\gamma > 1/2$ . By the Descarte's rule of sign, we know that equation (2.4.19) has no positive real root for  $\gamma \le 1/2$ , and equation (2.4.19) may have either 0 or 2 positive real roots for  $\gamma > 1/2$ . We have found numerically that local maximum and local minimum exist for  $\gamma > 4.960745$ . We now solve equation (2.4.19) numerically to obtain  $\lambda_{I(\max)}^{uni}(\gamma)$ ,  $\lambda_{I(\min)}^{uni}(\gamma)$ , and plot it in Figure 4.

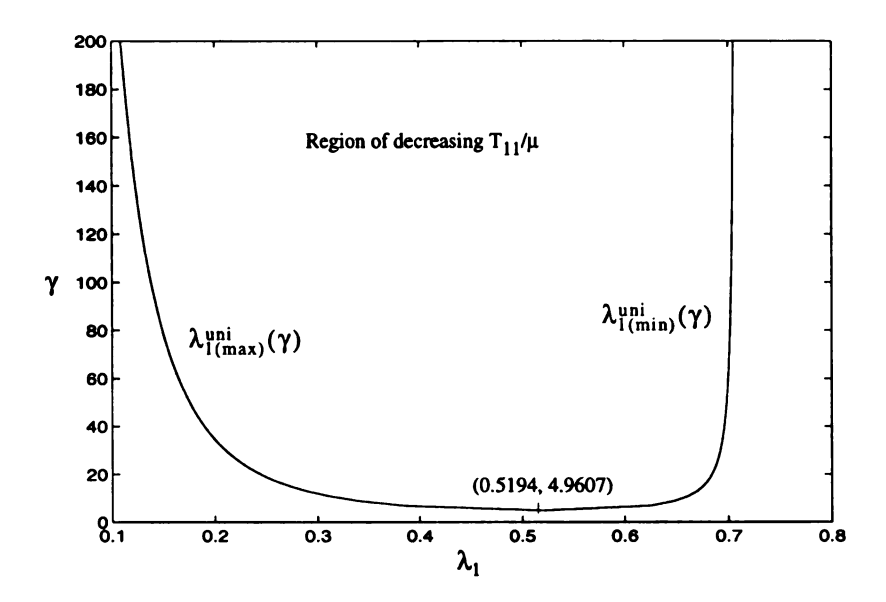


Figure 4. Curves of  $\lambda_{l(\max)}^{uni}(\gamma)$  and  $\lambda_{l(\min)}^{uni}(\gamma)$   $\lambda_{l(\min)}(\gamma)$  corresponding to the non-monotonic uniaxial response behavior of  $T_{11}/\mu$  which occurs in Figure 3 for  $\gamma > 4.960745$ .

#### (ii) Biaxial load associated with biaxial deformation

If the deformation is biaxial as given by (2.3.10), then

$$\mathbf{C} = \begin{bmatrix} \lambda_1^2 & 0 & 0 \\ 0 & \lambda_1^{-2} & 0 \\ 0 & 0 & 1 \end{bmatrix}. \tag{2.4.20}$$

For these deformations the Cauchy stress tensor is diagonal. If, in addition, the hydrostatic pressure p is chosen so that  $T_{22} = 0$ , corresponding to a traction free boundary with normal  $i_2$ , then the only nonzero components of the Cauchy stress tensor are

$$T_{11} = \mu(\lambda_1^2 - \lambda_1^{-2}) + 2\beta(\lambda_1^2 - 1)\lambda_1^2,$$
  

$$T_{33} = \mu(1 - \lambda_1^{-2}).$$
(2.4.21)

Here the hydrostatic pressure p which makes  $T_{22} = 0$  is

$$p = \mu \lambda_1^{-2}$$
. (2.4.22)

The nonzero component  $T_{33}$  (2.4.21)<sub>2</sub> is required to maintain biaxial deformation condition  $\lambda_3 = 1$ . Here  $T_{11}$  (2.4.21)<sub>1</sub> is plotted against  $\lambda_1$  for  $\gamma = 0$  (neo-Hookean), 1, 10 and 100 in Figure 5. As anticipated,  $|T_{11}(\lambda_1)|_{\text{biaxial load & biaxial deformation}} > |T_{11}(\lambda_1)|_{\text{uniaxial load & triaxial deformation}}$ , if  $\lambda_1 \neq 1$ .

Making use of (2.4.20) in (2.4.1), it is found that the normalized strain energy density function, expressed in terms of  $\lambda_1$  and  $\gamma$ , as well as its partial derivative with respect to  $\lambda_1$  are given by

$$\tilde{W}(\lambda_1, \gamma) = \frac{1}{\mu} W(C(\lambda_1), \mu, \beta) = \frac{1}{2} (\lambda_1^2 + \lambda_1^{-2} - 2) + \frac{1}{2} \gamma (\lambda_1^2 - 1)^2, \qquad (2.4.23)$$

$$\frac{\partial}{\partial \lambda_1} \tilde{W}(k, \psi, \gamma) = \lambda_1 - \lambda_1^{-3} + 2\gamma(\lambda_1^2 - 1)\lambda_1, \qquad (2.4.24)$$

for this biaxial deformation. Comparing (2.4.24) with  $(2.4.21)_1$  and noting (2.3.5), one verifies, again, the well-known result

$$\frac{1}{\mu}T_{11}(\lambda_1, \gamma) = \frac{\lambda_1}{\lambda_1\lambda_2\lambda_3}\frac{\partial}{\partial\lambda_1}\tilde{W}(\lambda_1, \gamma), \qquad (2.4.25)$$

in the anisotropic problem studied here.

Figure 5 indicates, for larger stiffness ratio  $\gamma$ , that the load responses  $T_{11}(\lambda_1)$  behaves non-monotonically in compression ( $\lambda_1 < 1$ ) and so also give rise to the possibility that three deformed configurations can correspond to one load level. The minimum  $\gamma$  at which  $T_{11}$  becomes non-monotonic for biaxial deformation is  $\gamma = 14.950393$  as shown below. Denoting the value of  $\lambda_1$  at which  $T_{11}/\mu$  takes its local maximum by  $\lambda_{1(\max)}^{bi}$ , and the value of  $\lambda_1$  at which  $T_{11}/\mu$  takes its local minimum by  $\lambda_{1(\min)}^{bi}$ , we now turn to locate  $\lambda_{1(\max)}^{bi}$  and  $\lambda_{1(\min)}^{bi}$  for changing  $\gamma$ . For this purpose, set the partial derivative of (2.4.25)

with respect to  $\lambda_1$  equal to zero:

$$\frac{\partial}{\partial \lambda_1} \left( \frac{1}{\mu} T_{11}(\lambda_1, \gamma) \right) = 2\lambda_1 + \lambda_1^{-3} + 2\gamma (4\lambda_1^3 - 2\lambda_1) = 0, \qquad (2.4.26)$$

which, for every given  $\gamma$ , determines possible values  $\lambda_{1(\max)}^{bi}$  and  $\lambda_{1(\min)}^{bi}$ . Since  $\lambda_1 > 0$ , the second equality in (2.4.18) is equivalent to

$$4\gamma\lambda_1^6 - (2\gamma - 1)\lambda_1^4 + 1 = 0. (2.4.27)$$

Expressing equation (2.4.27) in terms of  $C_{11}$  by noting  $C_{11} = \lambda_1^2$ , yields the following cubic equation

$$4\gamma C_{11}^3 - (2\gamma - 1)C_{11}^2 + 1 = 0. (2.4.28)$$

This cubic equation can be solved by following standard procedure. It is to be noted that equation (2.4.27) has a positive real root for  $\lambda_1$  if and only if equation (2.4.28) has a positive real root for  $C_{11}$ . It is to be further noted that the transition from monotonicity to nonmonotonicity of  $T_{11}/\mu$  corresponds to a positive real root of (2.4.28). Following the theory of cubic equations [Kurosh 1980] indicates that equation (2.4.28) has a double real root if and only if

$$8\gamma^3 - 120\gamma^2 + 6\gamma - 1 = 0. (2.4.29)$$

Following, again, the procedure as mentioned in [Kurosh 1980] indicates that (2.4.29) has only one real root  $\gamma = 14.950393$ . This is the lower bound for nonmonotonic behavior. For  $\gamma > 14.950393$ , one may then solve equation (2.4.28) ((2.4.27)) to obtain  $\lambda_{1(\max)}^{bi}(\gamma)$  and  $\lambda_{1(\min)}^{bi}(\gamma)$ , as shown in Figure 6. Figure 7 compares the nonmonotonicity regions for this response with that of the uniaxial response as given previously by Figure 4.

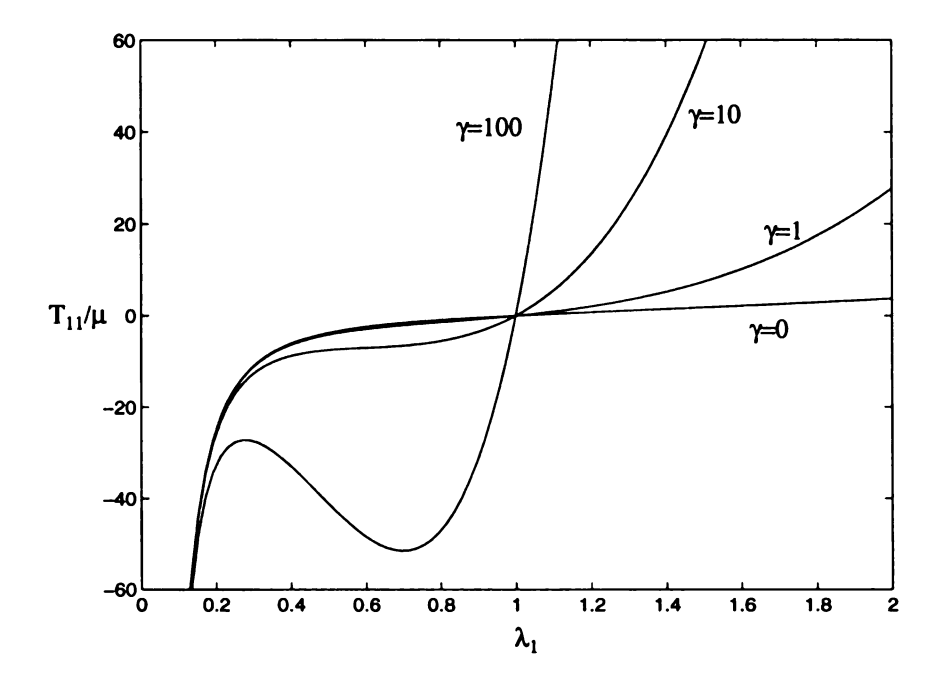


Figure 5. Dimensionless loading  $T_{11}/\mu$  vs. extension/contraction in the loading direction for the case of biaxial load (2.4.21) associated with biaxial deformation (2.3.10). The stiffness ratio  $\gamma$  takes the value:  $\gamma = 0$ , 1, 10 and 100. For  $\gamma > 14.950393$ ,  $T_{11}$  behaves non-monotonically for  $\lambda_1 < 1$ . Loss of non-monotonicity first takes place at  $\gamma = 14.950393$ ,  $\lambda_1 = 0.5676$ . This gives rise to the possibility that, in compression, three deformed configurations could correspond to one load level.  $\lambda_1 = 1$  represents the undeformed configuration.

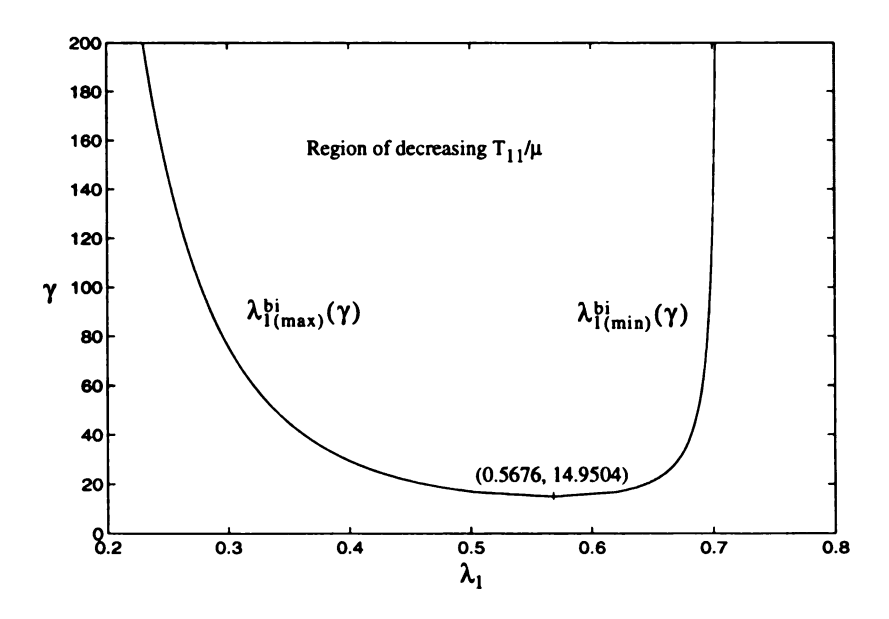


Figure 6. Curves of  $\lambda_{l(max)}^{bi}(\gamma)$  and  $\lambda_{l(min)}^{bi}(\gamma)$  corresponding to the nonmonotonic biaxial response behavior of  $T_{11}/\mu$  which occurs in Figure 5 for  $\gamma > 14.950393$ .

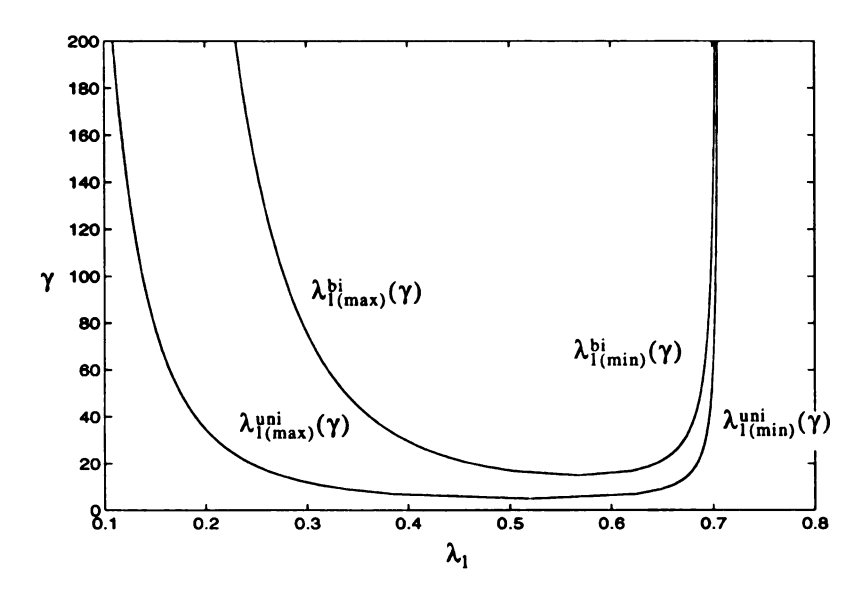


Figure 7. Comparison of the nonmonotonicity regions between the uniaxial response and the biaxial response.

# (iii) Uniaxial load in $X_2$ -direction (transverse to the fiber direction)

Here we seek the stress state of uniaxial traction in  $X_2$ -direction, given by (2.3.14) with i = 2, corresponding to the homogeneous deformation (2.3.3). We now show that there is a single family of such solutions and that they can be parametrized by  $\lambda_2$ . That is, we show that given  $\lambda_2$  we can obtain

$$\lambda_1 = \tilde{\lambda}_1(\lambda_2), \qquad T_{22} = \tilde{T}_{22}(\lambda_2), \qquad \lambda_3 = \tilde{\lambda}_3(\lambda_2).$$
 (2.4.30)

These relations are, however, not given explicitly.

The nonzero components of the Cauchy stress tensor, by substituting equations (2.3.3) and the incompressibility constraint (2.3.5) into equation (2.4.4), are

$$T_{11} = \mu \lambda_1^2 + 2\beta(\lambda_1^2 - 1)\lambda_1^2 - p,$$
 (2.4.31)

$$T_{22} = \mu \lambda_2^2 - p, \qquad (2.4.32)$$

$$T_{33} = \mu \lambda_3^2 - p. \tag{2.4.33}$$

Here  $T_{22}$  is the load required to produce such a deformation as described in equation (2.3.3). The uniaxial stress state (2.3.14) with i=2 requires that  $T_{11}=T_{33}=0$ . This permits the elimination of p between equations (2.4.31) and (2.4.33), and so gives the following relation between  $\lambda_1$  and  $\lambda_3$ 

$$\mu(\lambda_1^2 - \lambda_3^2) + 2\beta(\lambda_1^2 - 1)\lambda_1^2 = 0. \tag{2.4.34}$$

Then eliminating  $\lambda_3$  from equation (2.4.34) by using equation (2.3.5), yields

$$f_{12}(\lambda_1, \lambda_2) \equiv 2\beta\lambda_1^6 + (\mu - 2\beta)\lambda_1^4 - \mu\lambda_2^{-2} = 0.$$
 (2.4.35)

Alternatively eliminating  $\lambda_1$  from equation (2.4.34) by using equation (2.3.5), yields

$$f_{32}(\lambda_3, \lambda_2) = -\mu \lambda_3^6 + (\mu - 2\beta)\lambda_2^{-2}\lambda_3^2 + 2\beta\lambda_2^{-4} = 0.$$
 (2.4.36)

From equations (2.4.35) and (2.4.36), the corresponding  $\lambda_1$  and  $\lambda_3$  at every given  $\lambda_2$  can be determined. In fact, let  $x = \lambda_1^2$  or  $x = \lambda_3^2$  respectively in (2.4.35) or (2.4.36). We then get either

$$2\beta x^{3} + (\mu - 2\beta)x^{2} - \mu \lambda_{2}^{-2} = 0, \qquad (2.4.37)$$

or

$$-\mu x^3 + (\mu - 2\beta)\lambda_2^{-2}x + 2\beta\lambda_2^{-4} = 0.$$
 (2.4.38)

According to the Descarte's rule of sign, both equation (2.4.37) and equation (2.4.38) have exactly one positive real root for x. It follows that equation (2.4.35) or (2.4.36) each gives one positive real root to  $\lambda_1$  or  $\lambda_3$  respectively for every given  $\lambda_2>0$  and so define two functions  $\tilde{\lambda}_1$  and  $\tilde{\lambda}_3$  in (2.4.30)<sub>1,3</sub>. The load deflection relation (2.4.30)<sub>2</sub> is then

 $T_{22}(\lambda_2) = \mu\{\lambda_2' - \lambda_3'(\lambda_2)\}$ . Using a numerical procedure, we can graph the responses of the material defined in (2.4.1) in uniaxial load transverse to the fiber direction according to equations (2.3.5), (2.4.31)-(2.4.36). Figure 8-Figure 10 are examples of these responses plotted for  $\gamma = 0$  (neo-Hookean), 1, 10 and 100. This numerical procedure indicates that the dimensionless loading  $T_{22}/\mu$  monotonically increases with  $\lambda_2$ , so that for each value of load  $T_{23}$ , there is one corresponding deformed configuration of type (2.3.3).

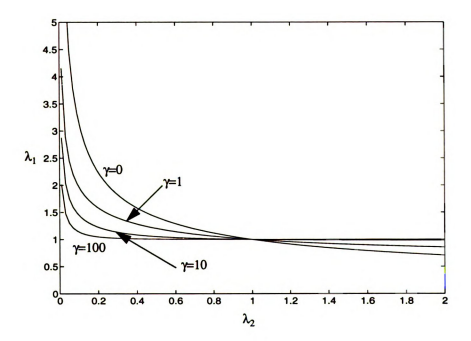


Figure 8. Lateral deformation in the fiber direction vs. extension/contraction in the loading direction, for the case of uniaxial load transverse to the fiber direction. The stiffness ratio  $\gamma$  takes the value:  $\gamma$  = 0, 1, 10 and 100.  $\lambda_2$  = 1 represents the undeformed configuration.

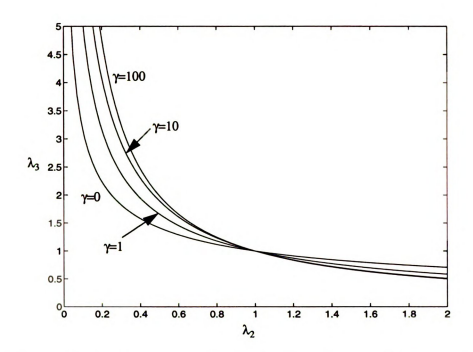


Figure 9. Lateral deformation orthogonal to the fiber direction vs. extension/contraction in the loading direction, for the case of uniaxial load transverse to the fiber direction. The stiffness ratio  $\gamma$  takes the value:  $\gamma=0,1,10$  and  $100,\,\lambda_2=1$  represents the undeformed configuration.

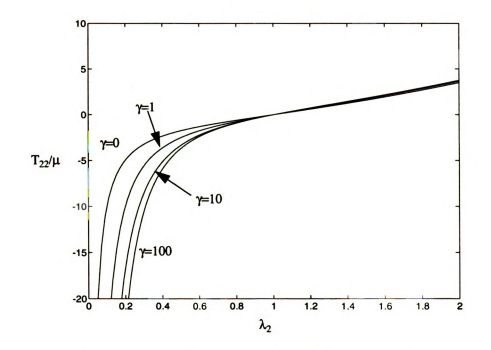


Figure 10. Dimensionless loading  $T_{22}/\mu$  vs. extension/contraction in the loading direction, for the case of uniaxial load transverse to fiber direction. The stiffness ratio  $\gamma$  takes the value:  $\gamma = 0, 1, 10$  and 100.  $\lambda_1 = 1$  represents the undeformed configuration.

Equations (2.3.5), (2.4.31)-(2.4.33) with  $T_{11} = T_{33} = 0$ , as well as equation (2.4.35) and (2.4.36) also yields the following asymptotes in terms of  $\lambda_2$ :

$$\lambda_{1} \sim \left(\frac{2\beta}{\mu}\right)^{-1/6} \lambda_{2}^{-1/3} \to \infty,$$

$$\lambda_{3} \sim \left(\frac{2\beta}{\mu}\right)^{1/6} \lambda_{2}^{-2/3} \to \infty,$$

$$T \sim -(2\mu^{2}\beta)^{1/3} \lambda_{2}^{-4/3} \to -\infty,$$
(2.4.39)

$$\lambda_{1} \sim \left(1 - \frac{2\beta}{\mu}\right)^{-1/4} \lambda_{2}^{-1/2} \rightarrow 0,$$

$$\lambda_{3} \sim \left(1 - \frac{2\beta}{\mu}\right)^{1/4} \lambda_{2}^{-1/2} \rightarrow 0,$$

$$T \sim \mu \lambda_{2}^{2} \rightarrow \infty,$$
as  $\lambda_{2} \rightarrow \infty$ . (2.4.40)

#### (iv) Simple shear deformation with respect to coordinate plane

We now turn to simple shear deformation in the  $(X_1, X_2)$ -plane. First, if the material is subjected to a simple shear in the  $X_1$ -direction (in the fiber direction) then the deformation gradient tensor is given by (2.3.12) with indices p = 1 and q = 2. The Cauchy stress tensor associated with this deformation is obtained from (2.4.4) as

$$\mathbf{T} = \begin{bmatrix} \mu(1+k^2) - p & \mu k & 0 \\ \mu k & \mu - p & 0 \\ 0 & 0 & \mu - p \end{bmatrix}.$$
 (2.4.41)

We note that the associated shear stress,

$$T_{12} = T_{21} = \mu k \tag{2.4.42}$$

is not affected by the additional stiffness in the  $X_1$ -direction, since this deformation (2.3.12) with i = 1 and j = 2 involves no stretching of the fiber.

If instead the simple shear is prescribed in the  $X_2$ -direction (transverse to the fiber direction) in the  $(X_1,X_2)$ -plane, then the deformation gradient tensor is given by (2.3.12) with indices p=2 and q=1. It then also follows from (2.4.4) that the Cauchy stress tensor is

$$\mathbf{T} = \begin{bmatrix} \mu - p + 2\beta k^2 & \mu k + 2\beta k^3 & 0\\ \mu k + 2\beta k^3 & \mu (1 + k^2) - p + 2\beta k^4 & 0\\ 0 & 0 & \mu - p \end{bmatrix}.$$
 (2.4.43)

Now, we find that

$$T_{12} = T_{21} = (\mu + 2\beta k^2)k$$
. (2.4.44)

The additional shear stiffness  $2\beta k^2$  to the total shear stiffness is due to the additional stiffness, introduced by the fiber reinforcement, in the  $X_1$ -direction. For infinitesimally small shear (|k| << 1), this additional shear stiffness is negligible, but this term has significant effect if the shear deformation is not infinitesimally small. For strongly anisotropic fiber-reinforced materials, the stiffness in the fiber direction can be greater, by orders of magnitude, than the stiffness in other direction. If  $\beta$  tends to infinity, as is the case that simulates an inextensible fiber, then  $T_{12}$  is required to be infinitely large to maintain nonzero amount of shear k in the  $X_2$ -direction. This is the same result as obtained by the ideal theory where the only direction for shear to take place is the fiber direction, due to the constraint of fiber inextensibility [Pipkin and Rogers 1971].

By symmetry of the  $X_2$  and  $X_3$ -directions, the results obtained above hold for simple shear in the  $(X_1,X_3)$ -plane if subscript 2 is everywhere replaced by subscript 3. On the other hand, for simple shear in the  $(X_2,X_3)$ -plane, the fiber stiffness  $\beta$  plays no role, and one easily finds that

$$T_{23} = T_{32} = \mu k \tag{2.4.45}$$

regardless of whether the simple shear is prescribed in the  $X_2$ -direction or in the  $X_3$ -direction.

The nonzero normal components of stress in (2.4.41) and (2.4.43) is due to the in-plane coupling effect (extension/shear), that, in finite elasticity, normal stresses are required to support simple shear deformation.

The simple shearing states (2.4.41) and (2.4.43) are supported by in-plane loads if  $T_{33} = 0$ . This corresponds to  $p = \mu$ , when utilized in (2.4.41) and (2.4.43) leads to the response diagrams given in Figure 11 and Figure 12. In Figure 11, the stress components  $T_{11}$ ,  $T_{12}$  and  $T_{22}$  in (2.4.41) are plotted, and in Figure 12, the stress components  $T_{11}$ ,  $T_{12}$  and  $T_{22}$  in (2.4.43) are plotted.

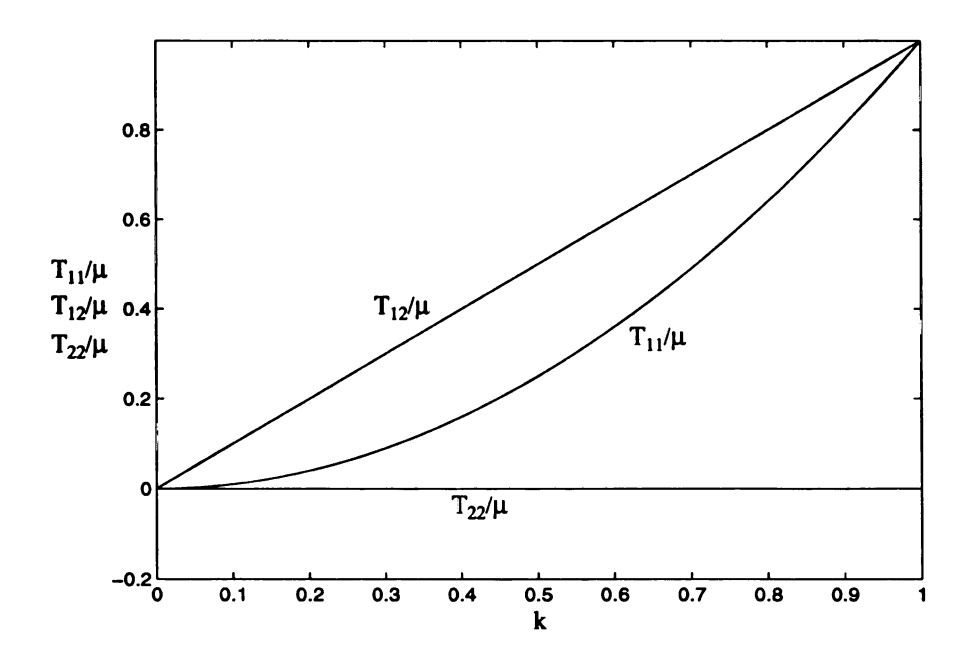


Figure 11. Simple shear in the fiber direction as given by equation (2.4.41) for  $\gamma = 10$ . This choice of  $\gamma$  corresponding to  $\mu = 4.9$  and  $\beta = 48.9$ , is motivated by the linear properties of the boron/epoxy material as exemplified later in Table 1.

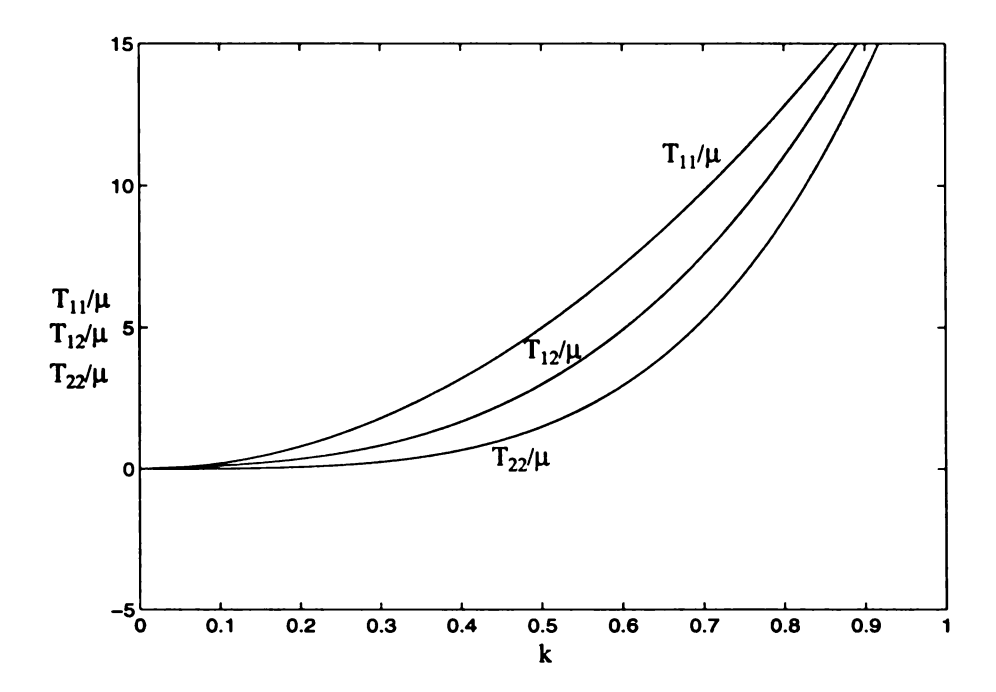


Figure 12. Simple shear transverse to the fiber direction as given by equation (2.4.43) for  $\gamma = 10$ .

# (v) General simple shear deformation in the $(X_1, X_2)$ -plane

For the more general simple shear in the  $(X_1, X_2)$ -plane with shear direction rotated from the fiber direction by an angle  $\psi$ , the Cauchy stress tensor is obtained, by substituting (2.3.13) into (2.4.4), in component form as

$$\begin{split} T_{11} &= \mu (k^2 cos^2 \psi - k sin 2 \psi) + 2\beta (k^2 sin^2 \psi - k sin 2 \psi) (1 - k sin 2 \psi + k^2 cos^2 \psi sin^2 \psi), \\ T_{12} &= \mu \Big( k cos 2 \psi + \frac{1}{2} k^2 sin^2 2 \psi \Big) + 2\beta (k^2 sin^2 \psi - k sin 2 \psi) (-k sin^2 \psi + k^2 cos \psi sin^2 \psi), \\ T_{22} &= \mu (k^2 sin^2 \psi + k sin 2 \psi) + 2\beta (k^2 sin^2 \psi - k sin 2 \psi) (k^2 sin^4 \psi). \end{split}$$

Here once again the hydrostatic pressure p is eliminated by equating  $p = \mu$  so as to give  $T_{33} = 0$ . Equation (2.4.46) reduces to (2.4.41) with  $p = \mu$  if  $\psi = 0$ , and reduces to (2.4.43) with  $p = \mu$  if  $\psi = \pi/2$  and k is replaced by -k. The responses under this simple shear (2.4.46) for single fiber family material with a number of shear directions are shown in Figure

13-Figure 15. These responses further reveal the in-plane coupling (extension/shear) effects, which present themselves not only in finite elasticity but also in linear anisotropic theory.

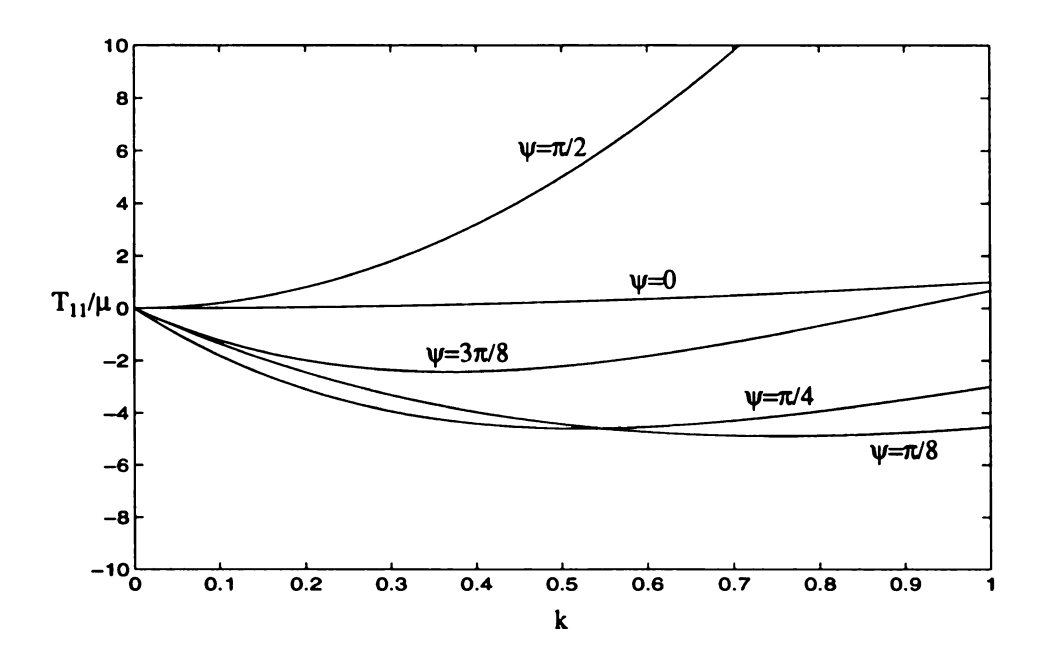


Figure 13. Normal stress  $T_{11}/\mu$  in (2.4.46) varies with simple shear k for material with one family of fibers, where  $\gamma = 10$  ( $\mu = 4.9$  and  $\beta = 48.9$ ). The material response to the simple shear (2.3.13) changes with the orientation  $\psi$ . The existence of normal stress in simple shear is characteristic of anisotropic materials.

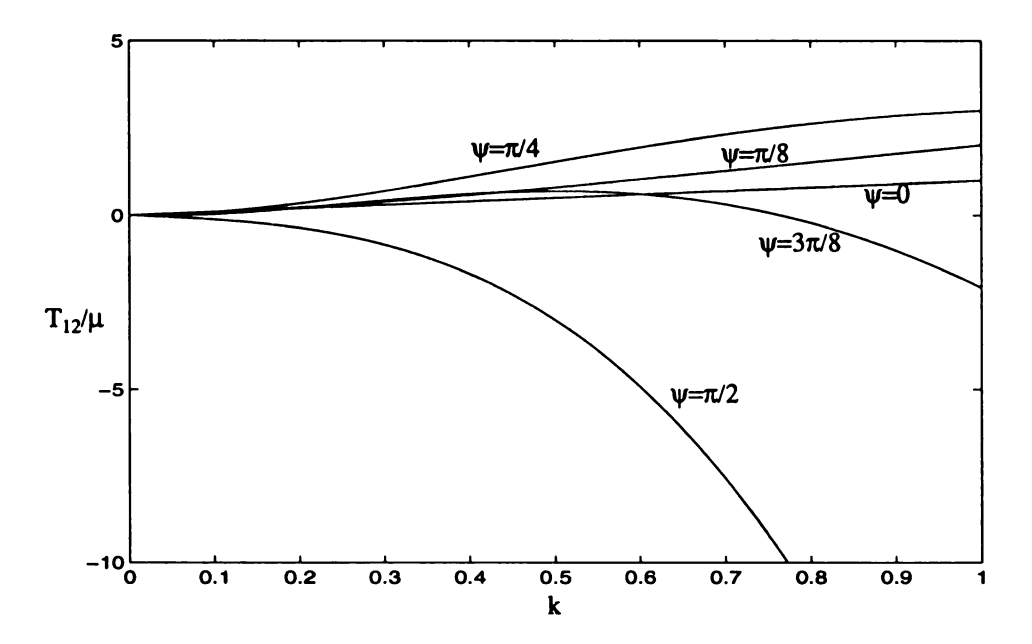


Figure 14. Shear stress  $T_{12}/\mu$  in (2.4.46) varies with simple shear k for material with one family of fibers, where  $\gamma = 10$  ( $\mu = 4.9$  and  $\beta = 48.9$ ). The material response to the simple shear (2.3.13) changes with the orientation  $\psi$ .

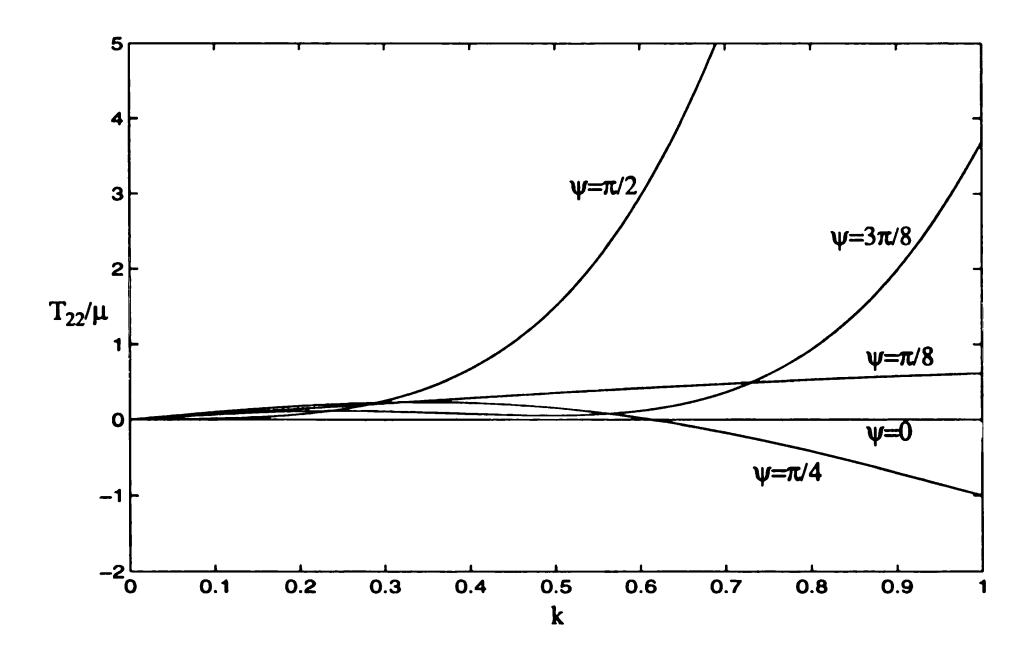


Figure 15. Normal stress  $T_{22}/\mu$  in (2.4.46) varies with simple shear k for material with one family of fibers, where  $\gamma = 10$  ( $\mu = 4.9$  and  $\beta = 48.9$ ). The material response to the simple shear (2.3.13) changes with the orientation  $\psi$ .

The in-plane shear stress resolved on surfaces parallel and perpendicular to the shearing

direction is then given by

$$T_{e_1e_2} = \mu k + \beta (k^2 \sin^2 \psi - k \sin 2\psi) (2k \sin^2 \psi - \sin 2\psi). \qquad (2.4.47)$$

This resolved shear stress is plotted in Figure 16 for various  $\psi$  at the fixed value  $\gamma = 10$ . The most immediate feature is the loss of monotonicity.

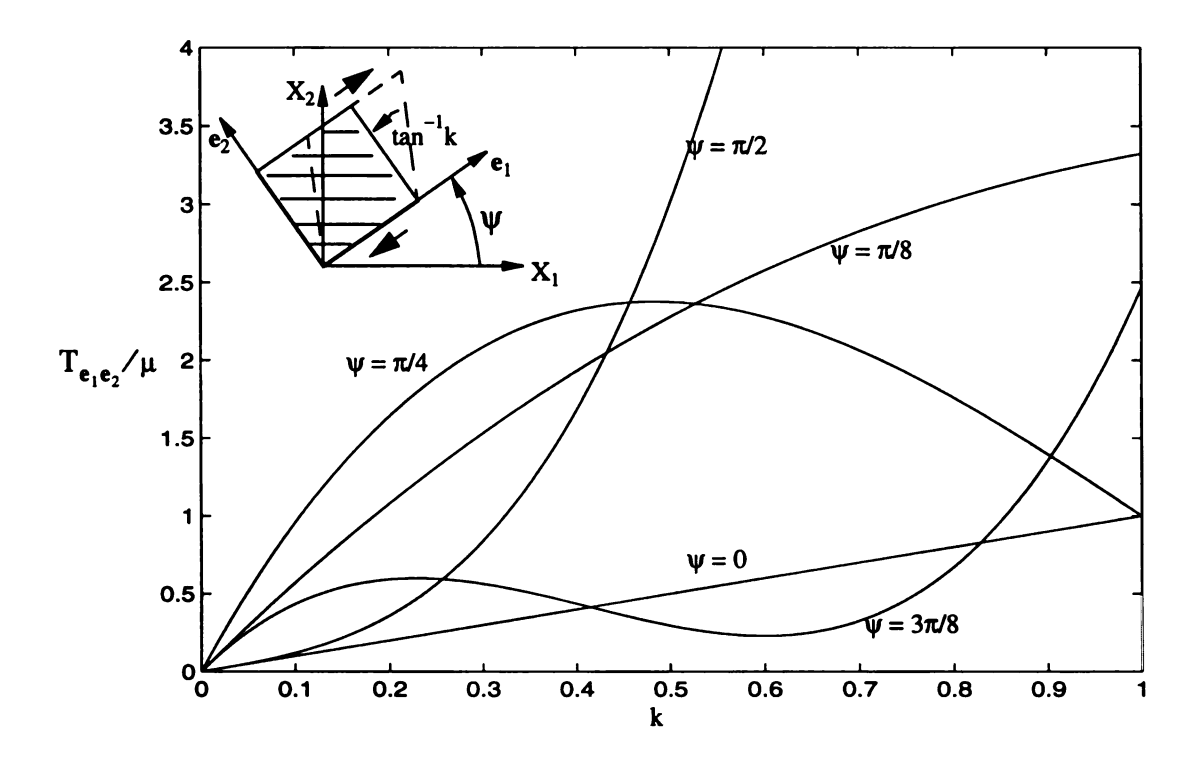


Figure 16. Shear stress  $T_{e_1e_2}/\mu$  in (2.4.47) varies with simple shear k for material with one family of fibers. As before  $\gamma = 10$ . The material response to the simple shear (2.3.13) changes with the orientation  $\psi$ .

This loss of monotonicity is correlated to a progressive contraction and subsequent relaxation/elongation of a material line element in the reinforcing direction. It is convenient to describe the associated line element deformation in terms of "fiber" shortening and lengthening. Then  $\sqrt{C_{11}}$  gives the fiber stretch, where, for this deformation, (2.3.13) yields

$$\mathbf{C} = \begin{bmatrix} 1 - 2k\cos\psi\sin\psi + k^2\sin^2\psi & k(\cos^2\psi - \sin^2\psi) - k^2\cos\psi\sin\psi & 0\\ k(\cos^2\psi - \sin^2\psi) - k^2\cos\psi\sin\psi & 1 + 2k\cos\psi\sin\psi + k^2\cos^2\psi & 0\\ 0 & 0 & 1 \end{bmatrix}. (2.4.48)$$

As shown in Figure 17, if  $0 < \psi < \pi/2$  this then gives rise to a regime of fiber contraction  $(C_{11} < 1)$  for moderate shear k which then gives way to fiber extension  $(C_{11} > 1)$  for large k.

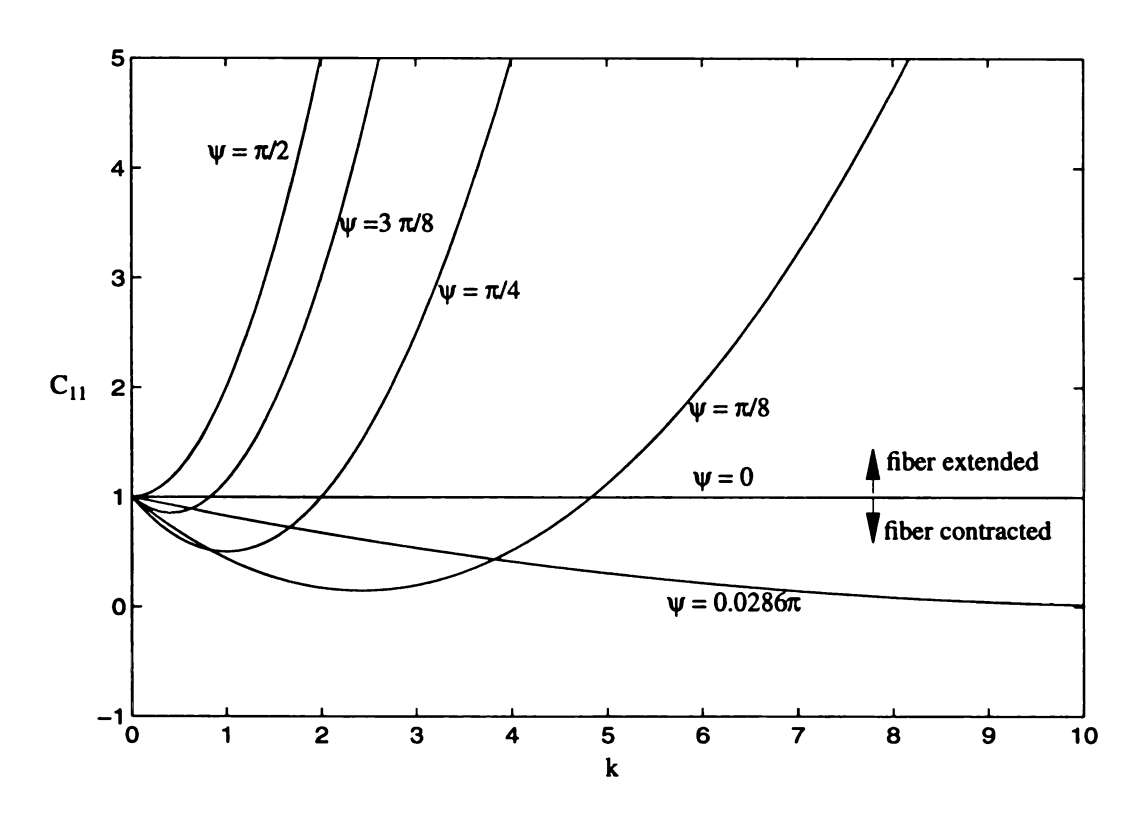


Figure 17. Fiber length changes with k, the amount of shear in general simple shear deformation. It is shown that fiber experiences first contraction  $(C_{11} < 0)$ , then elongation  $(C_{11} > 0)$  for  $0 < \psi < \pi/2$ .

This effect is due to the rotation that the fiber experiences under the deformation. Denoting this rotation by  $\phi$ , Figure 18 illustrates this phenomena for original fiber orientation  $\psi = \pi/4$ . For  $\psi = \pi/4$  the fiber is contracted for k:  $0 \to 2$  corresponding to  $\phi$ :  $0 \to -\pi/2$ , after which the fiber is extended for k:  $2 \to \infty$  corresponding to  $\phi$ :  $-\pi/2 \to -3\pi/4$ . More generally Figure 19 shows for any  $0 < \psi < \pi/2$  that the fiber is

contracted for k:  $k_{(0)} \equiv 0 \rightarrow k_{(b)} \equiv 2 \cot \psi$  corresponding to fiber rotation  $\phi$ :  $0 \rightarrow -\pi + 2\psi$ . The minimum deformed fiber length occurs at  $k_{(a)} \equiv \cot \psi$ , corresponding to  $C_{11} = \sin^2 \psi$  and  $\phi = -(\pi/2 - \psi)$ . The fiber is extended for k:  $k_{(b)} \rightarrow \infty$  corresponding to fiber rotation  $\phi$ :  $-\pi + 2\psi \rightarrow \psi - \pi$ . In particular, the fibers align with the simple shear direction  $\psi$  as  $k \rightarrow \infty$ .

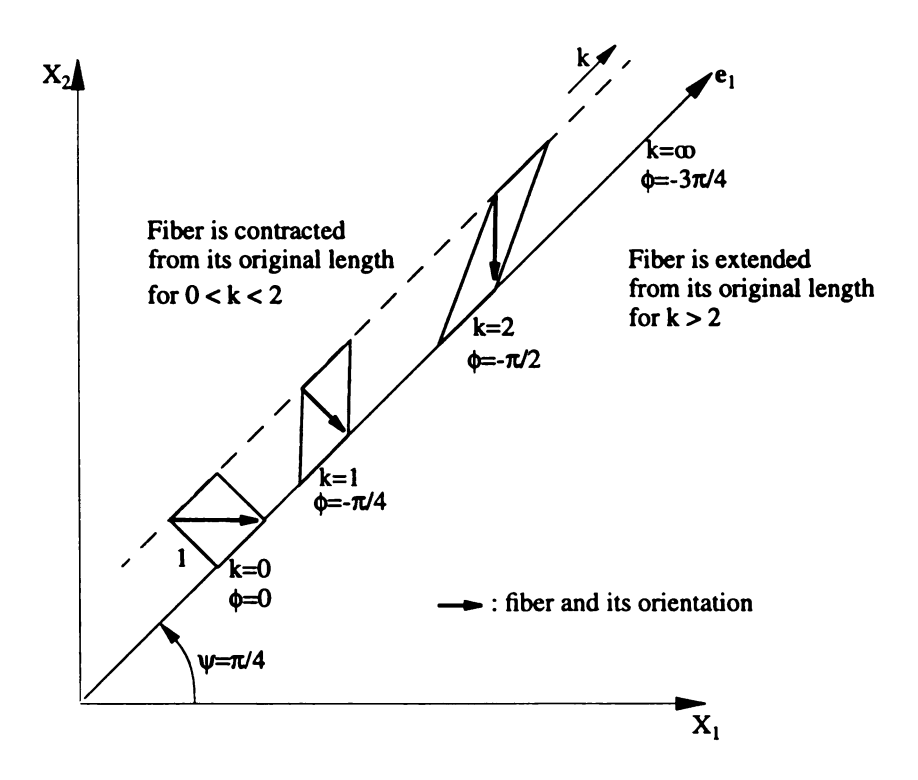


Figure 18. Simple shear deformation of a unit block with increasing k for  $\psi = \pi/4$ . The angle  $\phi$  is the fiber orientation with respect to the  $X_1$ -direction. Here, as k:  $0 \to \infty$ , the angle  $\phi$ :  $0 \to -3\pi/4$ . The fiber is first contracted and then extended. The maximum contraction occurs at  $\phi = -\pi/4$ .

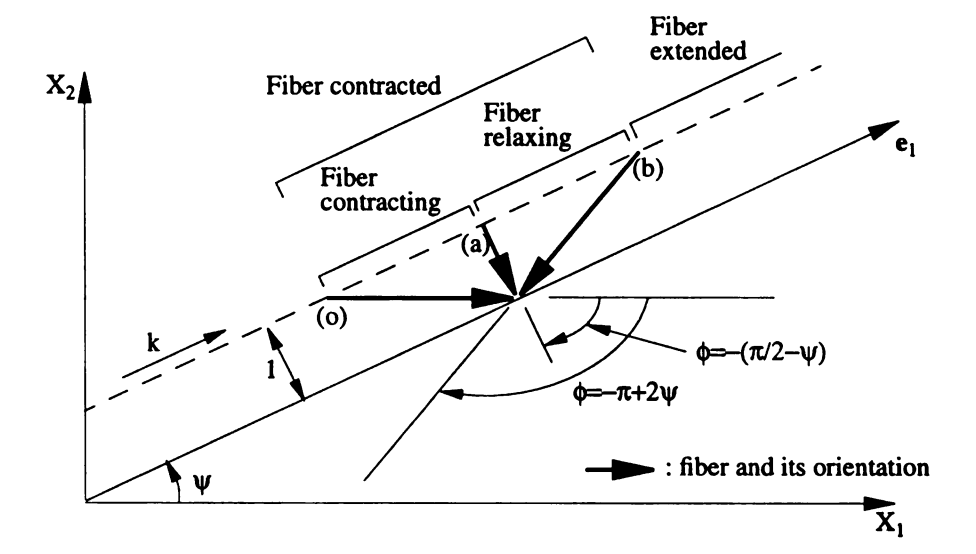


Figure 19. Deformation of a fiber under simple shear in arbitrary  $\psi$ -direction. Phases of fiber contraction, relaxation and extension are shown. Here point (o) represents the original fiber length and orientation. At point (a) the fiber is mostly contracted and at point (b) the fiber retrieves its original length. Angle  $\phi$  is the deformed fiber orientation with respect to  $X_1$ -direction.

To correlate this fiber contraction/relaxation/extension with the loss of monotonicity in the stress response (2.4.47), it is instructive to consider changes in the elastic strain energy density as a function of simple shear k. By making use of (2.4.48), the strain energy density function (2.1.13) gives that

$$\hat{W}(k, \psi, \gamma) = \frac{1}{\mu} W(C(k, \psi), \mu, \beta) = \frac{1}{2} k^2 + \frac{1}{2} \gamma (k^2 \sin^2 \psi - k \sin 2\psi)^2.$$
 (2.4.49)

The partial derivative of  $\hat{W}$  with respect to k is

$$\frac{\partial}{\partial k} \hat{W}(k, \psi, \gamma) = k + \gamma (k^2 \sin^2 \psi - k \sin 2\psi) (2k \sin^2 \psi - \sin 2\psi), \qquad (2.4.50)$$

so that (2.4.47) shows that

$$\frac{1}{\mu} T_{\mathbf{e}_1 \mathbf{e}_2}(\mathbf{k}, \mathbf{\psi}, \mathbf{\gamma}) = \frac{\partial}{\partial \mathbf{k}} \hat{\mathbf{W}}(\mathbf{k}, \mathbf{\psi}, \mathbf{\gamma}). \tag{2.4.51}$$

In Figure 20,  $T_{e_1e_2}/\mu$  for a material with  $\gamma = 10$  is plotted against k over a larger extent of

k than that plotted in Figure 16 for fiber orientations  $\psi=0$ ,  $\pi/8$ ,  $\pi/4$ ,  $3\pi/8$  and  $\pi/2$ . It is to be noted that  $T_{e_1e_2}/\mu$  for  $\psi=0$  is the normalized shear stress without the effect of fiber reinforcement. For other values of  $\psi$ , deviation of shear stress  $T_{e_1e_2}/\mu$  from that for  $\psi=0$  exhibits the effect of fiber reinforcement. Note that the curves for  $\psi=\pi/8$ ,  $\pi/4$ ,  $3\pi/8$  each cross the  $\psi=0$  (unreinforced) curve twice. This is due to the effect of fiber contraction-relaxation-elongation. On these curves the points corresponding to minimum fiber length are marked by '(a)' (when  $k=k_{(a)}$ ) and points corresponding to the retrieval of the original fiber length are marked by '(b)' (when  $k=k_{(b)}$ ). The fiber is continuously contracting for  $0 < k < k_{(a)}$ , it relaxes back to its original length for  $k_{(a)} < k < k_{(b)}$ , and it elongates for  $k > k_{(b)}$ . Points (a) and (b) are exactly the crossing points of these curves with the straight line for  $\psi=0$ . For each of these curves, it is seen from Figure 20 that

$$\begin{split} T_{e_1e_2}(k, \psi, 10) > T_{e_1e_2}(k, 0, 10), & \text{for } 0 < k < k_{(a)}, \\ T_{e_1e_2}(k, \psi, 10) < T_{e_1e_2}(k, 0, 10), & \text{for } k_{(a)} < k < k_{(b)}. \end{split} \tag{2.4.52}$$

For fixed reinforcing value  $\gamma$  and fiber orientation  $\psi$  one finds that local maxima and minima to these nonmonotonic response curves occur at

$$k_{max} = cot\psi - \sqrt{\frac{1}{3}cot^2\psi - \frac{1}{6\gamma}csc^4\psi}, \quad k_{min} = cot\psi + \sqrt{\frac{1}{3}cot^2\psi - \frac{1}{6\gamma}csc^4\psi}, \quad (2.4.53)$$

respectively. The quantity in the radical in (2.4.53) must be nonnegative for  $k_{max}$  and  $k_{min}$  to exist. This requires that

$$\gamma \ge 2$$
,  $\frac{1}{2} \arcsin\left(\sqrt{\frac{2}{\gamma}}\right) \le \psi \le \frac{\pi}{2} - \frac{1}{2} \arcsin\left(\sqrt{\frac{2}{\gamma}}\right)$ , (2.4.54)

for nonmonotonic response. For  $\gamma = 10$  this gives 0.2318 <  $\psi$  < 1.3390, so that all 3 curves  $\psi = \pi/8$ ,  $\pi/4$ ,  $3\pi/8$  in Figure 20 are nonmonotonic. In general, the corresponding shear stresses are

$$T_{e_1e_2}^{(max)}(\psi, \gamma) = T_{e_1e_2}(k_{max}, \psi, \gamma) \qquad T_{e_1e_2}^{(min)}(\psi, \gamma) = T_{e_1e_2}(k_{min}, \psi, \gamma) \quad (2.4.55)$$

These  $k_{max}$  and  $k_{min}$  are mapped to the (k,  $C_{11}$ )-plane and plotted in Figure 21 for  $\gamma = 10$ , together with the response previously given in Figure 17.

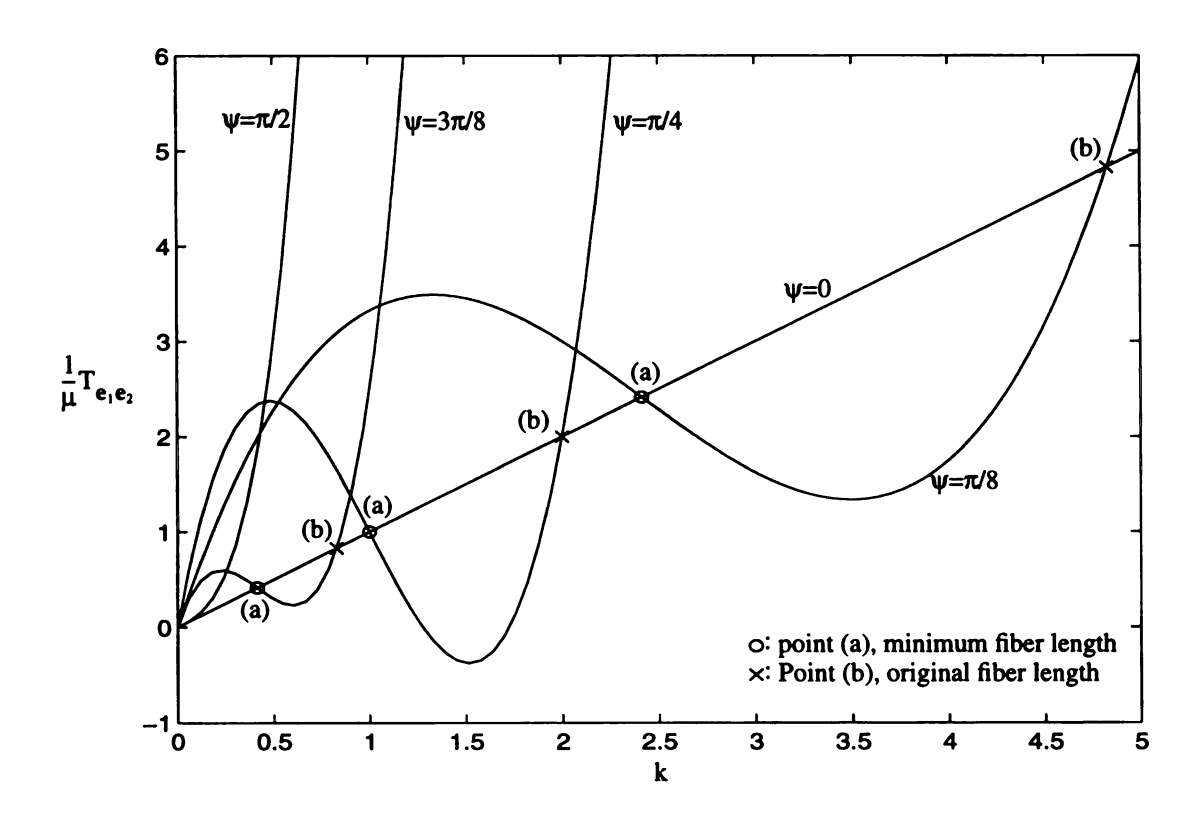


Figure 20. Shear stress  $T_{e_1e_2}/\mu$  in (2.4.51) ((2.4.47)) varies with simple shear k for a material with  $\gamma = 10$  and various fiber orientations  $\psi$  with respect to the direction of shearing. For each curve, the fibers contract from the origin to the point marked (a). The fibers then relax back to their original length between points (a) and (b). From point (b) onwards the fibers continue their elongation.

The energy relation (2.4.51) then shows that the decreasing portions of these response curves are associated with energetically unstable behavior in the standard sense of giving

 $\frac{\delta}{\partial k^2}W(k,\psi,\gamma)<0$ . This unstable regime includes the point of minimum fiber length  $k=k_{(a)}$ . It is also to be noted that the area between any  $0<\psi<\pi/2$  response curve and the  $\psi=0$  baseline curve for  $0< k< k_{(a)}$  is the same as the area between the two curves for  $k_{(a)}< k< k_{(b)}$ . This shows, with one exception, that the work required to obtain any of these k>0 deformations in the fiber reinforced materials with  $0<\psi<\pi/2$  is always greater than that required in the unreinforced material. The exception is the  $k=k_{(b)}$  deformation, associated with regain of original fiber length, which is work neutral with respect to the unreinforced response.

It is also apparent from Figure 20, for the  $\gamma=10$  material with fiber orientation  $\psi=\pi/4$ , that  $T_{e_1e_2}<0$  near the local minimum of the response curve. In particular, for relative fiber strength  $\gamma=10$  and original orientation  $\psi=\pi/4$ , one finds that  $T_{e_1e_2}=0$  is associated with shearing k=0, k=1.7236 and k=1.2764. For the  $\gamma=10$  material, one also finds that fiber orientation in the range  $0.5536<\psi<1.0172$  gives an interval of negative  $T_{e_1e_2}$  near the minimum of the response curve.

The effect of the relative fiber stiffness parameter  $\gamma$  is, according to (2.4.50), merely associated with a simple linear scaling of any  $\psi \neq 0$  response away from the unreinforced response (which is formally provided by the  $\psi = 0$  curve). Although nonmonotone response will occur in materials obeying  $\gamma \geq 2$  and  $\arcsin(\sqrt{2/\gamma}) \leq 2\psi < \pi - \arcsin(\sqrt{2/\gamma})$ , this does not necessarily ensure  $T_{e_1e_2} < 0$ . Instead,  $T_{e_1e_2}$  will only attain negative values for k near  $k_{\min}$  if the  $\gamma$ -scaling away from the unreinforced response is sufficiently large. We find that the lower bound value  $\gamma$  capable of providing such negative  $T_{e_1e_2}$  response is  $\gamma = 8$ . At this value  $\gamma = 8$  one finds that  $T_{e_1e_2} = 0$  for  $\psi = \pi/4$  at  $k = k_{\min} = 1.5$ . As  $\gamma$  increases from  $\gamma = 8$ , one finds that an increasing range

of original fiber orientations  $\psi$  are capable of supporting  $T_{e_1e_2} < 0$  for k near  $k_{min}$ . This negative  $T_{e_1e_2}$  response phenomenon is actually energy releasing under the general simple shear deformation. The region of  $(\psi, \gamma)$  supporting this energy releasing is plotted in Figure 22.

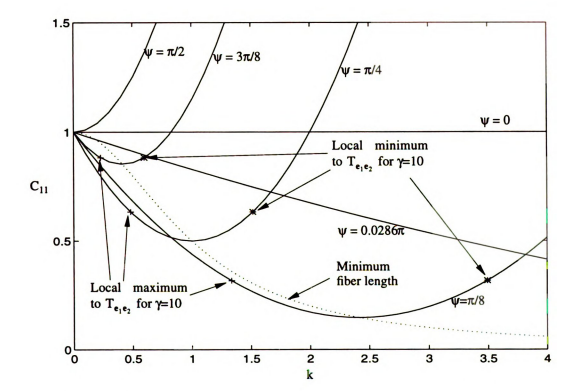


Figure 21. Changes of fiber length with k (Figure 17) are plotted again here together with the curve of minimum fiber length. Fibers are continuously contracted up to minimum length, then relaxed to their original length, and then are elongated, with increasing k for  $0 < \psi < \pi/2$ . The corresponding local maximums and local minimums are also plotted for the material with  $\gamma = 10$ .

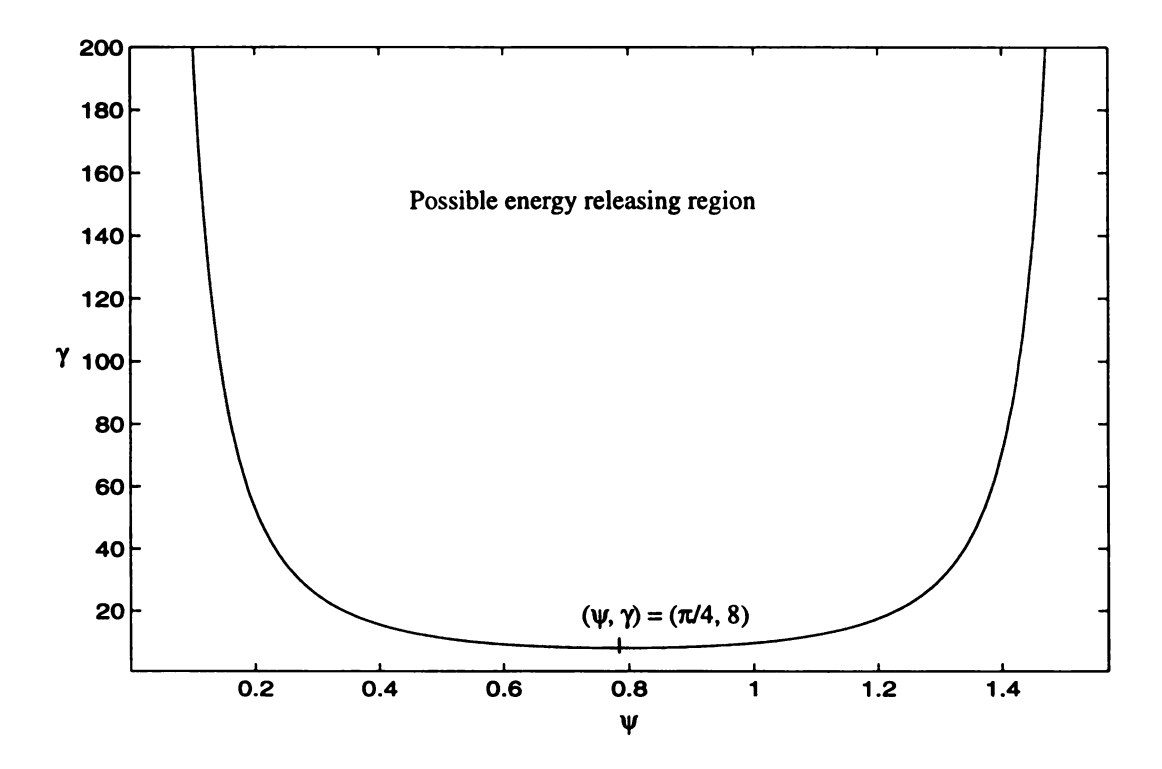


Figure 22. Region of  $(\psi, \gamma)$  supporting energy releasing behavior  $(T_{\mathbf{e}_1\mathbf{e}_2} < 0)$  under general simple shear deformation. Such behavior will occur if and only if  $\gamma \ge 8$ .

#### 2.4.2. Material Properties at Infinitesimal Limit

Here we consider the behaviors of the material given by (2.4.1) in the case that deformations are restricted in the neighborhood of the undeformed configuration. The corresponding elastic constants in linear elasticity are then derived. In the linear theory [Christensen 1979], a transversely isotropic material is described by five independent elastic constants, namely, the Young's moduli  $E_{11}$  and  $E_{22}$ , Poisson ratios  $v_{12}$  and  $v_{22}$  and shear modulus  $G_{12}$ . All other elastic constants can be obtained from  $E_{11}$ ,  $E_{22}$ ,  $v_{12}$ ,  $v_{22}$  and  $G_{12}$  by supplementing relations, such as

$$G_{23} = G_{32} = \frac{E_{22}}{2(1 + v_{23})}$$
 (2.4.56)

in the plane of isotropy, and

$$E_{11}v_{21} = E_{22}v_{12}, \qquad (2.4.57)$$

which is required by the symmetry of the elasticity tensor.

In the case of uniaxial load in the fiber direction, the relation between the load and the stretch in the load direction was found to be given by equation (2.4.12) and the lateral deformation was found to be given by equation (2.4.6). It follows from equation (2.4.12) that the corresponding Young's modulus  $E_{11}$  in the fiber direction is

$$E_{11} = \frac{dT}{d\lambda_1}\Big|_{\lambda_1 = 1} = 3\mu + 4\beta.$$
 (2.4.58)

From equation (2.4.6) it follows that the Poisson's ratio corresponding to uniaxial load in the fiber direction is

$$v_{21} = -\frac{d\lambda_2}{d\lambda_1}\Big|_{\lambda_1 = 1} = v_{31} = \frac{1}{2}.$$
 (2.4.59)

This is clearly due to the constraint of incompressibility. Here, the first subscript of  $\nu$  indicates the direction of lateral contraction/extension, and the second subscript of  $\nu$  indicates the direction of loading.

Similarly, the corresponding material properties in linear elasticity related to uniaxial load transverse to the fiber direction, derived from equations (2.3.5), (2.4.31)-(2.4.33) with  $T_{11} = T_{33} = 0$ , and equation (2.4.35) and (2.4.36), are given by

$$E_{22} = \frac{dT_{22}}{d\lambda_2}\bigg|_{\lambda_2 = 1} = \mu \frac{3\mu + 4\beta}{\mu + \beta},$$
 (2.4.60)

$$v_{12} = -\frac{d\lambda_1}{d\lambda_2}\Big|_{\lambda_1 = \lambda_2 = 1} = \frac{\mu}{2\mu + 2\beta},$$
 (2.4.61)

and

$$v_{32} = -\frac{d\lambda_3}{d\lambda_2}\bigg|_{\lambda_3 = \lambda_2 = 1} = \frac{\mu + 2\beta}{2\mu + 2\beta}.$$
 (2.4.62)

Note also that, by symmetry,  $E_{22} = E_{33}$ ,  $v_{12} = v_{13}$  and  $v_{32} = v_{23}$ . Here again, the subscripts of v are defined as before.

It is clear from (2.4.42) and (2.4.44), for infinitesimally small deformation of simple shear, that the shear modulus is

$$G_{12} = G_{21} = \frac{dT_{12}}{dk}\bigg|_{k=0} = \mu.$$
 (2.4.63)

By symmetry, the same results are obtained for  $G_{13} = G_{31} = \mu$ . Finally, it is seen from

(2.4.45) that 
$$G_{23} = G_{32} = \frac{dT_{23}}{dk}\Big|_{k=0} = \mu$$
.

Thus we have obtained the elastic constants corresponding to the linear elasticity for material (2.4.1) under the symmetry of transversely isotropy, and given by equations (2.4.58)-(2.4.63). It can be readily verified that relations (2.4.56) and (2.4.57) are satisfied. In comparison, since

$$\mu \ge 0$$
 and  $\beta \ge 0$ , (2.4.64)

it follows that

$$v_{13} = v_{12} \le v_{21} = v_{31} \le v_{32} = v_{23}$$
 (2.4.65)

and

$$E_{11} \ge E_{22} = E_{33} \ge G_{ij} = \mu,$$
 (i, j = 1, 2, 3, i \neq j). (2.4.66)

If  $\beta = 0$ , then the equality holds everywhere in equation (2.4.65) and in the first of (2.4.66). In this case the material defined in expression (2.4.1) reduces to the incompressible isotropic neo-Hookean material, and we have

$$E_{11} = E_{22} = 3\mu$$
,  $G_{12} = G_{21} = \mu$ ,  $V_{21} = V_{31} = V_{12} = V_{32} = \frac{1}{2}$ . (2.4.67)

In the extreme case that  $\mu = 0$ , material (2.4.1) has only stiffness in extension/contraction in the  $X_1$ -direction, and in such a case we have

$$E_{11} = 4\beta, E_{22} = 0, G_{12} = G_{21} = 0,$$
  
 $v_{21} = v_{31} = \frac{1}{2}, v_{12} = 0, v_{32} = 1.$  (2.4.68)

It should be noted in all cases that

$$v_{21} + v_{31} = 1$$
 and  $v_{12} + v_{32} = 1$ , (2.4.69)

which are required by incompressibility, and

$$E_{11}v_{12} = E_{22}v_{21}, \qquad (2.4.70)$$

which, again, is required by the symmetry of the elasticity tensor [Christensen 1979].

For the five independent elastic constants  $E_L \equiv E_{11}$ ,  $E_T \equiv E_{22}$ ,  $v_{LT} \equiv v_{21}$ ,  $v_{TT} \equiv v_{32}$  and  $G_{LT} \equiv G_{21}$ , four of them, namely  $E_L$ ,  $E_D$ ,  $G_{LT}$  and  $v_{LD}$ , are significant under the plane stress condition as regards the in-plane stress-strain relations. These four elastic constants,  $E_L$ ,  $E_D$ ,  $G_{LT}$  and  $v_{LD}$ , can be obtained from [Zweben et. al. 1989] for various fiber-reinforced composite materials as listed in Table 1. Here, the subscript L denotes the fiber direction and T denotes the transverse direction. For the elastic constants using L and T notation, we follow Zweben's convention in which the first subscript of v indicates the direction of loading, and the second subscript of v indicates the direction of lateral

contraction/extension. Although the strain density function of material (2.1.5) has only two parameters, it can still be used to approximate the elastic constants of these composite materials. Some results are listed in Table 1. We have obtained these results by using least square method to determine the values of the two parameters  $\mu$  and  $\beta$ , which make the elastic constants  $E_{L}$ ,  $E_{T}$  and  $G_{LT}$  derived the best fit to those of measured values of the various fiber-reinforced composite materials. Note that  $\nu_{LT}$  =  $\nu_{21}$  = 0.5 derived from (2.4.6) does not depend on  $\mu$  and  $\beta$ . In certain cases (e.g. boron/epoxy) the match is very good as regards  $E_{L}$ ,  $E_{T}$  and  $G_{LT}$ 

Composite Fiber/Matrix	Elastic Constants from [Zweben et. al. 1989]				Material Parameters in (2.1.5)		Derived Elastic Constants		
	E <sub>L</sub>	E <sub>T</sub>	G <sub>LT</sub>	$\nu_{ m LT}$	μ	β	E <sub>L</sub> '	E <sub>T</sub> '	G <sub>LT</sub> '
E Glass/ Epoxy	45.0	12.0	5.5	0.28	3.2	8.8	45.0	12.0	3.2
S Glass/ Epoxy	55.0	16.0	7.6	0.28	4.3	10.5	55.0	16.0	4.3
Kevlar 49 Aramid/ Epoxy	76.0	5.5	2.1	0.34	1.4	17.9	76.0	5.5	1.4
High-Strength Graphite/ Epoxy	145.0	10.0	4.8	0.25	2.5	34.3	145.0	10.0	2.5
High-Modulus Graphite/ Epoxy	220.0	6.9	4.8	0.25	1.7	53.7	220.0	6.9	1.7
Ultrahigh-Modulu s Graphite/ Epoxy	290.0	6.2	4.8	0.25	1.6	71.3	290.0	6.2	1.6
Boron/Epoxy	210.0	19.0	4.8	0.25	4.9	48.9	210.0	19.0	4.9
Alumina/ Epoxy	230.0	21.0	7.0	0.28	5.4	53.5	230.0	21.0	5.4

Table 1. Here  $E_L$ ,  $E_T$ ,  $G_{LT}$  and  $V_{LT}$  are obtained from Zweben et. al. (1989) with volume fraction of fiber = 0.6.  $E_L$ ',  $E_T$ ' and  $G_{LT}$ ' are given by equations (2.4.58), (2.4.60)-(2.4.63) for parameters  $\mu$  and  $\beta$  listed, which are determined by least square method to best fit to  $E_L$ ,  $E_T$  and  $G_{LT}$ . All the quantities except for  $V_{LT}$  have unit GPa.

#### 2.5. Material Properties (Two Balanced Fiber Families)

The material modeled by expression (2.1.10) is reinforced with two balanced families of fibers if M = 2 with  $\beta^{(1)} = \beta^{(2)}$ . Then, as discussed in section 2.1, it will, again, have three mutually orthogonal material principal directions and three mutually orthogonal planes of symmetry. This type of materials is classified as orthotropic material and is described by nine independent elastic constants in the scope of linear elasticity. This set of nine elastic constants can be chosen as  $E_{11}$ ,  $E_{22}$ ,  $E_{33}$ ,  $V_{12}$ ,  $V_{13}$ ,  $V_{23}$ ,  $G_{12}$ ,  $G_{13}$  and  $G_{23}$ .

Let us set up the rectangular Cartesian coordinate system in the way discussed in section 2.1 that the planes determined by the fibers from these two fiber families are normal to the  $X_2$ -direction and both the  $X_1$ -direction and the  $X_3$ -direction bisects the angle between fibers from these two families. Thus, the coordinates  $X_1$ ,  $X_2$  and  $X_3$  are in the three material principal directions, respectively. We thus have

$$\theta^{(1)} = -\theta^{(2)}$$
 and  $\beta^{(1)} = \beta^{(2)} = \beta$ , (2.5.1)

since the material considered here is reinforced with two balanced families of fibers. Now, the strain energy density function (2.1.10) becomes

$$W = \frac{\mu}{2}(I_1 - 3) + \frac{\beta}{2}(K^{(1)} - 1)^2 + \frac{\beta}{2}(K^{(2)} - 1)^2.$$
 (2.5.2)

The Cauchy stress tensor is given by

$$T_{ij} = \mu F_{ik} F_{jk} - p \delta_{ij} + 2\beta [(F_{rs} F_{rt} A_s^{(1)} A_t^{(1)} - 1) F_{ip} F_{jq} A_p^{(1)} A_q^{(1)} + (F_{rs} F_{rt} A_s^{(2)} A_t^{(2)} - 1) F_{ip} F_{jq} A_p^{(2)} A_q^{(2)}],$$
(2.5.3)

where

$$A^{(1)} = \{c, 0, -s\}^T$$
 and  $A^{(2)} = \{c, 0, s\}^T$ , (2.5.4)

and  $c = \cos\theta^{(1)}$  and  $s = \sin\theta^{(1)}$  (refer to Figure 1). With the coordinates so set, we shall call the reinforcement discussed here the reinforcement of two families of symmetrically balanced fibers.

For the triaxial deformation (2.3.3), together with (2.5.4), the potentially nonzero components of the Cauchy stress tensor, given by (2.5.3), are

$$T_{11} = \mu \lambda_1^2 - p + 4\beta (c^2 \lambda_1^2 + s^2 \lambda_3^2 - 1)c^2 \lambda_1^2,$$

$$T_{22} = \mu \lambda_1^2 - p,$$

$$T_{33} = \mu \lambda_3^2 - p + 4\beta (c^2 \lambda_1^2 + s^2 \lambda_3^2 - 1)c^2 \lambda_3^2.$$
(2.5.5)

By considering uniaxial loads in the  $X_1$ ,  $X_2$  and  $X_3$ -direction in turn, as given by (2.3.14), the equations (2.5.5) yield a set of three equations for  $\lambda_1$ ,  $\lambda_2$ ,  $\lambda_3$ , p and the uniaxial load. This set of equations, in connection with the incompressibility constraint (2.3.5), can be used to derive the corresponding elastic constants: Young's moduli and Poisson ratios, as proceeded in subsection 2.4.2 by considering the limit  $\lambda_1 \to \lambda_2 \to \lambda_3 \to 1$ . The results are written here

$$\begin{split} E_{11} &= \frac{3\mu^2 + 8\mu\beta c^4 + 8\mu\beta s^4 - 8\mu\beta c^2 s^2}{\mu + 2\beta s^4}, \\ E_{22} &= \frac{3\mu^2 + 8\mu\beta c^4 + 8\mu\beta s^4 - 8\mu\beta c^2 s^2}{\mu + 2\beta c^4 + 2\beta s^4 - 4\beta c^2 s^2}, \\ E_{33} &= \frac{3\mu^2 + 8\mu\beta c^4 + 8\mu\beta s^4 - 8\mu\beta c^2 s^2}{\mu + 2\beta c^4}, \\ v_{21} &= \frac{2\mu + 16\beta s^4 - 8\beta s^2}{4\mu + 8\beta s^4}, \\ v_{31} &= \frac{2\mu + 8\beta c^2 s^2}{4\mu + 8\beta s^4}, \\ v_{12} &= \frac{2\mu + 16\beta s^4 - 8\beta s^2}{4\mu + 16\beta c^4 + 16\beta s^4 - 8\beta}, \\ v_{32} &= \frac{2\mu + 16\beta c^4 - 8\beta c^2}{4\mu + 16\beta c^4 + 16\beta s^4 - 8\beta}, \\ v_{13} &= \frac{2\mu + 8\beta c^2 s^2}{4\mu + 8\beta c^4}, \\ v_{23} &= \frac{2\mu + 16\beta c^4 - 8\beta c^2}{4\mu + 8\beta c^4}. \end{split}$$

It is readily to verify that the following relations are satisfied,

$$E_{11}v_{12} = E_{22}v_{21},$$
  
 $E_{11}v_{13} = E_{33}v_{31},$  (2.5.7)  
 $E_{22}v_{23} = E_{33}v_{32},$ 

as required by the symmetry of the elasticity tensor.

If the material is subjected to a simple shear as described by (2.3.12), then the corresponding shear stress can be calculated from (2.5.3), and the corresponding shear moduli obtained, as proceeded in the limit  $k \to 0$ . The results are listed here

$$G_{12} = G_{21} = G_{23} = G_{32} = \mu,$$
  
 $G_{13} = G_{31} = \mu + 8\beta c^2 s^2.$  (2.5.8)

It can be seen that the shear moduli in the plane of fiber reinforcement are enhanced, if

 $\theta \neq 0$  and  $\theta \neq \pi/2$ . As one would expect, these  $\beta$ -dependent elastic constants in (2.5.6) and (2.5.8) reduce to those corresponding to transverse isotropy as discussed in subsection 2.4.2, if  $\theta^{(1)} = \theta^{(2)} = 0$  and  $\beta^{(1)} = \beta^{(2)} = \beta/2$ .

# 3. Ordinary Ellipticity in Planar Deformation

The ordinary ellipticity concerns the smoothness of the solution field. The loss of ordinary ellipticity corresponds to the possible appearance of discontinuity in the derivatives of the solution field. That is, if loss of ordinary ellipticity takes place, then, in the material body, there may exist certain surfaces across which the highest order directional derivative of the solution fields in the direction of the normal of these surfaces has finite jump. This kind of discontinuity is usually called weak discontinuity.

The analysis of ellipticity usually yields restrictions on deformation parameters, if loss of ellipticity is to be avoided. The deformation parameters are usually the principal stretches of the deformation gradient  $\lambda_1$ ,  $\lambda_2$  and  $\lambda_3$  or the left Cauchy-Green strain tensor  $C_{ij}$ . The restrictions are imposed on deformation parameters depending on material parameters, such as  $\mu$  and  $\beta$  in (2.4.1). It is convenient to choose principal stretches  $\lambda_1$ ,  $\lambda_2$  and  $\lambda_3$  as deformation parameters for isotropic materials, but not for anisotropic materials. The reason is that the principal directions of the deformation, i.e. the principal directions of the left Cauchy-Green strain tensor, will not coincide, in general, with the material symmetry axes, during deformation. For this reason and for the problem to be considered being more tractable, we shall choose the components of the left Cauchy-Green strain tensor as the deformation parameters.

In this chapter, we shall analyze the ordinary ellipticity of material (2.4.1) reinforced with one single family of fibers. We set, again, the rectangular Cartesian coordinate system as that set in section 2.4, with  $X_1$  in the fiber direction. In next two sections, we discuss, first the ordinary ellipticity condition given by [Zee and Sternberg 1983], and then the specification of this condition to planar deformation. The distinction

between local and global plane strain ellipticity is given. Basic results for both global and local plane strain ellipticity are presented in section 3.3 and 3.4. In section 3.5, we relate the global plane strain ellipticity condition to a root type problem for a polynomial of degree four. A parameter space representation for loss of global plane strain ellipticity is developed. This involves the clarification of the complex phenomena of loss of ellipticity. The orientation of discontinuity surface is also clarified, especially with respect to first loss of ellipticity. Then the loss of ellipticity is discussed in the context of the special deformations introduced in chapter 2.

### 3.1. The Ordinary Ellipticity Condition for Arbitrary Deformations

The necessary and sufficient condition for the ordinary ellipticity of the displacement field for an incompressible material was given by [Zee and Sternberg 1983]. Here, we outline their work in deriving this necessary and sufficient condition. The Piola-Kirchhoff stress tensor for incompressible hyperelastic materials is given by

$$S = \frac{\partial W}{\partial F} - pF^{-T}. \tag{3.1.1}$$

Denoting by  $\mathbf{u}$  the displacement field, and noting  $F_{ij} = \delta_{ij} + u_{i,j}$ , the equilibrium equation  $\text{div}\mathbf{S} = 0$  gives rise to the set of governing equations

$$c_{ijpq}u_{p,qj} - p_{,j}F_{ji}^{-1} = 0$$
  $det \mathbf{F} = 1$  (3.1.2)

for the displacement u and hydrostatic pressure p, where

$$c_{ijpq} = \frac{\partial^2}{\partial F_{ii} \partial F_{pq}} W(F)$$
 (3.1.3)

is the elasticity tensor. The result  $F_{ji,j}^{-1} = 0$  for volume preserving deformation has been

used in arriving at (3.1.2). Now consider a surface S lying within the reference configuration and described by

$$\mathbf{X} = \tilde{\mathbf{X}}(\zeta_1, \zeta_2), \tag{3.1.4}$$

where  $(\zeta_1, \zeta_2)$  is orthogonal curvilinear coordinate system on S. Further points near S in the reference configuration can be described in terms of a local orthogonal curvilinear coordinate system  $(\zeta_1, \zeta_2, \zeta_3)$ , such that

$$\mathbf{X} = \mathbf{X}(\zeta_1, \zeta_2, \zeta_3) = \tilde{\mathbf{X}}(\zeta_1, \zeta_2) + \zeta_3 \mathbf{n}(\zeta_1, \zeta_2), \tag{3.1.5}$$

in which **n** is the unit normal vector of S. Thus, fields **u** and p on and near S can be expressed in terms of  $(\zeta_1, \zeta_2, \zeta_3)$ . By the definition of ordinary ellipticity, the possible jumps in the derivatives of these fields across S are

$$[[u_{p,qj}]] = \left[\left[\frac{\partial^2 u_p}{\partial \zeta_3^2}\right]\right] \zeta_{3,q} \zeta_{3,j}, \qquad [[p_j]] = \left[\left[\frac{\partial p}{\partial \zeta_3}\right]\right] \zeta_{3,j}. \qquad (3.1.6)$$

Here [[h]] denotes the jump of a function h across S. Now, the governing equation (3.1.2) yield, on S,

$$c_{ijpq} \left[ \left[ \frac{\partial^{2} u_{p}}{\partial \zeta_{3}^{2}} \right] \right] \zeta_{3, q} \zeta_{3, j} - F_{ji}^{-1} \left[ \left[ \frac{\partial p}{\partial \zeta_{3}} \right] \right] \zeta_{3, j} = 0,$$

$$F_{qp}^{-1} \left[ \left[ \frac{\partial^{2} u_{p}}{\partial \zeta_{3}^{2}} \right] \right] \zeta_{3, q} \zeta_{3, j} = 0.$$
(3.1.7)

Note that  $\nabla \zeta_3 / |\nabla \zeta_3|$  on S coincides with the unit normal **n** of S. Defining

$$\mathbf{v} = \left[ \left[ \frac{\partial^2 \mathbf{u}}{\partial \zeta_3^2} \right] \right], \qquad \mathbf{q} = \left| \nabla \eta_3 \right|^{-1} \left[ \left[ \frac{\partial \mathbf{p}}{\partial \zeta_3} \right] \right], \tag{3.1.8}$$

equation (3.1.7) is now written as

$$\mathbf{Q}\mathbf{v} - \mathbf{q}\mathbf{F}^{-T}\mathbf{n} = \mathbf{0}, \qquad \mathbf{v} \cdot (\mathbf{F}^{-T}\mathbf{n}) = 0, \tag{3.1.9}$$

on S. Here

$$Q_{ip} = c_{ijpq} n_j n_q$$
,  $Q_{ip} = Q_{pi}$ , (3.1.10)

is the acoustic tensor. Equation (3.1.9) constitutes four linear homogeneous algebraic equations in the jumps v and q, which do not have nontrivial solution if and only if

$$\det\begin{bmatrix} \mathbf{Q} & -\mathbf{F}^{-1}\mathbf{n} \\ \mathbf{n}^{\mathsf{T}}\mathbf{F}^{-1} & 0 \end{bmatrix} \neq 0, \qquad \forall \ \mathbf{n} \in \mathcal{U}^{3}, \tag{3.1.11}$$

where  $\mathcal{U}^3 = \{\mathbf{n} \mid \mathbf{n}_m \mathbf{n}_m = 1, m = 1, 2, 3\}$ . In other words, if condition (3.1.11) is satisfied, there can exist only zero jumps  $\mathbf{v}$  and  $\mathbf{q}$ . Therefore, (3.1.11) is the necessary and sufficient condition for the ordinary ellipticity.

It is to be noted that the problem here is formulated in the reference configuration, so that the normal  $\mathbf{n}$  determines a surface of weak discontinuity in the reference configuration and  $\mathbf{Fn/|Fn|}$  determines the counterpart of the surface of weak discontinuity in the deformed configuration. If (3.1.11) is not true at some point  $\mathbf{P}$ , so that the inequality is replaced by equality for some  $\mathbf{n}$ , say  $\mathbf{n}^*$ , then a surface through  $\mathbf{P}$  with normal  $\mathbf{n}^*$  in the reference configuration is capable of supporting a weak discontinuity in the displacement field. Specifically, recalling that  $|\zeta_3|$  denotes perpendicular distance in the direction of  $\mathbf{n}^*$ , then  $\frac{\partial^2 \mathbf{u}_i}{\partial \zeta_3^2}$  and  $\frac{\partial \mathbf{p}}{\partial \zeta_3}$  may suffer finite discontinuities at  $\mathbf{P}$ . The associated discontinuity values in the vector  $[\mathbf{v}, \mathbf{q}]^T$  are given by nontrivial solutions to

$$\begin{bmatrix} \mathbf{Q}(\mathbf{n}^*) & -\mathbf{F}^{-1}\mathbf{n}^* \\ \mathbf{n}^{*T}\mathbf{F}^{-1} & 0 \end{bmatrix} \begin{bmatrix} \mathbf{v} \\ \mathbf{q} \end{bmatrix} = \mathbf{0}.$$
 (3.1.12)

Since

$$\begin{bmatrix} \mathbf{Q} & -\mathbf{F}^{-T}\mathbf{n} \\ \mathbf{n}^{T}\mathbf{F}^{-1} & 0 \end{bmatrix} = \begin{bmatrix} \mathbf{F}^{-T} & \mathbf{0} \\ \mathbf{0}^{T} & 1 \end{bmatrix} \begin{bmatrix} \mathbf{F}^{T}\mathbf{Q}\mathbf{F} & -\mathbf{n} \\ \mathbf{n}^{T} & 0 \end{bmatrix} \begin{bmatrix} \mathbf{F}^{-1} & \mathbf{0} \\ \mathbf{0}^{T} & 1 \end{bmatrix}, \tag{3.1.13}$$

we now have the relation

$$\det\begin{bmatrix} \mathbf{Q} & -\mathbf{F}^{-T}\mathbf{n} \\ \mathbf{n}^{T}\mathbf{F}^{-1} & 0 \end{bmatrix} = (\det \mathbf{F}^{-1})^{2} \det\begin{bmatrix} \mathbf{F}^{T}\mathbf{Q}\mathbf{F} & -\mathbf{n} \\ \mathbf{n}^{T} & 0 \end{bmatrix}. \tag{3.1.14}$$

Thus the necessary and sufficient condition for ordinary ellipticity can equivalently be expressed as

$$\det\begin{bmatrix} \mathbf{H} & -\mathbf{n} \\ \mathbf{n}^{\mathrm{T}} & \mathbf{0} \end{bmatrix} \neq 0 , \qquad \forall \mathbf{n} \in \mathcal{U}, \tag{3.1.15}$$

where

$$\mathbf{H} = \mathbf{F}^{\mathsf{T}}\mathbf{Q}\mathbf{F} , \qquad \mathbf{H}^{\mathsf{T}} = \mathbf{H} \tag{3.1.16}$$

is a  $3 \times 3$  symmetric matrix. With the coordinate system set-forth, it follows from (2.4.1) and (3.1.3) that the elements of c are given by

$$c_{iing} = \mu \delta_{in} \delta_{ig} + 2\beta \{ 2F_{i1}F_{n1} + (F_{s1}F_{s1} - 1)\delta_{in} \} \delta_{i1} \delta_{g1}, \qquad (3.1.17)$$

so that (3.1.10) and (3.1.16) then give

$$H_{pq} = \mu C_{pq} + 2\beta (C_{11} - 1)n_1^2 C_{pq} + 4\beta n_1^2 C_{p1} C_{1q}.$$
 (3.1.18)

For a given deformation, and hence given C, and given material parameters  $\mu$  and  $\beta$ ,

condition (3.1.15) with (3.1.18) suffices to determine whether or not surfaces of weak discontinuity may exist in the three-dimensional displacement field.

# 3.2. Specialization of the Ordinary Ellipticity Condition to

#### **Planar Deformation**

We henceforth restrict attention to deformations occurring in the  $(X_1, X_2)$ -plane either locally or globally. In turn, we restrict attention to possible surfaces of weak discontinuity with unit normals that have no component in the  $X_3$ -direction at a material point under consideration, so that the tangential planes of the surfaces of weak discontinuity at the material point are perpendicular to the  $(X_1, X_2)$ -plane.

Now, the elements of **H** can be calculated, for the plane deformation described by (2.3.7), as

$$\begin{split} H_{11} &= \mu C_{11} + 2\beta (3C_{11}^2 - C_{11})n_1^2 ,\\ H_{12} &= H_{21} = \mu C_{12} + 2\beta (3C_{11}C_{12} - C_{12})n_1^2 ,\\ H_{22} &= \mu C_{22} + 2\beta (C_{11}C_{22} - C_{22} + 2C_{12}^2)n_1^2 ,\\ H_{33} &= \mu + 2\beta (C_{11} - 1)n_1^2\\ H_{13} &= H_{31} = H_{23} = H_{32} = 0 . \end{split} \tag{3.2.1}$$

The restriction on possible surfaces of weak discontinuity,  $n_3 = 0$ , when combined with (3.1.15) and (3.2.1) gives

$$H_{33}(H_{11}n_2^2 + H_{22}n_1^2 - 2H_{12}n_1n_2) \neq 0$$
,  $\forall \mathbf{n} \in \mathcal{U}^2$ . (3.2.2)

Here,  $U^2 = \{ \mathbf{n} \mid n_{\alpha}n_{\alpha} = 1, \alpha = 1, 2, n_3 = 0 \}$ . The satisfaction of (3.2.2) is then the simultaneous satisfaction of both of the following two conditions

$$H_{33} \neq 0$$
,  $\forall \mathbf{n} \in \mathcal{U}^2$ , (3.2.3)

and

$$H_{11}n_2^2 + H_{22}n_1^2 - 2H_{12}n_1n_2 \neq 0$$
,  $\forall \mathbf{n} \in \mathcal{U}^2$ . (3.2.4)

Note that conditions (3.2.3) and (3.2.4) are derived from condition (3.1.11) for general 3-dimensional incompressible materials. Following a standard classification [Knowles and Sternberg 1975], a local plane strain state involves a displacement field that has no components in the  $X_3$ -direction at the material point under consideration, and the global plane strain state is a deformation in which the displacement components in  $X_3$ -direction vanish identically. Thus, the normal of the surface of weak discontinuity for local plane strain happens to be in the  $(X_1, X_2)$ -plane, and the surface of weak discontinuity for global plane strain is a cylindrical surface with generators parallel to the  $X_3$ -axis. Conditions (3.2.3) and (3.2.4) must be satisfied simultaneously for ellipticity in local plane strain deformation. For ellipticity of materials under global plane strain deformation the only condition required is (3.2.4). Actually, condition (3.2.4), which can be obtained here by eliminating the third row and the third column in the left hand side of condition (3.1.11), corresponds to the counterpart of condition (3.1.11) in the global plane strain deformation analysis given in [Abeyaratne 1980].

The ellipticity problem is now in terms of the deformation parameters  $C_{11}$ ,  $C_{12}$  and  $C_{22}$ , and the material parameters  $\mu$  and  $\beta$ , in seeking nonzero unit normal  $\mathbf{n} = [n_1, n_2, 0]$  to the surface of weak discontinuity. These five parameters are not independent. By making use of the stiffness ratio  $\gamma$  defined in (2.4.5) and the incompressibility constraint (2.3.9), the number of parameters is reduced to three, namely,  $C_{11}$ ,  $C_{12}$  and  $\gamma$ . Their respective domains are given by

$$C_{11} > 0, \quad -\infty < C_{12} < \infty, \quad \gamma \ge 0.$$
 (3.2.5)

Note, by replacing every appearance of  $C_{22}$  with  $(1 + C_{12}^2)/C_{11}$ , that  $C_{22}$  has been completely eliminated by using the incompressibility constraint (2.3.9). Hence, the restriction imposed by (2.3.9) on the remaining deformation parameters  $C_{11}$  and  $C_{12}$  has been released. Triplets ( $C_{11}$ ,  $C_{12}$ ,  $\gamma$ ) obeying (3.2.5) that satisfy (3.2.4) will be said to constitute the *global plane strain ellipticity set* (GPSE). Triplets ( $C_{11}$ ,  $C_{12}$ ,  $\gamma$ ) obeying (3.2.5) that satisfy both (3.2.4) and (3.2.3) will be said to constitute the *local plane strain ellipticity set* (LPSE). Thus, membership in LPSE implies membership in GPSE, but not vice versa.

It is to be noted for any pair  $(C_{11}, C_{12})$  obeying  $(3.2.5)_{1,2}$  that there exists an infinite number of associated plane strain homogeneous deformations. The infinite set of deformation gradients F can be parametrized by its  $F_{21}$  component on the range  $-\sqrt{C_{11}} \le F_{21} \le \sqrt{C_{11}}$  via

$$\begin{split} F_{13} &= F_{31} = F_{23} = F_{32} = 0, \\ F_{33} &= 1, \\ F_{11} &= \pm \sqrt{C_{11} - F_{21}^2} \;, \qquad \text{(either sign)}, \\ F_{12} &= (F_{11}C_{12} - F_{21})/(F_{11}^2 + F_{21}^2) = (-F_{21} \pm C_{12}\sqrt{C_{11} - F_{21}^2})/C_{11} \;, \\ F_{22} &= (1 + F_{12}F_{21})/F_{11} = (\pm (C_{11} - F_{21}^2) + C_{12}F_{21}\sqrt{C_{11} - F_{21}^2})/(C_{11}\sqrt{C_{11} - F_{21}^2}). \end{split}$$

In particular, choosing  $F_{21} = 0$  gives

$$\mathbf{F} = \begin{bmatrix} \pm \sqrt{C_{11}} & \pm C_{12} / \sqrt{C_{11}} & 0 \\ 0 & \pm 1 / \sqrt{C_{11}} & 0 \\ 0 & 0 & 1 \end{bmatrix}.$$
 (3.2.7)

The homogeneous deformation associated with the positive signed deformation gradient in (3.2.7) can be obtained as a sequence of two homogeneous deformations. First an axial expansion/contraction in the fiber direction with stretch  $\sqrt{C_{11}}$  accompanied by a volume preserving in-plane stretch  $1/(\sqrt{C_{11}})$ . This is followed by an in-plane simple shear of amount  $C_{12}$  in the fiber direction.

For  $-\sqrt{C_{11}} < F_{21} < \sqrt{C_{11}}$  the positive and negative roots in (3.2.6) represent two distinct branches of deformation gradients associated with the given C. These branches join together at both  $F_{21} = -\sqrt{C_{11}}$  and  $F_{21} = \sqrt{C_{11}}$ , where

$$\mathbf{F} = \begin{bmatrix} 0 & 1/\sqrt{C_{11}} & 0 \\ -\sqrt{C_{11}} & -C_{12}/\sqrt{C_{11}} & 0 \\ 0 & 0 & 1 \end{bmatrix}, \qquad \mathbf{F} = \begin{bmatrix} 0 & -1/\sqrt{C_{11}} & 0 \\ \sqrt{C_{11}} & C_{12}/\sqrt{C_{11}} & 0 \\ 0 & 0 & 1 \end{bmatrix}, \tag{3.2.8}$$

respectively. This forms a "loop" of deformation gradients associated with the given C. Any F on this loop will generate the full loop upon being post multiplied by the full range of an in-plane rigid body rotations, i.e. rotations about the  $X_3$ -axis. In particular, the member of this loop given by the positive roots in (3.2.6) for

$$F_{21} = \sqrt{\frac{C_{11}C_{12}^2}{(1 + C_{11})^2 + C_{12}^2}}$$
 (3.2.9)

gives the special symmetric, positive definite deformation gradient

$$\mathbf{U} = \begin{bmatrix} \frac{\sqrt{C_{11}}(1 + C_{11})}{\sqrt{(1 + C_{11})^2 + C_{12}^2}} & \frac{\sqrt{C_{11}}C_{12}}{\sqrt{(1 + C_{11})^2 + C_{12}^2}} & 0\\ \frac{\sqrt{C_{11}}C_{12}}{\sqrt{(1 + C_{11})^2 + C_{12}^2}} & \frac{1 + C_{11} + C_{12}^2}{\sqrt{C_{11}}\sqrt{(1 + C_{11})^2 + C_{12}^2}} & 0\\ 0 & 0 & 1 \end{bmatrix},$$
(3.2.10)

corresponding to the pure deformation U in the polar decomposition F = RU of any other member of this loop.

Since it can be noted from (3.2.1) that the ellipticity is affected by deformation only through the right Cauchy-Green strain tensor C, it will not be influenced by the rigid body rotation R. Actually, in view of (2.3.2), the mechanical effect of a deformation described by C to a material body is equivalent to the mechanical effect of the pure deformation given by U. The post rotation R is then viewed as post determined by requiring compatibility with the actual deformation field. One need not, however, consider this post rotation **R** to extract the pointwise material properties. That is, the post rotation **R** can be set to the identity for the consideration of mechanical response. So, the "putative normal" is Un/Un that determines the possible surface of weak discontinuity and is produced by the pure deformation part U of the overall deformation F as determined from the polar decomposition  $\mathbf{F} = \mathbf{R}\mathbf{U}$ . The "actual normal"  $\mathbf{F}\mathbf{n}/|\mathbf{F}\mathbf{n}|$  in the actual deformation field satisfying the compatibility condition will, in general, be rotated rigidly with the purely deformed material body, but we will not consider the rigid body rotation here. Similarly, regardless of the post rotation **R**, the deformed fiber putative direction given by (2.1.9) is now rewritten as  $UA/\sqrt{K}$ . Unless stated otherwise, all subsequent development will be with respect to quantities associated with the pure deformation part U of the overall deformation. For the plane deformation in the  $(X_1, X_2)$ -plane and the original fiber direction given by (2.4.3), we denote the angle from the  $X_1$ -axis to the deformed fiber direction by  $\phi$ , which is measured by a right hand rotation about the  $X_3$ -axis. In view of the above discussion, it is taken as

$$tan\phi = \frac{(\mathbf{UA})_2}{(\mathbf{UA})_1} = \frac{C_{12}}{1 + C_{11}}.$$
 (3.2.11)

### 3.3. Loss of Ellipticity in Local Plane Strain

A sufficient condition for loss of ellipticity in local plane strain is for the existence of  $\mathbf{n} \in \mathcal{U}^2$  such that  $H_{33} = 0$ . Now from  $(3.2.1)_4$ , it follows that  $H_{33} = 0$  if and only if  $n_1^2 = (2\gamma(1-C_{11}))^{-1}$ . Since  $0 \le n_1^2 \le 1$  it follows that the sufficient condition  $H_{33} = 0$  for loss of ellipticity in local plane strain is met if and only if

$$0 \le \frac{1}{2\gamma(1 - C_{11})} \le 1, \tag{3.3.1}$$

which, since  $1 - 1/2\gamma < 1$ , is equivalent to

$$C_{11} \le 1 - \frac{1}{2\gamma}. \tag{3.3.2}$$

In view of  $(3.2.5)_1$  this condition cannot be met if  $\gamma \le 1/2$ , which includes the neo-Hookean case  $\gamma = 0$ . For  $C_{11}$  obeying (3.3.2), it is sufficient to find an  $\mathbf{n} \in \mathcal{U}^2$  that violates (3.2.3). On the other hand, the satisfaction of the opposite inequality

$$C_{11} > 1 - \frac{1}{2\gamma} \tag{3.3.3}$$

is equivalent to the satisfaction of (3.2.3). Thus, (3.3.3) is necessary for ellipticity in local plane strain, however, sufficiency requires the satisfaction of both (3.2.4) and (3.3.3). Since (3.2.4) alone characterizes the ellipticity in global plane strain, it follows that triplets ( $C_{11}$ ,  $C_{12}$ ,  $\gamma$ ) in GPSE are also in LPSE if and only if  $C_{11}$  obey (3.3.3). In particular, triplets ( $C_{11}$ ,  $C_{12}$ ,  $\gamma$ ) obeying

$$C_{11} = 1 - \frac{1}{2\gamma} \tag{3.3.4}$$

constitute a cylindrical surface in the  $(C_{11}, C_{12}, \gamma)$ -space involving transitions from local plane strain ellipticity to the loss of this same property.

As an illustration of loss of ellipticity in local plane strain, consider the biaxial deformation (2.3.10) for which

$$\mathbf{C} = \begin{bmatrix} \lambda_1^2 & 0 & 0 \\ 0 & \lambda_1^{-2} & 0 \\ 0 & 0 & 1 \end{bmatrix}, \qquad \mathbf{T} = \mu \begin{bmatrix} (\lambda_1^2 - \lambda_1^{-2}) + 2\gamma(\lambda_1^2 - 1)\lambda_1^2 & 0 & 0 \\ 0 & 0 & 0 & 0 \\ 0 & 0 & 0 & (1 - \lambda_1^{-2}) \end{bmatrix}, \quad (3.3.5)$$

where the hydrostatic pressure p has been chosen so that  $T_{22}=0$ . Then, as  $\lambda_1$  is decreased from the undeformed value  $\lambda_1=1$ , the loss of ellipticity sufficiency condition (3.3.2) is never met if  $\gamma \leq 1/2$ , that is, if the additional stiffening due to the fibers is sufficiently weak. On the other hand, if  $\gamma > 1/2$ , that is, if the fibers are sufficiently stiff, then loss of ellipticity is ensured under decreasing  $\lambda_1$  starting with  $\lambda_1=\sqrt{1-1/2\gamma}$ . At this value of  $\lambda_1$  a surface of weak discontinuity with normal direction  $\mathbf{n}=[1,0,0]$  in the reference configuration can be sustained. Note that this corresponds to the surface with normal in the fiber direction. Under continued decrease of  $\lambda_1$  this potential surface of weak discontinuity rotates away from this initially perpendicular fiber intersection and such a rotation can occur either clockwise or counterclockwise. In particular, as  $\lambda_1 \to 0$ , the normal to the potential surface of weak discontinuity tends to the value  $\mathbf{n}=[1/2\gamma,\pm\sqrt{1-1/4\gamma^2},0]$ .

## 3.4. Basic Results for both Global and Local Plane Strain Ellipticity

The loss of ellipticity results obtained in the previous section were based solely on

the consideration of (3.2.3). The associated analysis was elementary. Now we turn to the consideration of (3.2.4) which, we recall, is the sole defining requirement for global plane strain ellipticity. In contrast to the analysis of (3.2.3), the analysis of (3.2.4) presents some challenge.

Condition (3.2.4) can be expressed as

$$\left[ n_1 \ n_2 \right] \left\{ (1 - 2n_1^2 \gamma) \mathbf{D} + 2n_1^2 \gamma \mathbf{E} \right\} \begin{bmatrix} n_1 \\ n_2 \end{bmatrix} \neq 0 , \qquad \forall \mathbf{n} \in \mathcal{U}^2,$$
 (3.4.1)

where we have introduced

$$\mathbf{D} = \begin{bmatrix} \frac{1 + C_{12}^2}{C_{11}} & -C_{12} \\ -C_{12} & C_{11} \end{bmatrix}, \qquad \mathbf{E} = \begin{bmatrix} 1 + 3C_{12}^2 & -3C_{11}C_{12} \\ -3C_{11}C_{12} & 3C_{11}^2 \end{bmatrix}.$$
(3.4.2)

We now examine the properties of matrices **D**, **E** and (**E-D**). It is verified directly from (3.4.2) using  $C_{11}>0$  and  $\det \mathbf{D}=1$ , that matrix **D** is positive-definite. In addition since  $E_{11}=1+3C_{12}^2>0$  and  $\det \mathbf{E}=3C_{11}^2>0$ , matrix **E** is also positive-definite. It can also be obtained from (3.4.2) that matrix (**E-D**) is positive-definite if and only if  $C_{11}>1$ . This is because  $(\mathbf{E-D})_{22}=C_{11}(3C_{11}-1)$  and  $\det(\mathbf{E-D})=(3C_{11}-1)(C_{11}-1)$ . If  $C_{11}=1$ , then (**E-D**) is positive-semidefinite.

According to the above discussion and following from the sufficiency conditions (3.3.3) and (3.4.1) for local plane strain ellipticity, we arrive at the following conclusions:

(EI) If  $C_{11} \ge 1$ , then local plane strain ellipticity is guaranteed. Here condition (3.4.1) is satisfied since **D** is positive-definite and (**E-D**) is positive-semidefinite. Condition (3.3.3) is also trivially satisfied. Hence, it is made clear that material (2.4.1) is

elliptic for planar deformations when fibers are in extension, so that loss of ellipticity can only take place when fibers are compressed.

(EII) If  $\gamma = 0$  ( $\beta = 0$ , the neo-Hookean material), local plane strain ellipticity is guaranteed. Here condition (3.4.1) is satisfied and, further, condition (3.3.3) is trivially satisfied. This result can be extended to materials obeying  $\gamma \le 1/2$ . Since E is positive-definite, (3.4.1) gives that loss of global plane strain ellipticity is possible only if  $1-2n_1^2\gamma < 0$ . This guarantees global plane strain ellipticity for  $\gamma < 1/2$ . Furthermore, when  $\gamma = 1/2$ , the first term in the left hand side of (3.4.1) may have its minimum value (zero) only if  $n_1^2 = 1$ , but now the second term in the left hand side of (3.4.1) is strictly greater than zero. Thus, global plane strain ellipticity is assured for materials obeying  $\gamma \le 1/2$ . Note, simultaneously, condition (3.3.3) is again trivially satisfied for  $\gamma \le 1/2$ . We can thus conclude that materials obeying  $\gamma \le 1/2$  guarantee local plane strain ellipticity.

(EIII) For all those unit normals  $\mathbf{n} \in \mathcal{U}^2$  with  $\mathbf{n}_1 = 0$ , both condition (3.2.3) with (3.2.1)<sub>4</sub> and condition (3.4.1) are satisfied. Thus, any possible unit normal describing a surface of weak discontinuity must have nonzero component  $\mathbf{n}_1$ .

## 3.5. An Alternative Form of the Global Plane Strain Ellipticity Condition

We now turn to examine condition (3.2.4) in more detail. This corresponds to the global plane strain deformation problem. Since that  $\mathbf{n} = [n_1, n_2, 0]^T$  is the unit normal of the surface of weak discontinuity of the displacement field taking place in the  $(X_1, X_2)$ -plane, this suggests the substitution  $n_1 = \cos\alpha$  and  $n_2 = \sin\alpha$ . In seeking the existence of this unit normal, and equivalently the existence of the surface of weak discontinuity,  $\mathbf{n}$  and  $-\mathbf{n}$  play the same role. Thus, noting (EIII), we restrict that  $-\pi/2 < \alpha < \pi/2$ . Here,  $\alpha$  is the angle

in the  $(X_1, X_2)$ -plane measured from the  $X_1$ -axis to  $\mathbf{n}$ . It is positive if it is a right hand rotation about the  $X_3$ -axis, and vice versa. By further making the substitution  $\mathbf{x} = \tan \alpha$ ,  $-\infty < \mathbf{x} < \infty$ , and expanding the left hand side of condition (3.2.4), using  $\mathbf{n}_1^2 = \frac{1}{1+\mathbf{x}^2}$ ,  $\mathbf{n}_2^2 = \frac{\mathbf{x}^2}{1+\mathbf{x}^2}$  and  $\mathbf{n}_1\mathbf{n}_2 = \frac{\mathbf{x}}{1+\mathbf{x}^2}$ , one obtains the following polynomial of  $\mathbf{x}$ ,  $\mathbf{P}(\mathbf{x}, \mathbf{C}_{11}, \mathbf{C}_{12}, \gamma)$ , of degree four:

$$P(x, C_{11}, C_{12}, \gamma) = \{x^2 + 2\gamma(3C_{11} - 1) + 1\}\{(C_{11}x - C_{12})^2 + 1\} - 4\gamma C_{11}.$$
 (3.5.1)

The polynomial  $P(x, C_{11}, C_{12}, \gamma)$  expressed in the form of a sum of powers of x is

$$P(x, C_{11}, C_{12}, \gamma) \equiv C_{11}^{2}(x^{4} + a_{1}x^{3} + a_{2}x^{2} + a_{3}x + a_{4}), \qquad (3.5.2)$$

where

$$a_{1} \equiv a_{1}(C_{11}, C_{12}) = -\frac{2C_{12}}{C_{11}},$$

$$a_{2} \equiv a_{2}(C_{11}, C_{12}, \gamma) = 2\gamma(3C_{11} - 1) + 1 + \frac{1 + C_{12}^{2}}{C_{11}^{2}},$$

$$a_{3} \equiv a_{3}(C_{11}, C_{12}, \gamma) = -\frac{4\gamma C_{12}(3C_{11} - 1) + 2C_{12}}{C_{11}},$$

$$a_{4} \equiv a_{4}(C_{11}, C_{12}, \gamma) = \frac{C_{12}^{2}\{2\gamma(3C_{11} - 1) + 1\} + 2\gamma(C_{11} - 1) + 1}{C_{11}^{2}}.$$
(3.5.3)

The condition (3.2.4) for global plane strain ellipticity is now equivalent to the requirement that the polynomial  $P(x, C_{11}, C_{12}, \gamma)$  has no real roots. That is, if for a given triplet  $(C_{11}, C_{12}, \gamma)$ , there exists no real x such that

$$P(x, C_{11}, C_{12}, \gamma) = 0, (3.5.4)$$

then the triplet is a member of the global plane strain ellipticity (GPSE) set.

It is evident from (3.5.1) that, if x is a root of equation (3.5.4) at  $(C_{11}, C_{12}, \gamma)$ , then

-x is a root of equation (3.5.4) at  $(C_{11}, -C_{12}, \gamma)$ , and vice versa. Further, the unit normal determined by -x is the reflection about the  $(X_1, X_3)$ -plane of the normal determined by x. The deformation described by  $(C_{11}, -C_{12})$  is a similar reflection to that described by  $(C_{11}, -C_{12})$ . One may, thus, restrict the discussion to the case  $C_{12} \ge 0$ .

#### 3.6. Loss of Ellipticity in Global Plane Strain

We begin analysis on (3.5.1) by giving an example of triplets  $(C_{11}, C_{12}, \gamma)$  that are associated with loss of global plane strain ellipticity. We consider here the triplets  $(C_{11}, C_{12}, \gamma)$  which support the existence of surfaces of weak discontinuity that are normal to the  $X_1$ -axis (x = 0). That is, the normal of the surface of weak discontinuity is in the fiber direction. Let x = 0 in (3.5.1), equation (3.5.4) becomes  $P(0, C_{11}, C_{12}, \gamma) = 0$ , and yields

$$C_{11} = \frac{(2\gamma - 1)(C_{12}^2 + 1)}{2\gamma(3C_{12}^2 + 1)} \equiv \tilde{C}_{11}(C_{12}, \gamma). \tag{3.6.1}$$

Equation (3.6.1) defines a surface in the  $(C_{11}, C_{12}, \gamma)$  parameter space as shown in Figure 23. In view of (3.2.5)<sub>1</sub> and the restriction  $C_{12} \ge 0$ , it is seen that this surface is associated with pairs  $(C_{12}, \gamma) \in \Sigma$ , where

$$\Sigma = \{ (C_{12}, \gamma) | C_{12} \ge 0, \gamma > 1/2 \}.$$
 (3.6.2)

For every triplet  $(\tilde{C}_{11}, C_{12}, \gamma)$  on this surface, the polynomial  $P(x, \tilde{C}_{11}, C_{12}, \gamma)$  has, at least, two real roots, one of which is x = 0. In addition to the root x = 0, the other root is, in general, nonzero and corresponds to a second possible surface of weak discontinuity whose normal is rotated away from the  $X_1$ -axis by an angle  $\tilde{\alpha}$ . The contours of this angle  $\tilde{\alpha}$  for triplet  $(\tilde{C}_{11}, C_{12}, \gamma)$  obeying (3.6.1) is plotted in Figure 24. These angles are found by substituting from (3.6.1) into (3.5.1) and determining the other real root x of the

resulting polynomial. The angle  $\alpha$  is then given by  $\alpha = \tan^{-1}x$ . This other real root is seen to coincide with x = 0, indicating a double root, on the boundary of  $\Sigma$ , that is on

$$\partial \Sigma = \{ (C_{12}, \gamma) | \text{ either } C_{12} = 0, \text{ or } \gamma = 1/2 \}.$$
 (3.6.3)

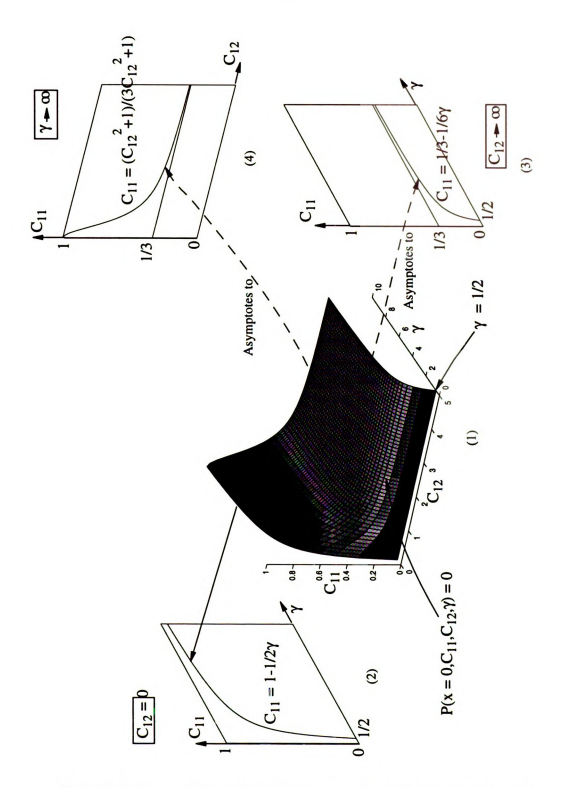


Figure 23. Surface consisting of triplets  $(C_{11}, C_{12}, \gamma)$  obeying (3.6.1). The asymptotes of this surface are also shown. Points associated with this surface are not members of GPSE and can support weak discontinuities with normals in the fiber-direction.

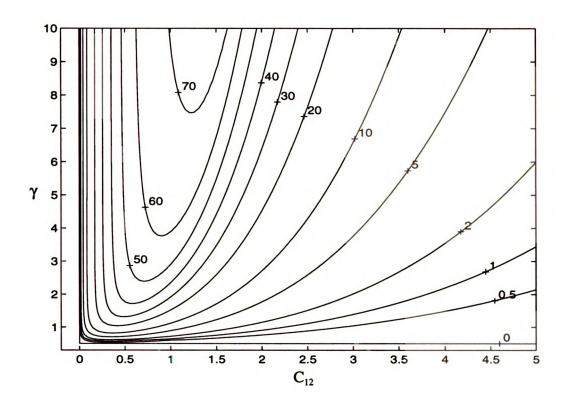


Figure 24. These contours give the angle  $\tilde{\alpha}$ , in degrees, for the direction of the normal to the second possible surface of weak discontinuity for triplets  $(\tilde{C}_{11}, C_{12}, \gamma)$  obeying (3.6.1).

According to (EI), plane strain ellipticity is guaranteed for  $C_{11} \ge 1$ ; on the other hand, for  $C_{11}$  given by (3.6.1), loss of plane strain ellipticity takes place. Consequently, it follows for each  $(C_{12}, \gamma) \in \Sigma$  that there exists at least one value  $\hat{C}_{11}$  obeying  $\tilde{C}_{11} \le \hat{C}_{11} \le 1$  associated with the transition from ellipticity to non-ellipticity. Defined at  $(C_{12}, \gamma) \in \Sigma$ , these  $\hat{C}_{11}$ 's associated with the transition between ellipticity and non-ellipticity furnish the global plane strain ellipticity boundary  $\mathfrak{B}$ :  $\hat{C}_{11} = \hat{C}_{11}(C_{12}, \gamma)$ . We shall find that there exist more than one such  $\hat{C}_{11}$  for certain  $(C_{12}, \gamma) \in \Sigma$  so that  $\hat{C}_{11} = \hat{C}_{11}(C_{12}, \gamma)$  may be multiple-valued. In general  $\mathfrak{B}$  is a two-dimensional manifold in the  $(C_{11}, C_{12}, \gamma)$  space.

Since P(x, C<sub>11</sub>, C<sub>12</sub>,  $\gamma$ ) is a polynomial in x of degree four, it has two pair of

complex conjugate roots for triplets  $(C_{11}, C_{12}, \gamma)$  in the ellipticity region. The transition from ellipticity to non-ellipticity then corresponds to the first transition of a pair of complex conjugate roots of P(x,  $C_{11}$ ,  $C_{12}$ ,  $\gamma$ ) to a pair of real roots. It is convenient to investigate this root type transition phenomenon in a "well-drilling" fashion. That is, for fixed  $(C_{12}, \gamma) \in \Sigma$ ,  $C_{11}$  is decreased from  $C_{11} = 1$  to  $C_{11}$  near zero. In the well-drilling process, a complex-real transition occurs if a pair of complex conjugate roots of P(x, C<sub>11</sub>,  $C_{12}$ ,  $\gamma$ ) changes to a pair of real roots. Accordingly, a real-complex transition occurs if a pair of real roots changes to a pair of complex roots. The C11 values at which a complex-real transition takes place will be denoted by  $\overline{C}_{11}$ , and the  $C_{11}$  values at which a real-complex transition takes place will be denoted by  $C_{11}$ . It will be shown that more than one complex-real transition and more than one real-complex transition may take place in a single well-drilling, depending on the value of  $(C_{12}, \gamma)$ . Thus, the manifold in the  $(C_{11}, C_{12}, \gamma)$ . γ)-space associated with changes in global plane strain ellipticity is much more complicated than the smooth manifold (3.6.1). In general,  $\overline{C}_{11}$  and  $\underline{C}_{11}$  are multiple-valued functions of  $(C_{12}, \gamma) \in \Sigma$ , and each branch will be written in the form  $\overline{C}_{11} = \overline{C}_{11}(C_{12}, \gamma)$ and  $\underline{C}_{11} = \underline{C}_{11}(C_{12}, \gamma)$ , respectively. In the following discussion, a superscript in parentheses will be used to mark each single-valued branch of  $\overline{C}_{11}(C_{12}, \gamma)$  and each single-valued branch of  $\underline{C}_{11}(C_{12}, \gamma)$ . The set of all triplets  $(\overline{C}_{11}, C_{12}, \gamma)$  and  $(\underline{C}_{11}, C_{12}, \gamma)$  will, in general, form a two-dimensional transition manifold S. In general, B is a submanifold of S since real-complex transitions and complex-real transitions may or may not involve the root pair associated with loss or gain of ellipticity.

We now seek to determine the properties of this manifold S. Consequently, triplets  $(\overline{C}_{11}(C_{12}, \gamma), C_{12}, \gamma)$  and  $(\underline{C}_{11}(C_{12}, \gamma), C_{12}, \gamma)$  on S in the  $(C_{11}, C_{12}, \gamma)$  parameter space, are

associated with values  $x^*$  that are double real roots of (3.5.4). That is they simultaneously satisfy the following equations

$$P(x, C_{11}, C_{12}, \gamma) = 0$$
 and  $\frac{\partial}{\partial x} P(x, C_{11}, C_{12}, \gamma) = 0$ . (3.6.4)

# 3.7. Global Plane Strain Ellipticity Boundary: Cross-Sections at Constant C<sub>12</sub>

It is convenient to explore the properties of S by considering its cross section at various fixed values of  $C_{12}$ . In general one find that this cross section then evolves in a fairly complicated way as  $C_{12}$  increases from zero. In particular we find that there exist 6 special values of  $C_{12}$ :

$$C_{12}^{(1)} = 1.4444,$$
  $C_{12}^{(2)} = 2,$   $C_{12}^{(3)} = 2.026,$   $C_{12}^{(4)} = 2.0945,$   $C_{12}^{(5)} = 2.13,$   $C_{12}^{(6)} = 2.2635,$  (3.7.1)

at which the cross section of S changes its qualitative form.

The cross section of S for  $C_{12}=0$  is given by those  $(C_{11}, \gamma)$  pairs that support real roots x satisfying both equations in (3.6.4). For  $C_{12}=0$ , one obtains from (3.5.3) that  $a_1=a_3=0$ , so that  $P(x, C_{11}, 0, \gamma)$  is quadratic in  $x^2$ . Accordingly x=0 is a root of  $\frac{\partial}{\partial x}P(x, C_{11}, 0, \gamma)=0$ . Then one finds that  $P(0, C_{11}, 0, \gamma)=0$  gives  $C_{11}=1-\frac{1}{2\gamma}$  ((3.3.4)) as an exact expression for the cross section of S at  $C_{12}=0$  (Figure 25). Note this expression coincides both with (3.3.4) and with (3.6.1) for  $C_{12}=0$ . This completes the analysis of S for  $C_{12}=0$  since it can be shown that the other two roots X of  $\frac{\partial}{\partial x}P(x, C_{11}, 0, \gamma)=0$  do not satisfy  $P(x, C_{11}, 0, \gamma)=0$  for triplets  $(C_{11}, 0, \gamma)$  obeying (3.2.5).

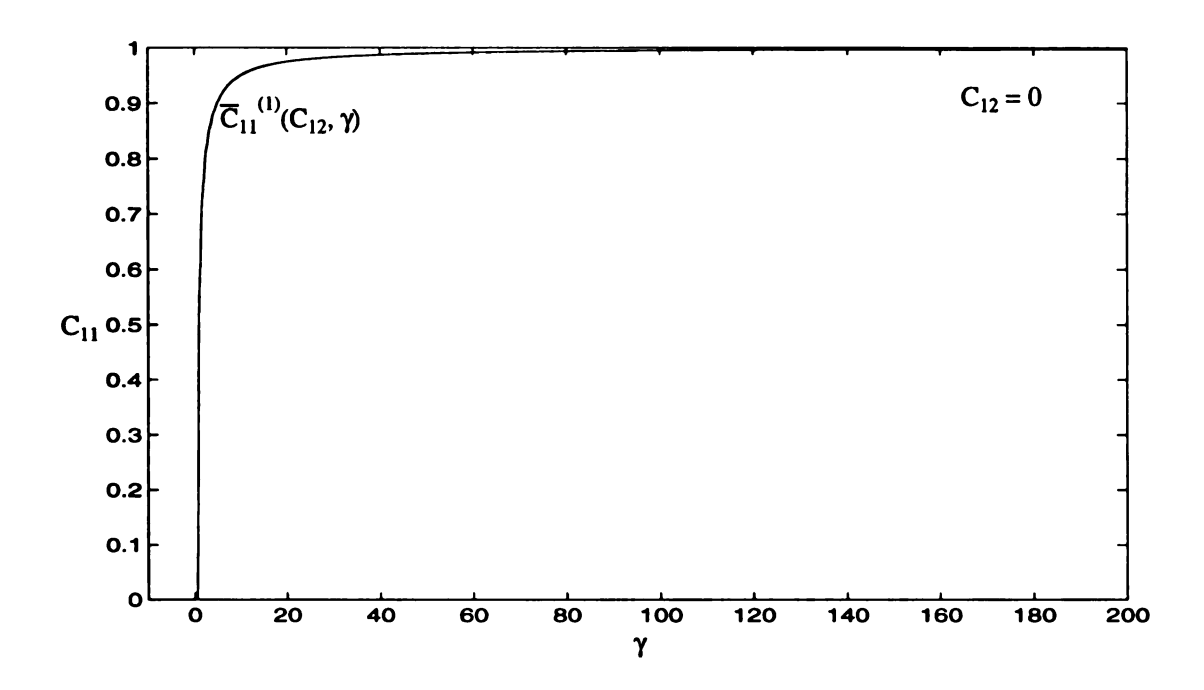


Figure 25. The cross section of S for  $C_{12} = 0$  is given by  $C_{11} = 1-1/2\gamma$  and so coincides with both (3.3.4) and with  $\tilde{C}_{11}(0, \gamma)$ . Here S coincides with B.

We now turn to the consideration of cross-sections of S for  $C_{12} > 0$ . Some results are plotted in Figure 26-Figure 33. The procedure employed here and in what follows for generating these cross sections is based on the discussion in Appendix A. There it is shown that a point  $(C_{11}, C_{12}, \gamma)$  is a member of S if and only if it satisfies the equation  $\vartheta(C_{11}, C_{12}, \gamma) = 0$ , where  $\vartheta = 27\xi_1^2 + 4\xi_2^3$ . The two functions  $\xi_1 \colon \mathcal{R}^3 \to \mathcal{R}$  and  $\xi_2 \colon \mathcal{R}^3 \to \mathcal{R}$  are given by (A.1). It is also shown that cusp points (see  $I^{(4)}$  and  $I^{(5)}$  in Figure 29-Figure 33) to S are associated with the *simultaneous* solution of the equations  $\xi_1(C_{11}, C_{12}, \gamma) = 0$  and  $\xi_2(C_{11}, C_{12}, \gamma) = 0$ . Such cusp solutions exist only if  $C_{12} \ge 2$ . This simultaneous set of equations can be treated numerically to locate potential cusp points. In addition, it is shown that self intersection points (see  $I^{(3)}$  in Figure 29-Figure 33) of the manifold S are associated with the simultaneous solution of  $b_3(C_{11}, C_{12}, \gamma) = 0$  and  $b_2(C_{11}, C_{12}, \gamma)^2 - 4b_4(C_{11}, C_{12}, \gamma) = 0$ , where  $b_1 \colon \mathcal{R}^3 \to \mathcal{R}$ ,  $b_2 \colon \mathcal{R}^3 \to \mathcal{R}$  and

b<sub>3</sub>:  $\mathcal{R}^3 \to \mathcal{R}$  are given by (A.1). These self intersection points also occur only if  $C_{12} \ge 2$  and can again be located numerically. Consequently, the cross section of S at fixed  $C_{12}$  is found from a numerical root search of the equation  $\vartheta(C_{11}, C_{12}, \gamma) = 0$ , where the cusp points and the self intersection points are given by the separate analysis of (A.1), and (A.1)<sub>3,4</sub>, respectively. These special values of  $(C_{11}, \gamma)$  associated with the limit points  $I^{(1)}$ ,  $I^{(2)}$  and  $I^{(6)}$  in Figure 28-Figure 33 are located by refining the numerical root search of the equation  $\vartheta(C_{11}, C_{12}, \gamma) = 0$ . The special values  $C_{12}^{(i)}$ , i = 1,3,4,5,6 are also determined numerically. On the other hand,  $C_{12}^{(2)} = 2$  is an exact result associated with the unique location on S corresponding to a quadruple root of (3.5.1).

For  $C_{12}$  in the interval  $0 < C_{12} < C_{12}^{(1)} = 1.4444$ , two additional cross sections of S at fixed  $C_{12} = 0.5$  and  $C_{12} = 1.4$  are plotted in Figure 26, Figure 27, respectively. Well-drilling at  $(C_{12}, \gamma)$  obeying  $C_{12} < C_{12}^{(1)}$  intersect S only once, and this intersection is associated with the first and only complex-real transition. This root transition is hence a transition associated with loss of global plane strain ellipticity. We denote this single-valued part of S by  $\overline{C}_{11}^{(1)} = \overline{C}_{11}^{(1)}(C_{12}, \gamma)$ , which is part of the ellipticity boundary  $\mathfrak{B}$ :  $\hat{C}_{11} = \hat{C}_{11}(C_{12}, \gamma)$ , for  $C_{12} < C_{12}^{(1)}$ . In the well-drilling process at  $(C_{12}, \gamma)$  obeying  $C_{12} < C_{12}^{(1)}$ , equation (3.5.4) has, in turn, no real roots if  $C_{11} > \overline{C}_{11}^{(1)}$ , and two real roots if  $C_{11} < \overline{C}_{11}^{(1)}$ . Values  $(C_{12}, \gamma) \in \Sigma$  that give rise to this type of behavior, i.e. a single transition from no real roots to two real roots, will be called the <0, 2>-points of  $\Sigma$ , and the corresponding subregion of  $\Sigma$  possessing this property will be denoted by  $\Sigma_1$ .

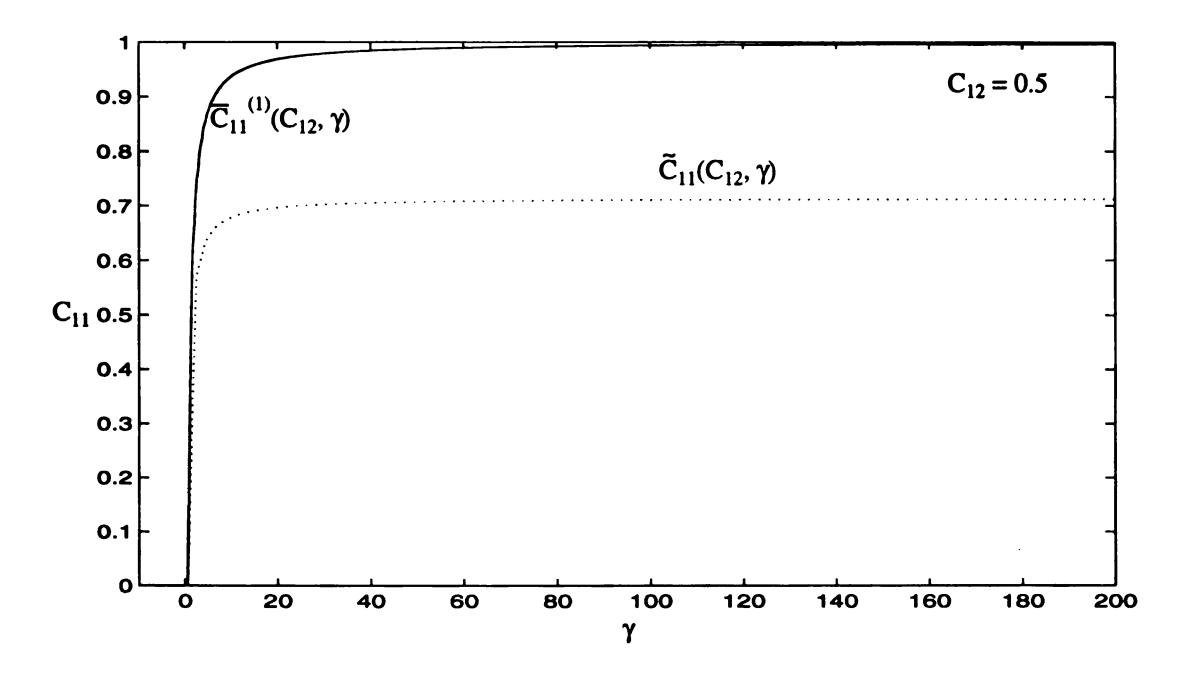


Figure 26. Cross section of S for  $C_{12} = 0.5$ , showing the global plane strain ellipticity boundary B. Pairs  $(C_{12}, \gamma)$  above S are in the GPSE, and pairs below S involve loss of global plane strain ellipticity. The dotted line shows the cross section of the surface previously given in Figure 23, which is now interior to the loss of ellipticity region.

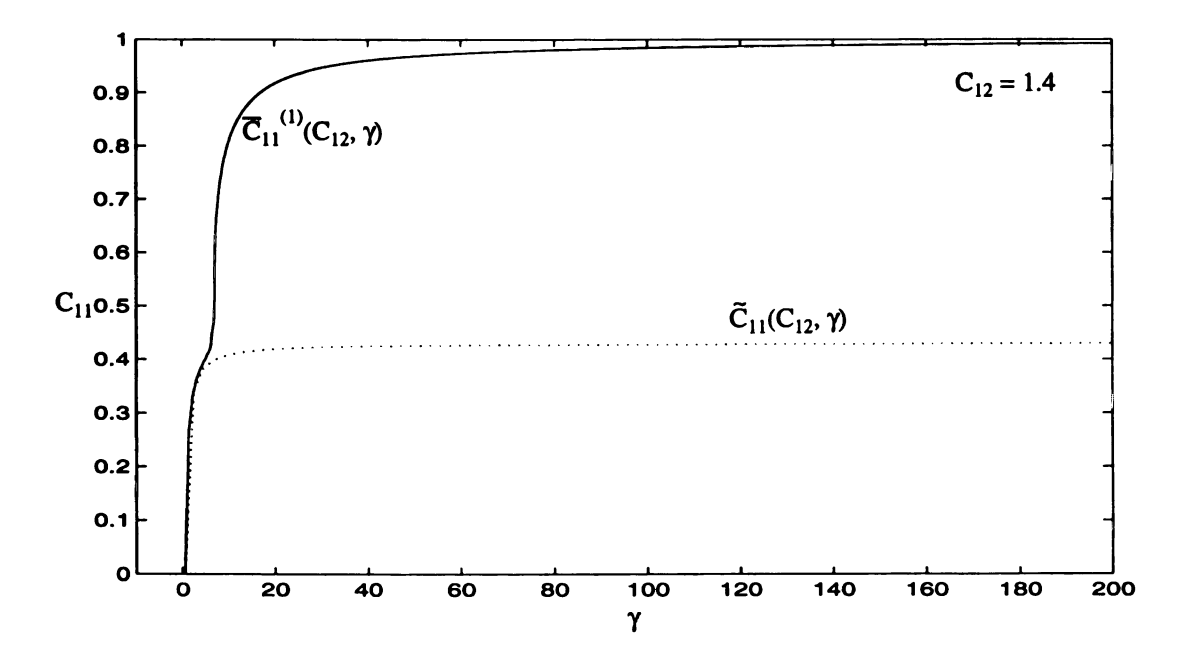


Figure 27. Cross section of S for  $C_{12} = 1.4$ , showing the global plane strain ellipticity boundary B. As in Figure 26, the cross section of the surface associated with (3.6.1) is again shown by the dotted line.

It can be noted from Figure 26 and Figure 27 that, with the increase of  $C_{12}$ ,

manifold S is beginning to develop an inflection point. At  $C_{11} = 0.5181$ ,  $C_{12} = C_{12}^{(1)} = 1.4444$  and  $\gamma = 7.4009$ , this inflection point begins to yield two limit points  $l^{(1)}$  and  $l^{(2)}$ . These two limit points  $l^{(1)}$  and  $l^{(2)}$ , with the further increase of  $C_{12}$ , generate two space curves in the  $(C_{11}, C_{12}, \gamma)$  parameter space. The associated  $(C_{11}, \gamma)$  values may be parametrized in terms of  $C_{12}$  as

$$\mathbf{l}^{(1)} \equiv (\widehat{\mathbf{C}}_{11}^{(1)}, \widehat{\boldsymbol{\gamma}}^{(1)}) = (\Theta^{(1)}(\mathbf{C}_{12}), \Gamma^{(1)}(\mathbf{C}_{12})), \quad \text{for } \mathbf{C}_{12} \ge \mathbf{C}_{12}^{(1)}, \quad (3.7.2)$$

$$I^{(2)} \equiv (\widehat{C}_{11}^{(2)}, \widehat{\gamma}^{(2)}) = (\Theta^{(2)}(C_{12}), \Gamma^{(2)}(C_{12})), \quad \text{for } C_{12}^{(1)} \le C_{12} \le C_{12}^{(6)}. \quad (3.7.3)$$

These vertical tangency points are shown in Figure 28 for  $C_{12}=1.8$ . This is a typical cross section for  $C_{12}^{(1)} < C_{12} < C_{12}^{(2)}=2$ . For  $C_{12}$  in this interval, manifold  $\mathcal{S}$  is no longer single-valued with respect to  $\Sigma$ . It is triple-valued for  $\Gamma^{(1)}(C_{12}) < \gamma < \Gamma^{(2)}(C_{12})$ . Well-drilling at  $(C_{12}, \gamma)$  obeying  $C_{12}^{(1)} < C_{12} < C_{12}^{(2)}$  and  $\Gamma^{(1)}(C_{12}) < \gamma < \Gamma^{(2)}(C_{12})$  intersect  $\mathcal{S}$  three times. These intersections are, in turn, associated with complex-real transition, real-complex transition and complex-real transition. Manifold  $\mathcal{S}$  is thus split into three single-valued branches by  $\Gamma^{(1)}$  and  $\Gamma^{(2)}$ . We denote these three single-valued branches of  $\mathcal{S}$  by  $\overline{C}_{11}^{(1)} = \overline{C}_{11}^{(1)}(C_{12}, \gamma)$ ,  $C_{11}^{(1)} = C_{11}^{(1)}(C_{12}, \gamma)$  and  $\overline{C}_{11}^{(2)} = \overline{C}_{11}^{(2)}(C_{12}, \gamma)$ , as illustrated in Figure 28. The second intersection at  $C_{11}^{(1)}$  corresponds to the recovery of ellipticity with increasing compression  $C_{11}^{(1)}$  decreasing of a material particle. Values  $C_{12}^{(1)} = C_{12}^{(1)} < C_{12}^{(1)} < C_{12}^{(2)} < C_{12}^{(2)}$  and  $C_{11}^{(1)} < C_{12}^{(2)} < C_{12}^{(2)} < C_{12}^{(2)}$  and  $C_{11}^{(1)} < C_{12}^{(2)} < C_{12}^{(2)} < C_{12}^{(2)}$  are classified as  $C_{11}^{(1)} < C_{12}^{(2)} < C_{12}^{$ 

Well-drilling at  $(C_{12}, \gamma)$  obeying  $C_{12}^{(1)} < C_{12} < C_{12}^{(2)}$  and either  $1/2 < \gamma < \Gamma^{(1)}(C_{12})$  or  $\gamma > \Gamma^{(2)}(C_{12})$ , intersects the manifold S only once. This intersection is associated with complex-real transition, and so these  $(C_{12}, \gamma)$  pairs are <0, 2>-points of  $\Sigma$ , i.e.

 $(C_{12}, \gamma) \in \Sigma_1$ . All  $\overline{C}_{11}^{(1)} = \overline{C}_{11}^{(1)}(C_{12}, \gamma)$ ,  $\underline{C}_{11}^{(1)} = \underline{C}_{11}^{(1)}(C_{12}, \gamma)$  and  $\overline{C}_{11}^{(2)} = \overline{C}_{11}^{(2)}(C_{12}, \gamma)$  for  $C_{12}^{(1)} < C_{12} < C_{12}^{(2)} = 2$  are part of the ellipticity boundary  $\mathcal{B}$ :  $\hat{C}_{11} = \hat{C}_{11}(C_{12}, \gamma)$ .

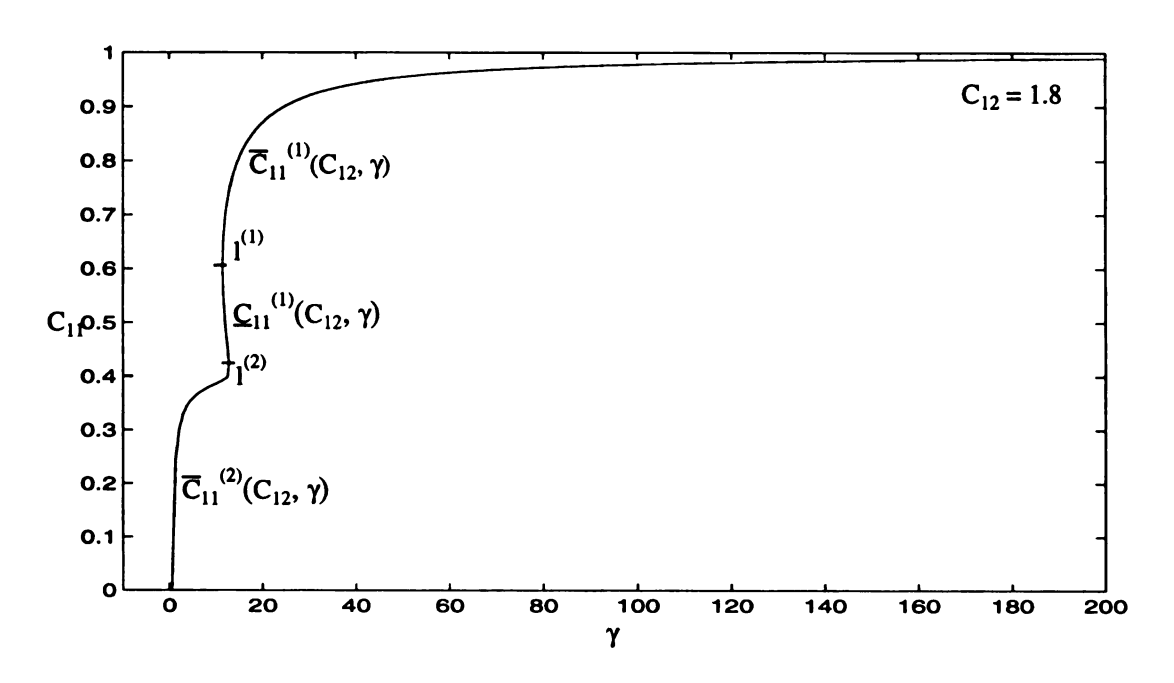


Figure 28. Cross section of S for  $C_{12} = 1.8$ , showing the global plane strain ellipticity boundary B. Here  $I^{(1)}$  and  $I^{(2)}$  are limit points associated with vertical tangency. In this and future figures for S at constant  $C_{12}$ , the cross section associated with (3.6.1) is no longer shown.

Note in Figure 28 that there is a sharp bend in the  $\overline{C}_{11}^{(2)}$  branch of S just below  $I^{(2)}$ . Starting at  $C_{11} = 0.3883$ ,  $C_{12} = C_{12}^{(2)} = 2$  and  $\gamma = 17.0815$ , this bend unfolds into three branches. Two of these, denoted by  $\overline{C}_{11}^{(21)} = \overline{C}_{11}^{(21)}(C_{12}, \gamma)$  and  $\overline{C}_{11}^{(22)} = \overline{C}_{11}^{(22)}(C_{12}, \gamma)$ , continue to be associated with complex-real transition. In between them, the third unfolded branch, denoted by  $\underline{C}_{11}^{(2)} = \underline{C}_{11}^{(2)}(C_{12}, \gamma)$ , is associated with real-complex transition, as illustrated in Figure 29-Figure 32. This generates 3 special points on each cross-section, which are denoted by  $I^{(3)}$ ,  $I^{(4)}$  and  $I^{(5)}$ . As  $C_{12}$  increases from  $C_{12} = 2$ , this generates 3 new space curves. All 3 curves originate at  $\mathcal{P} = (C_{11}, C_{12}, \gamma) = (0.3883, 2, 17.0815)$  which is the *sole quadruple root to*  $(3.6.4)_{I}$ . The associated  $(C_{11}, \gamma)$ -values on

these curves can also be parametrized in terms of C<sub>12</sub> as

$$\mathbf{1}^{(3)} \equiv (\widehat{\mathbf{C}}_{11}^{(3)}, \widehat{\boldsymbol{\gamma}}^{(3)}) = (\Theta^{(3)}(\mathbf{C}_{12}), \Gamma^{(3)}(\mathbf{C}_{12})), \quad \text{for } \mathbf{C}_{12} \ge \mathbf{C}_{12}^{(2)}, \quad (3.7.4)$$

$$l^{(4)} \equiv (\widehat{C}_{11}^{(4)}, \widehat{\gamma}^{(4)}) = (\Theta^{(4)}(C_{12}), \Gamma^{(4)}(C_{12})), \quad \text{for } C_{12} \ge C_{12}^{(2)}, \quad (3.7.5)$$

$$I^{(5)} \equiv (\widehat{C}_{11}^{(5)}, \widehat{\gamma}^{(5)}) = (\Theta^{(5)}(C_{12}), \Gamma^{(5)}(C_{12})), \quad \text{for } C_{12} \ge C_{12}^{(2)}.$$
 (3.7.6)

The space curve  $l^{(3)}$  is the intersection of  $\overline{C}_{11}^{(21)}(C_{12}, \gamma)$  with  $\overline{C}_{11}^{(22)}(C_{12}, \gamma)$  for  $C_{12}^{(2)}=2 \cdot C_{12} \cdot C_{12}^{(4)} \cong 2.0945$ , and is the intersection of  $\overline{C}_{11}^{(21)}(C_{12}, \gamma)$  with  $\underline{C}_{11}^{(1)}(C_{12}, \gamma)$  for  $C_{12} \cdot C_{12}^{(4)} \cong 2.0945$ . Curve  $l^{(3)}$  corresponds to two distinct root transitions, and triplets  $(\Theta^{(3)}(C_{12}), C_{12}, \Gamma^{(3)}(C_{12}))$  thus provide two double real roots for equation (3.5.4). Triplets  $(\Theta^{(4)}(C_{12}), C_{12}, \Gamma^{(4)}(C_{12}))$  and  $(\Theta^{(5)}(C_{12}), C_{12}, \Gamma^{(5)}(C_{12}))$ , which are the cusp points in Figure 29-Figure 32, on the space curves  $l^{(4)}$  and  $l^{(5)}$  respectively provide triple real roots for equation (3.5.4). Now, branch  $\overline{C}_{11}^{(21)}(C_{12}, \gamma)$  is bounded by  $\gamma = 1/2$  and  $l^{(5)}$ , branch  $\overline{C}_{11}^{(22)}(C_{12}, \gamma)$  is bounded by  $l^{(4)}$  and  $l^{(5)}$ .

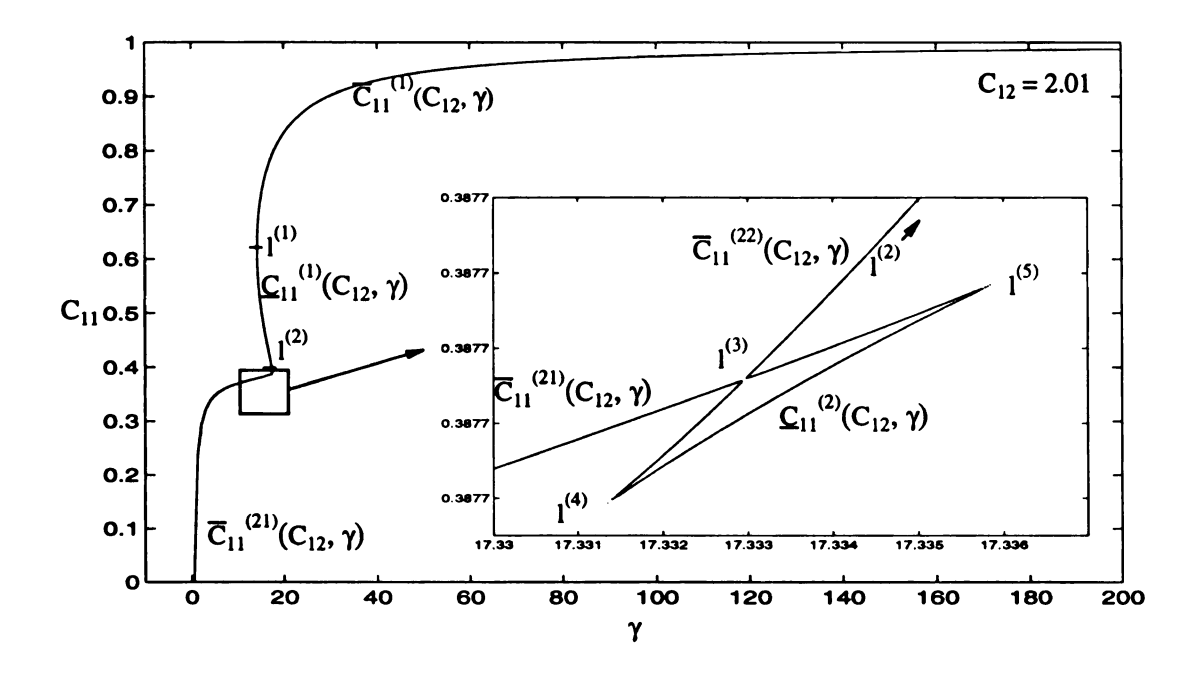


Figure 29. Cross section of S for  $C_{12} = 2.01$  is typical of  $C_{12}$  values obeying  $C_{12}^{(2)} < C_{12} < C_{12}^{(3)}$ . Unlike the cross sections for  $C_{12} < C_{12}^{(2)} = 2$ , the cross section now intersects itself (inset). Points on the internal branches created by this intersection are members of S but not members of S. Triplets  $(C_{11}, C_{12}, \gamma)$  within the triangular region enclosed by these internal branches have 4 real roots to  $(3.6.4)_1$ .

In the well-drilling process, branches  $\overline{C}_{11}^{(21)}(C_{12},\gamma)$  and  $\overline{C}_{11}^{(22)}(C_{12},\gamma)$  are associated with complex-real transition and branch  $\underline{C}_{11}^{(2)}(C_{12},\gamma)$  is associated with real-complex transition. For  $C_{12}^{(2)} < C_{12} < C_{12}^{(3)} \cong 2.026$ , we have

$$\Gamma^{(1)}(C_{12}) < \Gamma^{(4)}(C_{12}) < \Gamma^{(3)}(C_{12}) < \Gamma^{(5)}(C_{12}) < \Gamma^{(2)}(C_{12}),$$
for  $C_{12}^{(2)} < C_{12} < C_{12}^{(3)}$ . (3.7.7)

Thus, for  $C_{12}^{(2)} < C_{12} < C_{12}^{(3)}$ , the values of  $(C_{12}, \gamma) \in \Sigma$  are classified according to the parameter  $\gamma$  as follows: <0, 2> for  $1/2 < \gamma < \Gamma^{(1)}(C_{12})$ , <0, 2, 0, 2> for  $\Gamma^{(1)}(C_{12}) < \gamma < \Gamma^{(4)}(C_{12})$ , <0, 2, 0, 2, 4, 2> for  $\Gamma^{(4)}(C_{12}) < \gamma < \Gamma^{(5)}(C_{12})$ , <0, 2, 0, 2> for  $\Gamma^{(5)}(C_{12}) < \gamma < \Gamma^{(2)}(C_{12})$ , <0, 2> for  $\gamma > \Gamma^{(2)}(C_{12})$ . The subregion of  $\Sigma$  containing <0, 2, 0, 2, 4, 2>-points will be denoted by  $\Sigma_3$ .

At  $C_{12}^{(3)} \cong 2.026$ , it is found that  $\Gamma^{(2)}(C_{12}) = \Gamma^{(3)}(C_{12})$ . This gives

$$\begin{split} \Gamma^{(1)}(C_{12}) < \Gamma^{(4)}(C_{12}) < \Gamma^{(3)}(C_{12}) < \Gamma^{(2)}(C_{12}) < \Gamma^{(5)}(C_{12}), \\ \Theta^{(3)}(C_{12}) < \Theta^{(2)}(C_{12}), \\ \text{for } C_{12}^{(3)} < C_{12} < C_{12}^{(4)} \cong 2.0945. \end{split} \tag{3.7.8}$$

The values of  $(C_{12}, \gamma) \in \Sigma$ , for  $C_{12}^{(3)} < C_{12} < C_{12}^{(4)}$ , are classified according to the parameter  $\gamma$  as follows: <0, 2> for  $1/2 < \gamma < \Gamma^{(1)}(C_{12})$ , <0, 2, 0, 2> for  $\Gamma^{(1)}(C_{12}) < \gamma < \Gamma^{(4)}(C_{12})$ , <0, <0, <0, <0, <0, <0, <0, <0, <0, <0, <0, <0, <0, <0, <0, <0, <0, <0, <0, <0, <0, <0, <0, <0, <0, <0, <0, <0, <0, <0, <0, <0, <0, <0, <0, <0, <0, <0, <0, <0, <0, <0, <0, <0, <0, <0, <0, <0, <0, <0, <0, <0, <0, <0, <0, <0, <0, <0, <0, <0, <0, <0, <0, <0, <0, <0, <0, <0, <0, <0, <0, <0, <0, <0, <0, <0, <0, <0, <0, <0, <0, <0, <0, <0, <0, <0, <0, <0, <0, <0, <0, <0, <0, <0, <0, <0, <0, <0, <0, <0, <0, <0, <0, <0, <0, <0, <0, <0, <0, <0, <0, <0, <0, <0, <0, <0, <0, <0, <0, <0, <0, <0, <0, <0, <0, <0, <0, <0, <0, <0, <0, <0, <0, <0, <0, <0, <0, <0, <0, <0, <0, <0, <0, <0, <0, <0, <0, <0, <0, <0, <0, <0, <0, <0, <0, <0, <0, <0, <0, <0, <0, <0, <0, <0, <0, <0, <0, <0, <0, <0, <0, <0, <0, <0, <0, <0, <0, <0, <0, <0, <0, <0, <0, <0, <0, <0, <0, <0, <0, <0, <0, <0, <0, <0, <0, <0, <0, <0, <0, <0, <0, <0, <0, <0, <0, <0, <0, <0, <0, <0, <0, <0, <0, <0, <0, <0, <0, <0, <0, <0, <0, <0, <0, <0, <0, <0, <0, <0, <0, <0, <0, <0, <0, <0, <0, <0, <0, <0, <0, <0, <0, <0, <0, <0, <0, <0, <0, <0, <0, <0, <0, <0, <0, <0, <0, <0, <0, <0, <0, <0, <0, <0, <0, <0, <0, <0, <0, <0, <0, <0, <0, <0, <0, <0, <0, <0, <0, <0, <0, <0, <0, <0, <0, <0, <0, <0, <0, <0, <0, <0, <0, <0, <0, <0, <0, <0, <0, <0, <0, <0,

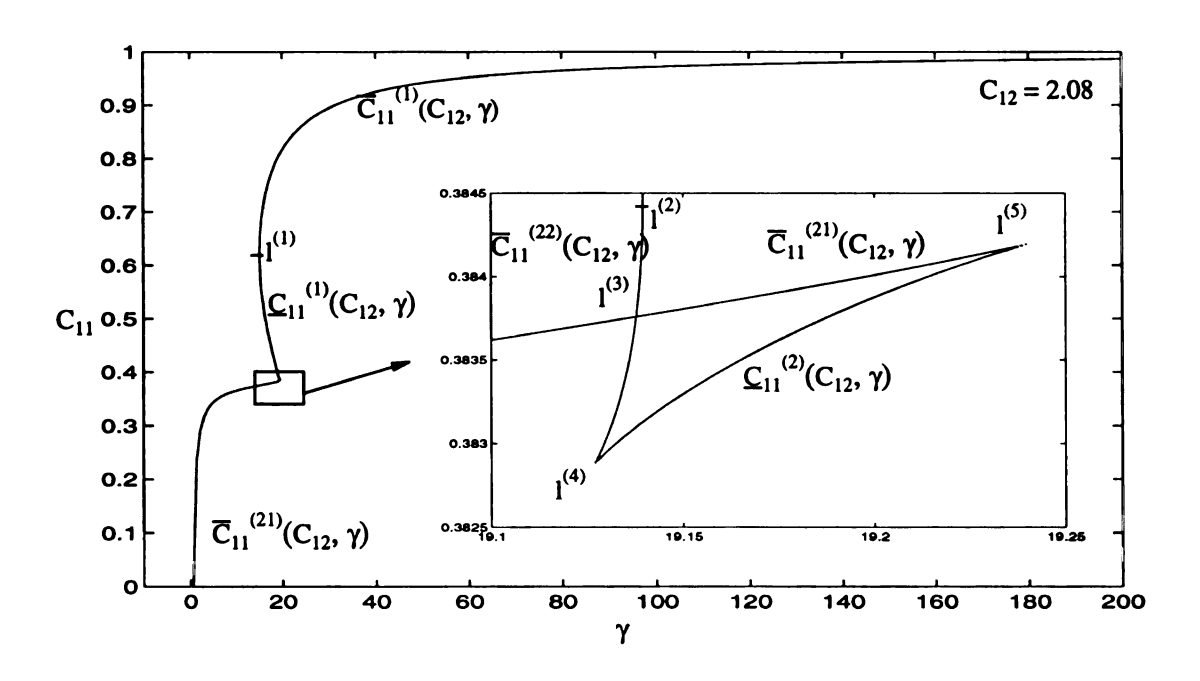


Figure 30. Cross section of S for  $C_{12} = 2.08$  is typical of  $C_{12}$  values obeying  $C_{12}^{(3)} < C_{12} < C_{12}^{(4)}$ . Note that the vertical tangency point  $I^{(2)}$  is approaching the self intersection point  $I^{(3)}$ .

At  $C_{12}^{(4)}\cong 2.0945$ , it is found that  $\Gamma^{(2)}(C_{12})=\Gamma^{(3)}(C_{12})\cong 19.52$  and  $\Theta^{(2)}(C_{12})$  =  $\Theta^{(3)}(C_{12})\cong 0.3828$ . This gives

$$\Gamma^{(1)}(C_{12}) < \Gamma^{(4)}(C_{12}) < \Gamma^{(3)}(C_{12}) < \Gamma^{(2)}(C_{12}) < \Gamma^{(5)}(C_{12}),$$

$$\Theta^{(3)}(C_{12}) > \Theta^{(2)}(C_{12}),$$
for  $C_{12}^{(4)} < C_{12} < C_{12}^{(5)} \cong 2.13.$ 
(3.7.9)

The values of  $(C_{12}, \gamma) \in \Sigma$ , for  $C_{12}^{(4)} < C_{12} < C_{12}^{(5)}$ , are classified according to the parameter  $\gamma$  as: <0, 2>-points, <0, 2, 0, 2>-points, <0, 2, 4, 2>-points, <0, 2, 4, 2>-points, <0, 2, 4, 2>-points, <0, 2, 4, 2>-points and <0, 2>-points, in turn, for  $\gamma$  intervals divided by  $\Gamma^{(1)}$ ,  $\Gamma^{(4)}$ ,  $\Gamma^{(3)}$ ,  $\Gamma^{(2)}$  and  $\Gamma^{(5)}$ , as can be seen in Figure 31. The subregion of  $\Sigma$  containing <0, 2, 4, 2, 4, 2>-points will be denoted by  $\Sigma_5$ .

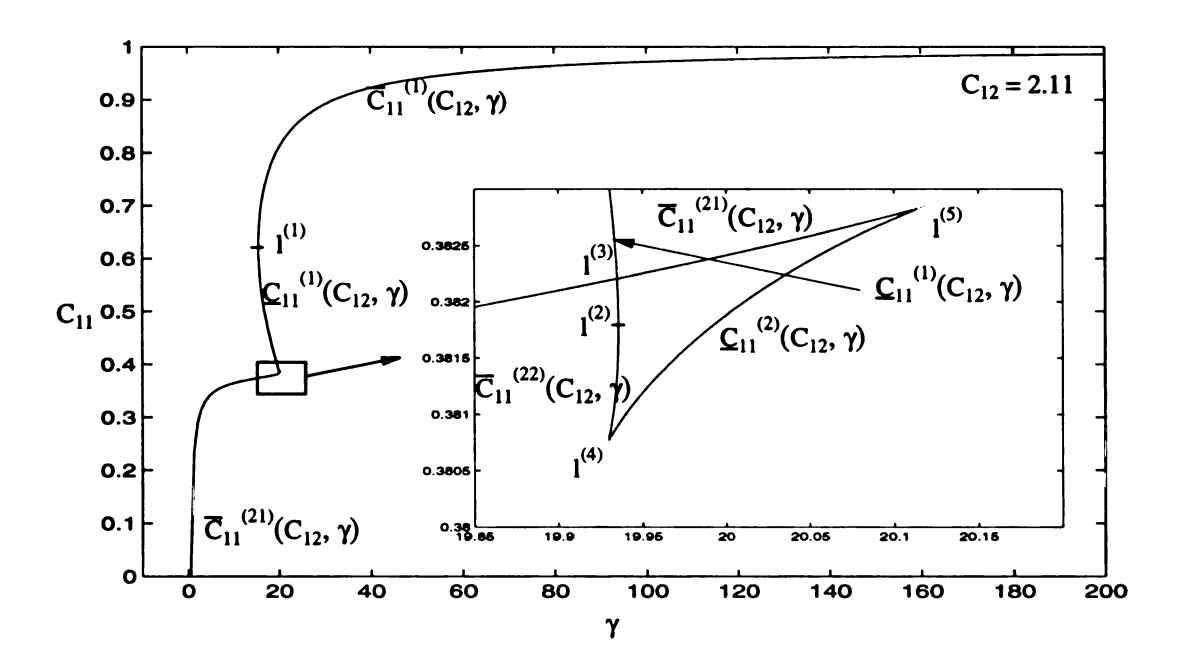


Figure 31. Cross section of S for  $C_{12} = 2.11$  is typical of  $C_{12}$  values obeying  $C_{12}^{(4)} < C_{12} < C_{12}^{(5)}$ . Here the vertical tangency point  $I^{(2)}$  has passed through the self intersection point  $I^{(3)}$ . These two points coincide only at the special value  $C_{12} = C_{12}^{(4)}$ , which is intermediate between that of Figure 30 and the present figure.

At  $C_{12}^{(5)} \cong 2.13$ , it is found that  $\Gamma^{(3)}(C_{12}) = \Gamma^{(4)}(C_{12})$ . This gives

$$\Gamma^{(1)}(C_{12}) < \Gamma^{(3)}(C_{12}) < \Gamma^{(4)}(C_{12}) < \Gamma^{(2)}(C_{12}) < \Gamma^{(5)}(C_{12}),$$
for  $C_{12}^{(5)} < C_{12} < C_{12}^{(6)} \cong 2.2635$ . (3.7.10)

The values of  $(C_{12}, \gamma) \in \Sigma$ , for  $C_{12}^{(5)} < C_{12} < C_{12}^{(6)}$ , are classified according to the parameter  $\gamma$  as: <0, 2>-points, <0, 2, 0, 2>-points, <0, 2, 4, 2>-points, and <0, 2>-points, in turn, for  $\gamma$  intervals divided by  $\Gamma^{(1)}$ ,  $\Gamma^{(3)}$ ,  $\Gamma^{(4)}$ ,  $\Gamma^{(2)}$  and  $\Gamma^{(5)}$ , as can be seen in Figure 32.

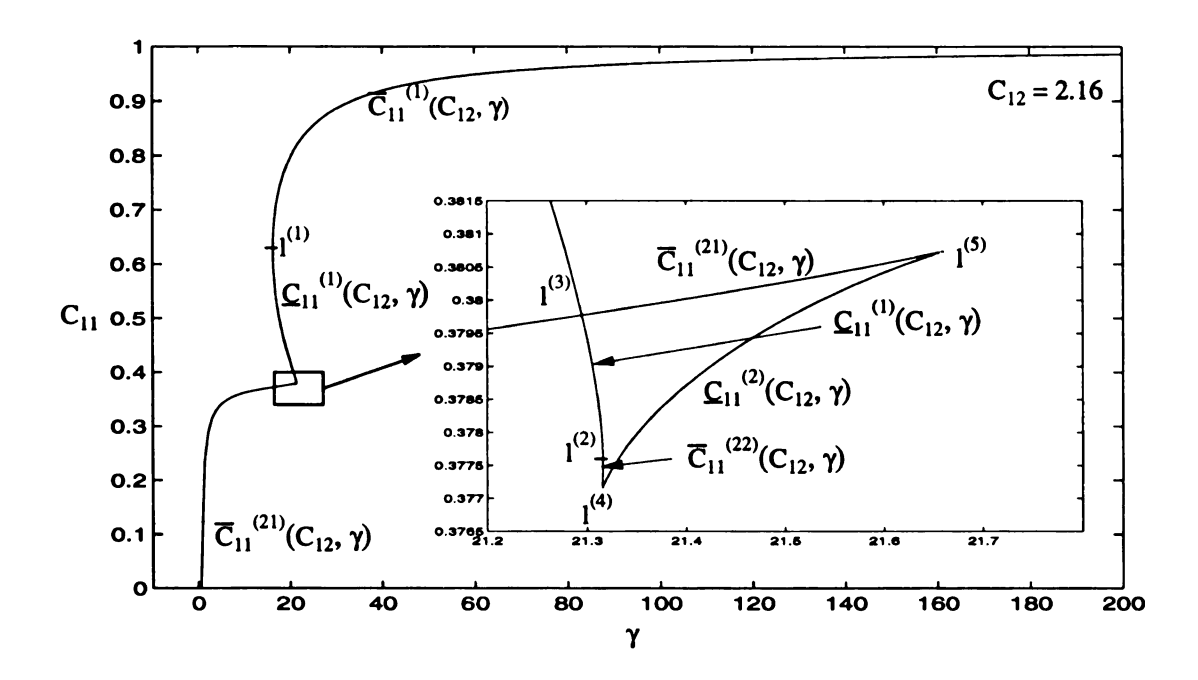


Figure 32. Cross section of S for  $C_{12} = 2.16$  is typical of  $C_{12}$  values obeying  $C_{12}^{(5)} < C_{12} < C_{12}^{(6)}$ . Note that the vertical tangency point  $I^{(2)}$  is approaching the cusp point  $I^{(4)}$ .

At  $C_{12}^{(6)} \cong 2.2635$ , it is found that  $\Gamma^{(2)}(C_{12}) = \Gamma^{(4)}(C_{12}) \cong 24.4047$  and  $\Theta^{(2)}(C_{12}) = \Theta^{(4)}(C_{12}) \cong 0.3694$ . Hence the branch associated with  $\overline{C}_{11}^{(22)}(C_{12}, \gamma)$  and the limit point  $I^{(2)}$  no longer exist for  $C_{12} > C_{12}^{(6)}$ . However, a new branch  $\overline{C}_{11}^{(3)} = \overline{C}_{11}^{(3)}(C_{12}, \gamma)$  is generated along with the new limit point  $I^{(6)}$ , parametrized by the space curve

$$1^{(6)} \equiv (\widehat{C}_{11}^{(6)}, \widehat{\gamma}^{(6)}) = (\Theta^{(6)}(C_{12}), \Gamma^{(6)}(C_{12})), \quad \text{for } C_{12} \ge C_{12}^{(6)}.$$
 (3.7.11)

Now, branch  $\overline{C}_{11}^{(3)}(C_{12}, \gamma)$  is bounded by  $l^{(6)}$  and  $l^{(4)}$ , and branch  $\underline{C}_{11}^{(2)}(C_{12}, \gamma)$  is bounded by  $l^{(6)}$  and  $l^{(5)}$ . This new branch  $\overline{C}_{11}^{(3)}(C_{12}, \gamma)$  is associated with complex-real transition. Figure

33 is a typical cross section of S for  $C_{12} > C_{12}^{(6)}$ . In this  $C_{12}$  range:

$$\begin{split} \Gamma^{(1)}(C_{12}) < \Gamma^{(3)}(C_{12}) < \Gamma^{(6)}(C_{12}) < \Gamma^{(4)}(C_{12}) < \Gamma^{(5)}(C_{12}), \\ C_{12} > C_{12}^{(6)} &\cong 2.2635. \end{split} \tag{3.7.12}$$

The values of  $(C_{12}, \gamma) \in \Sigma$ , for  $C_{12} > C_{12}^{(6)}$ , are classified according to the parameter  $\gamma$  as: <0, 2>-points, <0, 2, 0, 2>-points, <0, 2, 4, 2>-points, <0, 2, 4, 2>-points, <0, 2, 4, 2>-points, and <0, 2>-points, for  $\gamma$  intervals divided by  $\Gamma^{(1)}$ ,  $\Gamma^{(3)}$ ,  $\Gamma^{(6)}$ ,  $\Gamma^{(4)}$  and  $\Gamma^{(5)}$ , in turn, as can be seen in Figure 33.

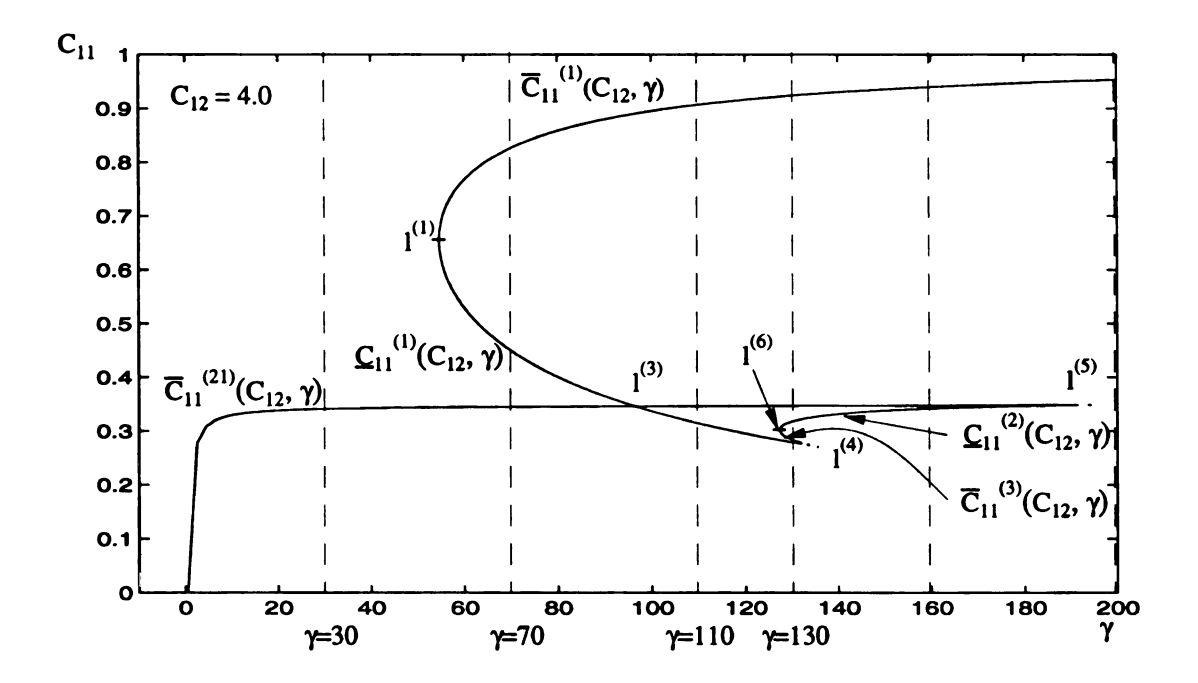


Figure 33. Cross section of S for  $C_{12} = 4.0$  is typical of  $C_{12}$  values obeying  $C_{12} > C_{12}^{(6)}$ . The dashed lines at fixed  $\gamma = 30$ , 70, 110, 130, 160 and 200 provide correlation with Figure 35.

## 3.8. Projection of the Ellipticity Boundary onto the $(C_{12}, \gamma)$ -Plane

The cross-section analysis of the previous section reveals how the manifold S is divided into branches by the space curves  $l^{(1)}-l^{(6)}$ . The penetration of each branch provides a root transition, only some of which are associated with loss or gain of global plane strain

ellipticity. Changes in  $C_{11}$  at fixed  $(C_{12}, \gamma) \in \Sigma$  involve different root transition sequences depending on the value of  $(C_{12}, \gamma)$  and motivated the classifications  $\Sigma_1 - \Sigma_5$  as an exhaustive subregion decomposition of  $\Sigma$ . The projections of the space curves  $l^{(1)}-l^{(6)}$  onto the  $(C_{12}, \gamma)$ -plane give plane curves  $\Gamma^{(1)}-\Gamma^{(6)}$ , which provide the boundaries of these subregions. The curve projections and subregions are plotted in Figure 34.

We find that  $\gamma$ -values on the  $\Gamma$ -curves are monotonically increasing with  $C_{12}$ . The curves  $\Gamma^{(1)}$  and  $\Gamma^{(3)}$ - $\Gamma^{(6)}$  involve  $C_{12} \rightarrow \infty$ . In contrast, curve  $\Gamma^{(2)}$  terminates at  $(C_{12}^{(6)}, \gamma^{(6)})$  at which point  $\Gamma^{(6)}$  begins. The curves  $\Gamma^{(1)}$ - $\Gamma^{(6)}$  intersect at the 6 points:

$$C_{12}^{(1)} = 1.4444, \qquad \gamma^{(1)} = 7.4009,$$
 $C_{12}^{(2)} = 2, \qquad \gamma^{(2)} = 17.0815,$ 
 $C_{12}^{(3)} = 2.026, \qquad \gamma^{(3)} = 17.782,$ 
 $C_{12}^{(4)} = 2.0945, \qquad \gamma^{(4)} = 19.521,$ 
 $C_{12}^{(5)} = 2.13, \qquad \gamma^{(5)} = 20.47,$ 
 $C_{12}^{(6)} = 2.2635, \qquad \gamma^{(6)} = 24.3891.$ 
(3.8.1)

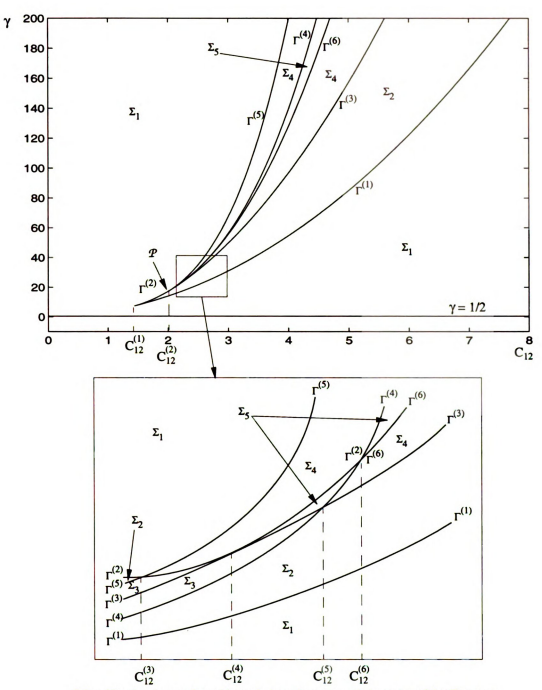
The interpretation of these 6 points are as follows:

- $(C_{12}^{(1)}, \gamma^{(1)})$  is the origin of the curves  $\Gamma^{(1)}$  and  $\Gamma^{(2)}$  associated with the development of  $C_{11}$  tangency (vertical tangency) on S.
- $(C_{12}^{(2)}, \gamma^{(2)})$  is the  $(C_{12}, \gamma)$  value of  $\mathcal{P}$ , the unique quadruple root of  $(3.6.4)_1$ .

  This point is the origin of curves  $\Gamma^{(3)}$ ,  $\Gamma^{(4)}$ ,  $\Gamma^{(5)}$  associated with the creation of internal branches of  $\mathcal{S}$  that are not on  $\mathcal{B}$ .
- $(C_{12}^{(3)}, \gamma^{(3)})$  is associated with the intersection of the projection curves  $\Gamma^{(2)}$  and  $\Gamma^{(5)}$  even though the parent space curves  $I^{(2)}$  and  $I^{(5)}$  do not intersect.

- $(C_{12}^{(4)}, \gamma^{(4)})$  is associated with the intersection of the vertical tangency space curve  $l^{(2)}$  with branch intersection space curve  $l^{(3)}$ . Hence the projection curves  $\Gamma^{(2)}$  and  $\Gamma^{(3)}$  also intersect.
- $(C_{12}^{(5)}, \gamma^{(5)})$  is associated with the intersection of the projection curves  $\Gamma^{(3)}$  and  $\Gamma^{(4)}$  even though the parent space curves  $I^{(3)}$  and  $I^{(4)}$  do not intersect.
- $(C_{12}^{(6)}, \gamma^{(6)})$  is associated with the transition of vertical tangency between branches of S. Specifically, vertical tangency space curve  $l^{(2)}$  is converted to vertical tangency space curve  $l^{(6)}$ due to the intersection of the combined space curve  $l^{(2)}/l^{(6)}$  with cusp curve  $l^{(4)}$ .

It is useful to note that the 4 points:  $(C_{12}^{(1)}, \gamma^{(1)})$ ,  $(C_{12}^{(2)}, \gamma^{(2)})$ ,  $(C_{12}^{(4)}, \gamma^{(4)})$ ,  $(C_{12}^{(6)}, \gamma^{(6)})$  are associated with the intersection of actual space curves  $l^{(i)}$ . In contrast, the 2 points  $(C_{12}^{(3)}, \gamma^{(3)})$  and  $(C_{12}^{(5)}, \gamma^{(5)})$  are only associated with the intersection of the space curve projections  $\Gamma^{(i)}$ .



Magnification is not plotted in scale in order to reveal the order of the  $\Gamma$ -curves.

Figure 34. The projections of the special space curves  $\Gamma^{(1)}.\Gamma^{(6)}$  onto the  $(C_{12},\gamma)$ -plane give plane curves  $\Gamma^{(1)}.\Gamma^{(6)}$ . These, in turn, divide  $\Sigma$  into regions  $\Sigma_1, \Sigma_2, \Sigma_3, \Sigma_4$  and  $\Sigma_5$  associated with different root transition sequences as  $C_{11}$  is decreased from  $C_{11}=1$ . The root transition sequences are  $\Sigma_1 \Leftrightarrow \mathcal{O}, 2 \Rightarrow \mathcal{O}, \Sigma_2 \Leftrightarrow \mathcal{O}, 2, 0, 2, 4, 2 \Rightarrow \mathcal{O}, 2, 4, 2 \Rightarrow \mathcal{O}, 2, 4, 2, 4, 2, 4, 2 \Rightarrow \mathcal{O}, 2, 4, 2 \Rightarrow \mathcal$ 

# 3.9. Multiplicity and Orientation of the Discontinuity Surfaces for $C_{12}=4$

In this section we examine the change in the normal direction of the surfaces of weak discontinuity associated with the well-drilling process at the fixed cross-section of S corresponding to  $C_{12} = 4$ . The cross-section of S was given in Figure 33, and is chosen here in view of its irregular character. We consider well drillings at  $\gamma = 30$ , 70, 110, 130, 160 and 200 respectively. These well-drillings are marked by vertical dash lines in Figure 33. Figure 35(a)-(f) present the corresponding normal directions in terms of the angles  $\alpha$ , which are measured in degree in the  $(X_1, X_2)$ -plane from the  $X_1$ -axis to the normal direction. This measurement is positive if it is the result of a right hand rotation about  $X_3$ -axis, and vice versa.

Figure 35(a) corresponds to  $\gamma = 30$ . Here, for  $C_{11} \le \overline{C}_{11}^{(21)}(4,30)$  two families of normals  $\bf n$  form a half loop, which is initiated at  $C_{11} = \overline{C}_{11}^{(21)}(4,30)$  where the normals from these two families have the same direction (double real root of  $P(x, C_{11}, C_{12}, \gamma)$ ). This behavior persists for all  $\gamma < 54.6295$ . At  $\gamma = \Gamma^{(1)}(4) = 54.6295$ , two new families of normals  $\bf n$  make appearance and begin to form a separate upper loop near  $C_{11} = \widehat{\theta}^{(1)} \approx 0.6566$ . A well-developed (and very thin) upper loop of normals for  $C_{11}^{(1)}(4,70) \le C_{11} \le \overline{C}_{11}^{(1)}(4,70)$  is shown in Figure 35(b), together with the lower half loop of normals for  $C_{11} \le \overline{C}_{11}^{(2)}(4,70)$ . Each tip of the upper loop, at  $C_{11} = C_{11}^{(1)}(4,70)$  and  $C_{11} = \overline{C}_{11}^{(1)}(4,70)$  respectively, corresponds to a double real root of  $P(x, C_{11}, C_{12}, \gamma)$ . The upper full loop is separate from the lower half loop for 54.6295  $< \gamma < 127.31$ . At  $\gamma = \Gamma^{(3)}(4) = 96.5469$ , the lower tip of the upper loop reaches the top level (at  $C_{11} = \overline{C}_{11}^{(21)}(4,96.5469)$ ) of the lower half loop, and this situation corresponds to two double real roots of  $P(x, C_{11}, C_{12}, \gamma)$ . For further increased  $\gamma > \Gamma^{(3)}(4)$ , there is an overlap

in the  $C_{11}$ -values of the upper loop with the lower half loop for  $C_{11}^{(1)}(4, \gamma) \le C_{11} \le \overline{C}_{11}^{(21)}(4, \gamma)$  as shown in Figure 35(c). In this situation  $P(x, C_{11}, C_{12}, \gamma)$ has four real roots. At  $\gamma = \Gamma^{(6)}(4) \approx 127.31$ , the further developed upper loop touches the lower half loop at  $C_{11} = \Theta^{(6)}(4) = 0.3025$ . This contact point is also a double real root of P(x, C<sub>11</sub>, C<sub>12</sub>,  $\gamma$ ). For  $\gamma > \Gamma^{(6)}(4)$ , this contact point splits both the upper loop and the lower half loop, and forms two extremum points at  $C_{11} = \overline{C}_{11}^{(3)}(4, \gamma)$  and  $C_{11} = C_{11}^{(2)}(4, \gamma)$ , as can been seen in Figure 35(d). Now in two  $C_{11}$ -intervals:  $C_{11}^{(1)}(4,\gamma) \le C_{11} \le \overline{C}_{11}^{(3)}(4,\gamma)$  and  $C_{11}^{(2)}(4,\gamma) \le C_{11} \le \overline{C}_{11}^{(21)}(4,\gamma)$ , it follows that  $P(x,C_{11},x)$  $C_{12}$ ,  $\gamma$ ) again has four real roots. With the further increase of  $\gamma$ , the extremum points at  $C_{11} = \overline{C}_{11}^{(3)}(4, \gamma)$  and  $C_{11} = \underline{C}_{11}^{(1)}(4, \gamma)$  approach each other; these two points finally merge at  $(C_{11}, \gamma) = (\Theta^{(4)}(4), \Gamma^{(4)}(4)) = (0.2660, 138.57)$ , so that the interval of four real roots  $\underline{C}_{11}^{(1)}(4,\gamma) < C_{11} < \overline{C}_{11}^{(3)}(4,\gamma)$  vanishes and  $P(x, C_{11}, C_{12}, \gamma)$  has a triple real root. Figure 35(e) displays the normal directions after this merge. At  $(C_{11}, \gamma) = (\Theta^{(5)}(4), \gamma)$  $\Gamma^{(5)}(4)$ ) = (0.3488, 197.87), the remaining two extremum points at  $C_{11} = C_{11}^{(2)}(4, \gamma)$ and  $C_{11} = \overline{C}_{11}^{(21)}(4,\gamma)$  also merge and ends the four real root interval  $\underline{C}_{11}^{(2)}(4,\gamma) < C_{11} < 0$  $\bar{C}_{11}^{(21)}(4,\gamma)$ . This merge point corresponds to another triple root of  $P(x, C_{11}, C_{12}, \gamma)$ . For  $\gamma > \Gamma^{(5)}(4)$  there are, once again, at most 2 discontinuity surfaces. A typical picture of the normal directions for  $\gamma > \Gamma^{(5)}(4)$  is plotted in Figure 35(f). Note in all six subfigures of Figure 35 that the angle  $\alpha$  is typically close to  $\pm 90^{\circ}$ . This corresponds to fibers which intersect the discontinuity surface at a shallow angle. Recall however from (EIII) that  $\alpha$  = ±90° is not allowed so that the discontinuity surface can not actually be a fiber containing plane.

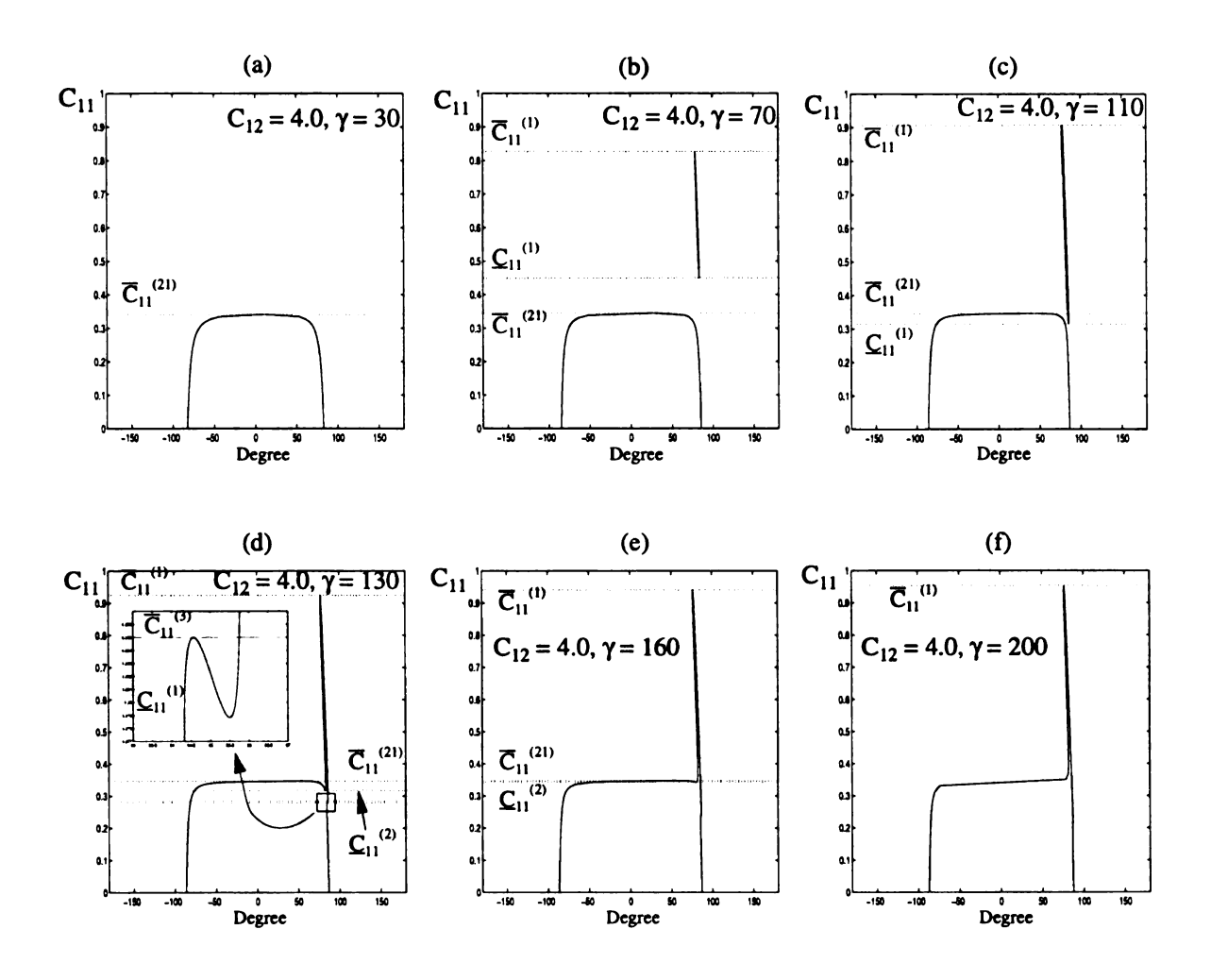


Figure 35. The evolution of normal direction  $\alpha$  of the surfaces of the weak discontinuity along well-drillings at fixed  $(C_{12},\gamma)$ . The six separate subfigures all correspond to  $C_{12} = 4.0$ , and to six separate values of  $\gamma$ . These subfigures correspond to the six dashed lines in Figure 33.

## 3.10. Orientation of the Discontinuity Surface at First Loss of Ellipticity

According to the results of the previous section, the only significant deviation from  $\alpha$  near  $\pm 90^{\circ}$  will typically only occur near the first loss of ellipticity. Accordingly, in this section, we examine the normal direction of the surface of weak discontinuity when it is first initiated. The triplets  $(C_{11}, C_{12}, \gamma)$  that are associated with this situation are those that form part of the global plane strain ellipticity boundary, across which the first occurrence of loss of GPSE takes place in the deformation process. For the purposes of this section we

consider deformation corresponding to the well-drilling process: decrease of  $C_{11}$  at fixed  $C_{12}$ . The set of these triplets, denoted by  $\mathcal{B}^{(1)}$ :  $\hat{C}_{11}^{(1)} = \hat{C}_{11}^{(1)}(C_{12}, \gamma)$  for  $(C_{12}, \gamma) \in \Sigma$ , is given by

$$\begin{split} \hat{C}_{11} &= \overline{C}_{11}^{(1)}(C_{12}, \gamma) & \text{for } (0 \leq C_{12} < C_{12}^{(1)}) \text{ or } (C_{12} > C_{12}^{(1)}) \text{ and } \gamma > \Gamma^{(1)}(C_{12})), \\ \hat{C}_{11} &= \overline{C}_{11}^{(2)}(C_{12}, \gamma) & \text{for } C_{12}^{(1)} < C_{12} < C_{12}^{(2)} \text{ and } 1/2 < \gamma < \Gamma^{(1)}(C_{12}), \\ \hat{C}_{11} &= \overline{C}_{11}^{(21)}(C_{12}, \gamma) & \text{for } C_{12} \geq C_{12}^{(2)} \text{ and } 1/2 < \gamma < \Gamma^{(1)}(C_{12}). \end{split}$$
(3.10.1)

It is to be noted that  $\hat{C}_{11}^{(1)} = \hat{C}_{11}^{(1)}(C_{12}, \gamma)$  is discontinuous across  $I^{(1)}(C_{12}, \gamma)$ . Projecting to the  $(C_{12}, \gamma)$ -plane, this discontinuity occurs across  $\Gamma^{(1)}(C_{12})$ . The double real roots  $x^*$  to the equation  $P(x, \hat{C}_{11}^{(1)}, C_{12}, \gamma) = 0$  can be obtained by solving the simultaneous equations (3.6.4) using a numerical root searcher at the values  $\hat{C}_{11}^{(1)}$  as determined by the methodology outlined in section 3.7. The normal directions associated with the triplets given by (3.10.1) are then measured by angles  $\alpha$  in the  $(X_1, X_2)$ -plane from the  $X_1$ -axis to the normal direction, and the angle  $\alpha$  is given by  $\alpha = \tan^{-1}(x^*)$ . The angle  $\alpha$  is positive if it is the result of a right hand rotation about  $X_3$ -axis, and vice versa.

Figure 36, plotted in the  $(C_{12},\gamma)$ -plane, shows the angle  $\alpha$  in degrees for  $(C_{12},\gamma) \in \Sigma$ . All these angles  $\alpha$  are positive except those for triplets  $(C_{11}, C_{12}, \gamma)$  along either  $C_{12} = 0$  or  $\gamma = 1/2$ , where  $\alpha = 0$  as discussed previously. We find that  $\alpha = 0$  as  $C_{12} \to \infty$  and  $\alpha = \tan^{-1}(C_{12})$  as  $\gamma \to \infty$ , these results will be verified later in section 3.12.

Regardless the rigid body rotation  $\mathbf{R}$ , the normal direction  $\alpha$  can be mapped to the deformed material configuration by using  $\mathbf{U}$  given in (3.2.10) to obtain  $\alpha$ 's deformed counterpart  $\hat{\alpha}$ . The corresponding angles  $\hat{\alpha}$  are plotted in Figure 37.

Recall that the deformed fiber direction  $\phi$  is given by (3.2.11). For triplets (C<sub>11</sub>, C<sub>12</sub>,  $\gamma$ ) on  $\mathcal{B}^{(1)}$  given by (3.10.1), one obtains directly from (3.2.11) that  $\phi$  is always positive.

The positive direction of  $\phi$  is similarly defined as that for  $\alpha$ . Figure 38 plots the angles  $\phi$  and Figure 39 plots the angles  $(\hat{\alpha}-\phi)$ , that is, the normal direction of the surface of weak discontinuity with respect to deformed fiber. It is to be noted that  $\hat{\alpha}-\phi$ , being a difference of directions in the deformed configuration is, in fact, independent of the choice of **F=RU** used for obtaining the deformed counterpart.

An interesting question concerns the maximum value of  $\hat{\alpha}$ - $\phi$  on the global plane strain ellipticity boundary  $\mathcal{B}$ . Figure 39, for example, shows a 27° contour. Here it is important to realize that the values given on Figure 39 are associated with only the portion of  $\mathcal{B}$  corresponding to the largest  $C_{11}$  at fixed  $(C_{12},\gamma)$ . For comparison,  $\mathcal{P}$ =(0.3883,2,17.0815) which locates the unique quadruple root of (3.6.4)<sub>1</sub> is on  $\mathcal{B}$  but is not on  $\mathcal{B}_1$  and so is not represented on Figure 36-Figure 39. We find at  $\mathcal{P}$ =(0.3883,2,17.0815) that x = 2.5754, so that  $\hat{\alpha}$ - $\phi = 24.9^\circ$ .

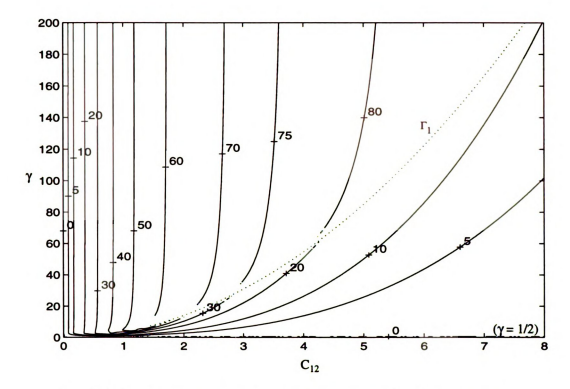


Figure 36. Constant value contours of angle  $\alpha$  (in degree) associated with first contact of  $\mathcal{B}$  by decreasing  $C_{11}$  from 1 at fixed  $(C_{12}, \gamma)$ . This gives the orientation of the discontinuity surface in the reference configuration. The contours are discontinuous across  $\Gamma^{(1)}$ , the projection of the  $\Gamma^{(1)}$  vertical tangency curve associated with the termination of the upper branch of  $\mathfrak{B}$ .

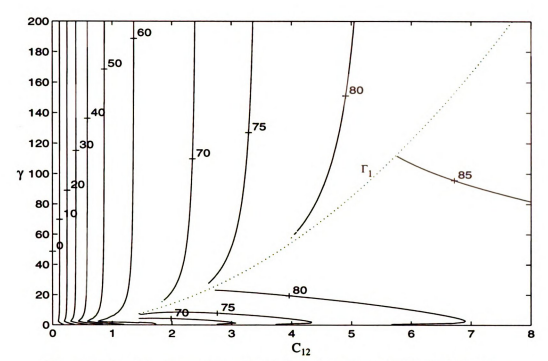


Figure 37. Constant value contours of angle  $\hat{\alpha}$  (in degree) associated with first contact of  $\mathcal{B}$  by decreasing  $C_{11}$  from 1 at fixed  $(C_{12}, \gamma)$ . This gives the orientation of the discontinuity surface in the deformed configuration, where the deformation is determined on the basis of the pure part of the polar decomposition.

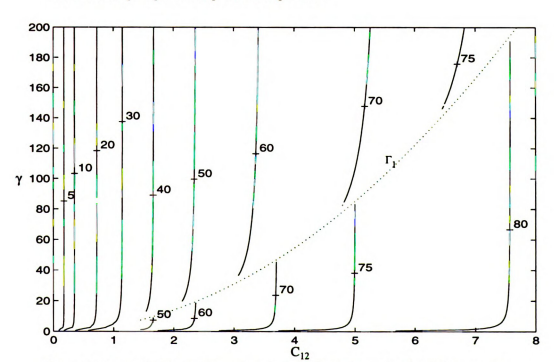


Figure 38. Constant value contours of angle  $\phi$  (in degree) associated with first contact of  $\mathcal{B}$  by decreasing  $C_{11}$  from 1 at fixed  $(C_{12}, \gamma)$ . This gives the orientation of the deformed fibers in the deformed configuration, where the deformation is determined on the basis of the pure part of the polar decomposition.

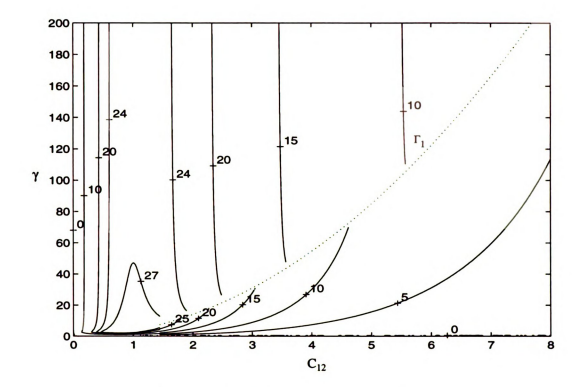


Figure 39. Constant value contours of angle  $\hat{\alpha}$  -  $\phi$  (in degree) associated with first conact of  $\mathcal{B}$  by decreasing  $C_{11}$  from 1 at fixed  $(C_{12}, \gamma)$ . This gives the angle between the deformed fiber direction and the normal to the discontinuity surface in the deformed configuration. This difference angle is independent of the choice of F used for describing the deformed configuration.

#### 3.11. Cross Sections of Sat Fixed y

Six cross sections of the manifold S at fixed  $\gamma$  are plotted here to illustrate the evolution of S with increasing  $\gamma$ . The six values of  $\gamma$ . 5, 10, 20, 50, 100, 200 were chosen for this purpose. Since  $\gamma$  is the sole parameter defining the material, each cross-section gives the loss of ellipticity boundary for a fixed material. It is to be noted that

$$5 < \gamma^{(1)} < 10 < \gamma^{(2)} < \gamma^{(3)} < \gamma^{(4)} < 20 < \gamma^{(5)} < \gamma^{(6)} < 50. \tag{3.11.1}$$

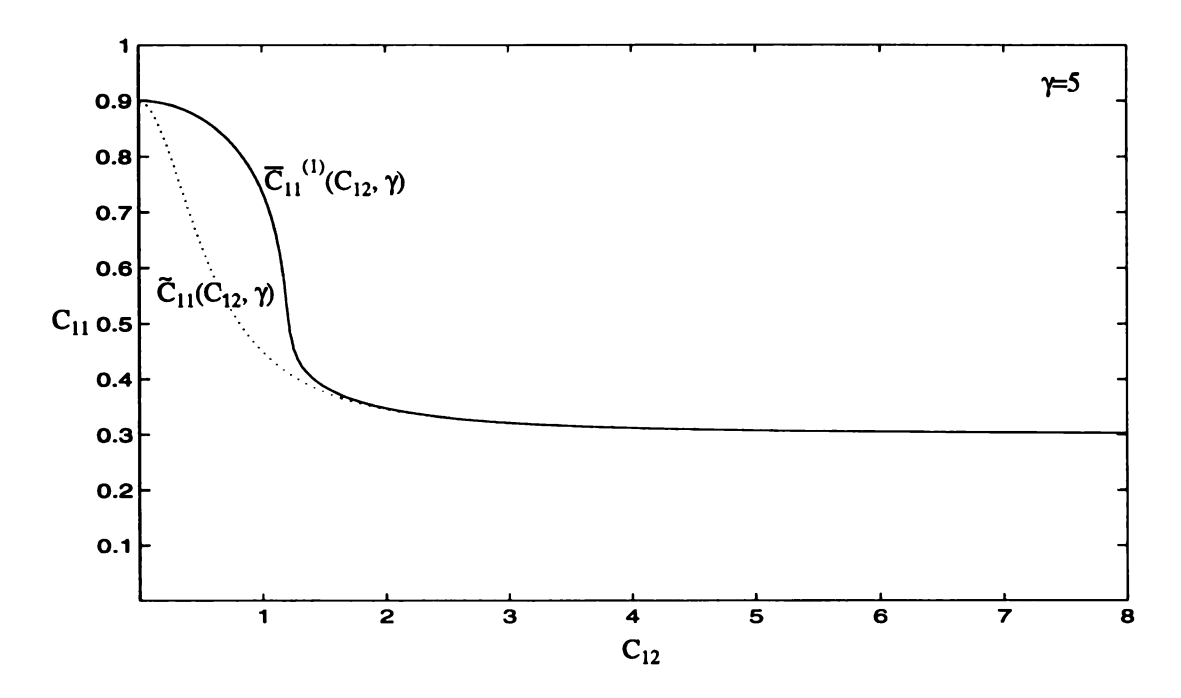


Figure 40. Cross section of S for  $\gamma = 5$ , showing the global plane strain ellipticity boundary B, is typical of  $\gamma$  values obeying  $\gamma < \gamma^{(1)} \equiv 7.4009$ . The dotted line shows the cross section of the surface previously given in Figure 23, which is now interior to the loss of ellipticity region.

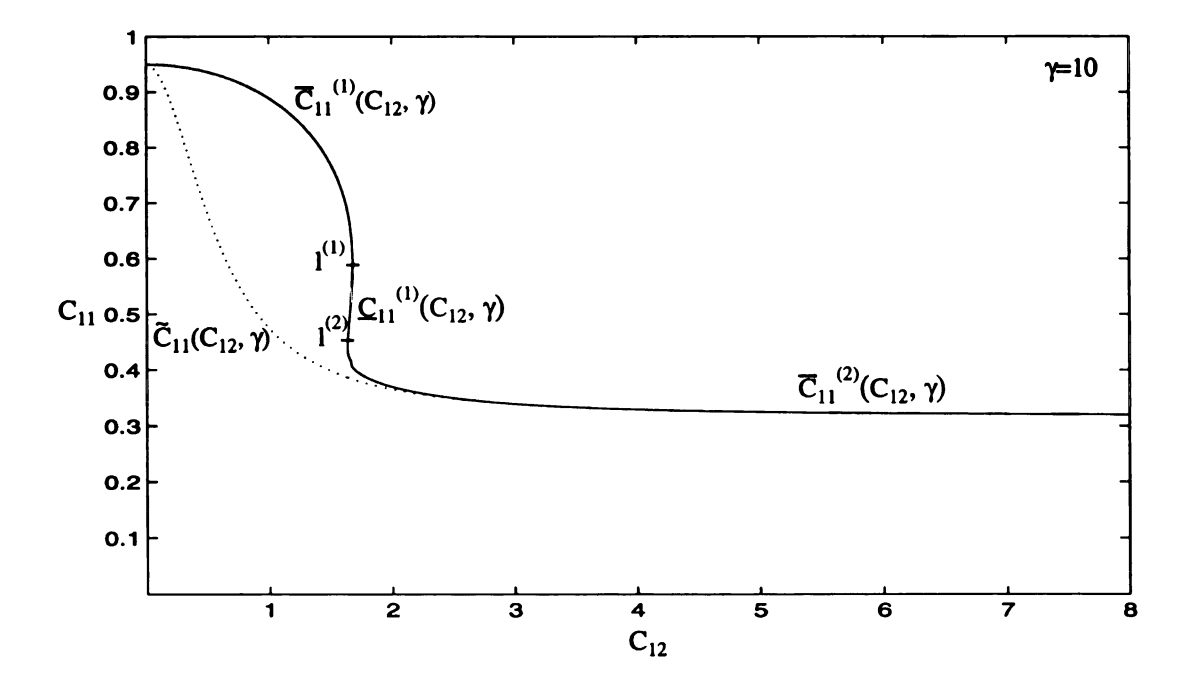


Figure 41. Cross section of S for  $\gamma = 10$ , showing the global plane strain ellipticity boundary B, is typical of  $\gamma$  values obeying  $\gamma^{(1)} \equiv 7.4009 < \gamma < \gamma^{(2)} \equiv 17.0815$ . The dotted line shows the cross section of the surface previously given in Figure 23 and will no longer be plotted in the future figures for S at constant  $\gamma$ . The value of  $\gamma = 10$  gives correlation to the boron/epoxy composite discussed in subsection 2.4.2.

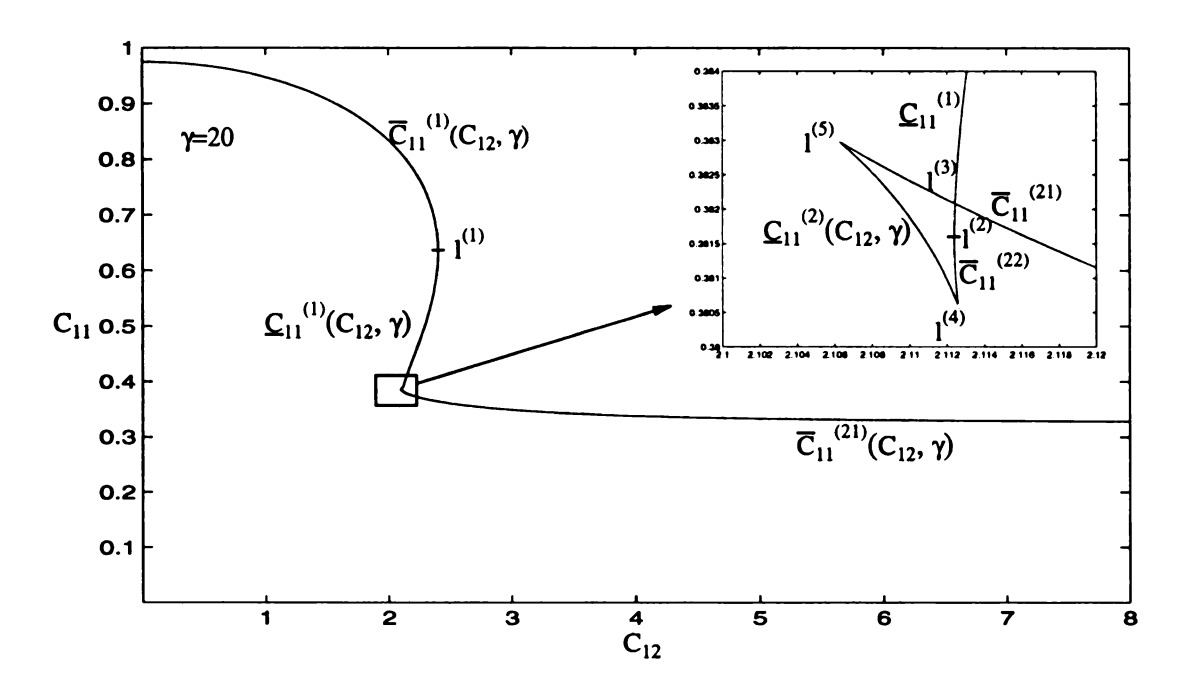


Figure 42. Cross section of S for  $\gamma = 20$  is typical of  $\gamma$  values obeying  $\gamma^{(4)} \equiv 19.521 < \gamma < \gamma^{(5)} \equiv 20.47$ . The unfolding of S has already taken place. Points on the internal branches created by this unfolding are members of S but not members of S. Triplets  $(C_{11}, C_{12}, \gamma)$  within the triangular region have 4 real roots to  $(3.6.4)_1$ . Points  $I^{(1)}$  and  $I^{(2)}$  are locations of vertical tangency, cusp points  $I^{(4)}$  and  $I^{(5)}$  are triple roots of  $(3.6.4)_1$  and self intersection point  $I^{(3)}$  gives a pair of double root real roots to  $(3.6.4)_1$ .

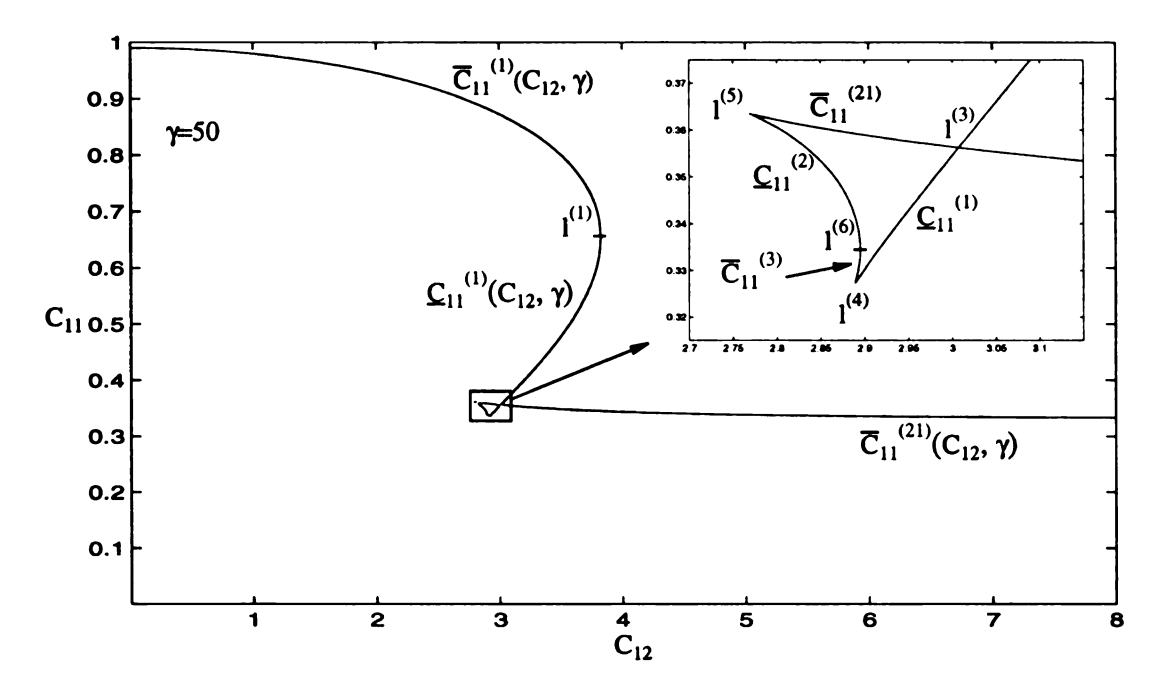


Figure 43. Cross section of S for  $\gamma = 50$  is typical of  $\gamma$  values obeying  $\gamma > \gamma^{(6)} = 24.3891$ . The unfolding of S has further developed. In particular the former vertical tangency point  $l^{(2)}$  has transferred to a different branch in the guise of point  $l^{(6)}$ .

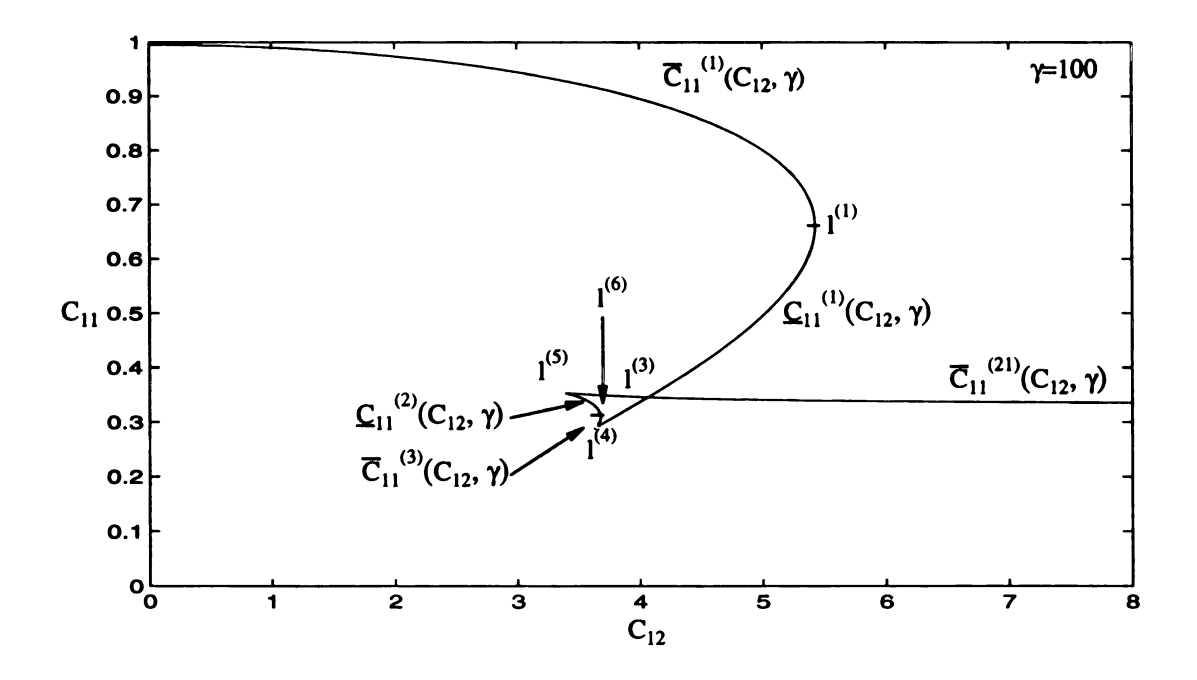


Figure 44. Another typical cross section of S for  $\gamma$  values obeying  $\gamma > \gamma^{(6)}$ . The unfolding of S is now well developed. A value of  $\gamma$  at this order of magnitude is not uncommon in fiber reinforced materials.

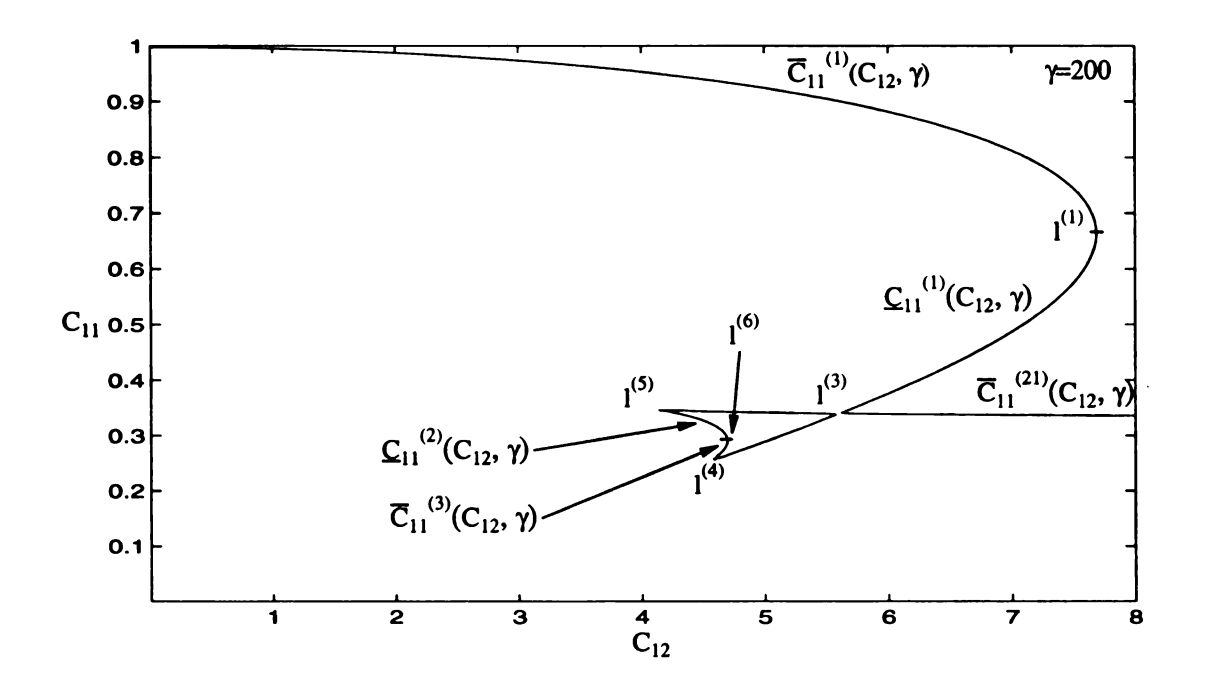


Figure 45. Cross section of S for even larger  $\gamma$ . For this  $\gamma$  value and practical values of  $C_{12}$ , loss of ellipticity takes place at  $C_{11}$  very close to 1.

### 3.12. Asymptotic Properties of the Global Plane Strain Ellipticity Boundary

Although the manifold S as given by the values  $\hat{C}_{11}(C_{12}, \gamma)$  for  $(C_{12}, \gamma) \in \Sigma$  are not determined explicitly by the numerical procedure that generated Figure 25-Figure 33 and Figure 40-Figure 45, the asymptotic form of S can be found by an explicit analysis of (3.6.4) using (3.5.1)-(3.5.4) as we now show. With respect to the octant  $C_{11} > 0$ ,  $C_{12} \ge 0$ ,  $\gamma \ge 0$  we have in section 3.7 shown that S is given by  $C_{11} = 1 - 1/2\gamma$  when  $C_{12} = 0$ , whereas in EII it was shown that S does not intersect  $\gamma = 0$ . Here we complete the analysis of the boundaries of this octant by considering the separate special cases  $C_{11} \rightarrow 0$ ,  $C_{12} \rightarrow \infty$  and  $\gamma \rightarrow \infty$  (since EI ensures ellipticity for  $C_{11} \ge 0$  there is no need to consider  $C_{11} \rightarrow \infty$ ).

(i)  $C_{11} = 0$ . In this case, equation (3.5.4) in conjunction with (3.5.1) becomes

$$(x^2 - 2\gamma + 1)(C_{12}^2 + 1) = 0. (3.12.1)$$

The global plane strain ellipticity requirement that (3.5.4) has no real root is met if and only if

$$\gamma < \frac{1}{2}$$
, when  $C_{11} = 0$ . (3.12.2)

This result is not in contradiction to the previous result discussed in (EII), since there we consider only  $C_{11}>0$ . This confirms that the global plane strain ellipticity boundary encounters the plane  $C_{11}=0$  along the line  $\gamma=1/2$ , where equation (3.12.1) has double real root x=0.

(ii)  $C_{12} \to \infty$  at fixed  $\gamma$ . To analyze the asymptotic form of S as  $C_{12} \to \infty$ , we rewrite equations (3.6.4) in full as

$$P(x, C_{11}, C_{12}, \gamma) = C_{12}^{2} \{x^{2} + 2\gamma(3C_{11} - 1) + 1\}$$

$$- C_{12} \{2C_{11}x[x^{2} + 2\gamma(3C_{11} - 1) + 1]\}$$

$$+ (C_{11}^{2}x^{2} + 1)\{x^{2} + 2\gamma(3C_{11} - 1) + 1\} - 4\gamma C_{11} = 0,$$
(3.12.3)

and

$$\frac{\partial}{\partial x}P(x,C_{11},C_{12},\gamma) = 2C_{12}^2x - C_{12}\{2C_{11}[x^2 + 2\gamma(3C_{11} - 1) + 1] + 4C_{11}x^2\}$$

$$2C_{11}^2x[x^2 + 2\gamma(3C_{11} - 1) + 1] + 2x(C_{11}^2x^2 + 1) = 0.$$
(3.12.4)

Neglecting  $O(C_{12})$  in (3.12.3) and (3.12.4) gives that the dominant balance equations as  $C_{12} \rightarrow \infty$  are

$$x^2 + 2\gamma(3C_{11} - 1) + 1 = 0$$
 and  $x = 0$ . (3.12.5)

Thus one obtains that

$$C_{11} \sim \frac{1}{3} \left( 1 - \frac{1}{2\gamma} \right)$$
 and  $x \sim 0$  as  $C_{12} \to \infty$ . (3.12.6)

For the next order correction, let

$$C_{11} = \frac{1}{3} \left( 1 - \frac{1}{2\gamma} \right) + C_{11}^{\Delta}.$$
 (3.12.7)

Expanding the left hand sides of equations  $P\left(x, \frac{1}{3}\left(1 - \frac{1}{2\gamma}\right) + C_{11}^{\Delta}, C_{12}, \gamma\right) = 0$  and  $\frac{\partial}{\partial x}P\left(x, \frac{1}{3}\left(1 - \frac{1}{2\gamma}\right) + C_{11}^{\Delta}, C_{12}, \gamma\right) = 0$  in the Taylor's series to the first order near x = 0 and  $C_{11}^{\Delta} = 0$ , gives

$$2\gamma - 1 - 9C_{12}^{2}\gamma C_{11}^{\Delta} = 0,$$

$$C_{12}^{2}x - (2\gamma - 1)C_{12}C_{11}^{\Delta} = 0.$$
(3.12.8)

Equation (3.12.8)<sub>1</sub> yields  $C_{11}^{\Delta} = \frac{2\gamma - 1}{9\gamma C_{12}^2}$ , which, in conjunction with (3.12.7) and (3.12.8)<sub>2</sub> gives

$$C_{11} = \frac{1}{3} \left( 1 - \frac{1}{2\gamma} \right) + \frac{2\gamma - 1}{9\gamma C_{12}^2} + o(C_{12}^{-2})$$
 and  $x = \frac{(2\gamma - 1)^2}{9\gamma C_{12}^3} + o(C_{12}^{-3})$  (3.12.9)

as  $C_{12} \to \infty$ . This also verifies the consistency of the procedure and delivers the horizontal asymptotes seen in Figure 40-Figure 45. Notice that  $x \to 0$  as  $C_{12} \to \infty$  implies  $\alpha \to 0$  which is consistent with Figure 36. The leading order behavior of  $C_{11}$  as  $C_{12} \to \infty$  yields the same asymptote as that given by (3.6.1) which, not surprisingly, followed from the direct consideration of x=0.

(iii)  $\gamma \to \infty$  at fixed  $C_{12}$ . For this case, we rewrite equation (3.6.4) in full as

$$P(x, C_{11}, C_{12}, \gamma) = \gamma \{2(3C_{11} - 1)[(C_{11}x - C_{12})^2 + 1] - 4C_{11}\} + (x^2 + 1)[(C_{11}x - C_{12})^2 + 1] = 0,$$
(3.12.10)

and

$$\frac{\partial}{\partial x} P(x, C_{11}, C_{12}, \gamma) = \gamma \{4(3C_{11} - 1)C_{11}(C_{11}x - C_{12})\} 
+2x[(C_{11}x - C_{12})^2 + 1] + 2(x^2 + 1)C_{11}(C_{11}x - C_{12}) = 0.$$
(3.12.11)

Neglecting  $O(\gamma^0)$ , one obtains the dominant balance equations

$$(3C_{11}-1)(C_{11}x-C_{12})^2+C_{11}-1=0,$$
  

$$(3C_{11}-1)(C_{11}x-C_{12})=0.$$
(3.12.12)

Equation (3.12.12) indicates that

$$C_{11} \sim 1$$
 and  $x \sim C_{12}$  as  $\gamma \rightarrow \infty$ . (3.12.13)

For the next order correction, let

$$C_{11} = 1 + C_{11}^{\Delta}$$
 and  $x = C_{12} + x^{\Delta}$ . (3.12.14)

Expanding the left hand sides of equations  $P(C_{12} + x^{\Delta}, 1 + C_{11}^{\Delta}, C_{12}, \gamma) = 0$  and  $\frac{\partial}{\partial x}P(C_{12} + x^{\Delta}, 1 + C_{11}^{\Delta}, C_{12}, \gamma) = 0$  in a Taylor's series to the first order near  $x^{\Delta} = 0$  and  $C_{11}^{\Delta} = 0$ , gives

$$1 + C_{12}^{2} + 2C_{12}x^{\Delta} + 2\gamma C_{11}^{\Delta} = 0,$$

$$C_{12} + 4\gamma x^{\Delta} + 4\gamma C_{12}C_{11}^{\Delta} = 0.$$
(3.12.15)

Solving equations  $(3.12.15)_{1,2}$  one obtains

$$C_{11}^{\Delta} = -\frac{1 + C_{12}^2}{2\gamma} + o(\gamma^{-1})$$
 and  $x^{\Delta} = \frac{C_{12}(1 + 2C_{12}^2)}{4\gamma} + o(\gamma^{-1}),$  (3.12.16)

as  $\gamma \to \infty$ . This verifies the consistency of the procedure, which, in summary, gives

$$C_{11} = 1 - \frac{1 + C_{12}^2}{2\gamma} + o(\gamma^{-1}), \qquad x = C_{12} + \frac{C_{12}(1 + 2C_{12}^2)}{4\gamma} + o(\gamma^{-1})$$
 (3.12.17)

as  $\gamma \to \infty$ . Hence  $\alpha \to tan$  ' $(C_{12})$  as  $\gamma \to \infty$ , corresponding to the eventual straight vertical nature of the constant  $\alpha$  curves in Figure 36. The asymptote  $C_{11} \sim 1$  as  $\gamma \to \infty$  is consistent with Figure 25-Figure 33. Since x does not approach 0, the asymptote  $C_{11} \sim 1$  does not match the  $\gamma \to \infty$  asymptotic value for  $C_{11}$  in Figure 23.

# 3.13. Ellipticity under Special Deformations

We now turn to examine the possible loss of global plane strain ellipticity under certain plane deformations.

#### Simple Shear

For simple shear in the fiber direction, the deformation gradient tensor is given by (2.3.12) with i = 1 and j = 2. The right Cauchy-Green strain tensor is then given by

$$\mathbf{C} = \begin{bmatrix} 1 & k & 0 \\ k & 1 + k^2 & 0 \\ 0 & 0 & 1 \end{bmatrix}, \tag{3.13.1}$$

where k is the amount of shear. We have, under this deformation, that  $C_{11} = 1$  and  $C_{12} = k$ . Parametrized in terms of k, the loading path of this deformation can be plotted in the  $(C_{11}, C_{12})$ -plane, as shown in Figure 46. Hence, the material (2.4.1) is elliptic with regard to both the global and the local plane strain criteria.

For simple shear perpendicular to the fiber direction, the deformation gradient tensor is given by (2.3.12) with i = 2 and j = 1, and the right Cauchy-Green strain tensor is given by

$$\mathbf{C} = \begin{bmatrix} 1 + k^2 & k & 0 \\ k & 1 & 0 \\ 0 & 0 & 1 \end{bmatrix}, \tag{3.13.2}$$

where, again, k is the amount of shear. Since under this deformation we have  $C_{11} = 1 + k^2 \ge 1$ , the material (2.4.1) is, again, elliptic, for both types of plane deformations, i.e., global plane strain deformation or local plane strain deformation. Parametrized, again, in terms of k, the loading path of this simple shear perpendicular to the fiber direction is plotted also in Figure 46.

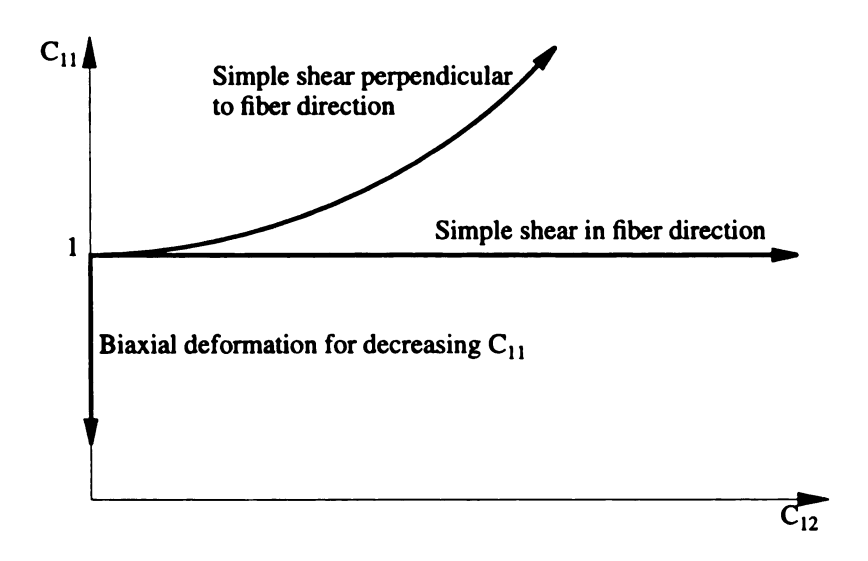


Figure 46. Loading paths for some plane deformations.

#### Biaxial Deformation

For incompressible materials, a plane deformation (2.3.7) in the  $(X_1, X_2)$ -plane is a biaxial deformation if  $C_{12} = 0$ . Following directly from (2.3.10) with the incompressibility constraint (2.3.11), and noting that  $\lambda_1 = C_{11}^{1/2}$ , the right Cauchy-Green strain tensor for this biaxial deformation is rewritten as

$$\mathbf{C} = \begin{bmatrix} \mathbf{C}_{11} & 0 & 0 \\ 0 & \mathbf{C}_{11}^{-1} & 0 \\ 0 & 0 & 1 \end{bmatrix}. \tag{3.13.3}$$

As plotted in Figure 46, the loading path for this deformation goes vertically down with decreasing  $C_{11}$ . According to the discussion in section 3.7, loss of ellipticity (both local and global) takes place, if  $\gamma > 1/2$ , as soon as  $C_{11} \le 1 - 1/2\gamma$ . Since  $C_{11} = \lambda_1^2$  this corresponds to  $\lambda_1 \le \sqrt{1 - 1/2\gamma}$ . It is to be noted from Figure 47 that there is no obvious correlation of loss of ellipticity with the loss of monotonicity phenomena associated with materials obeying  $\gamma > 14.95$  as discussed in (ii) of section 2.4.1.

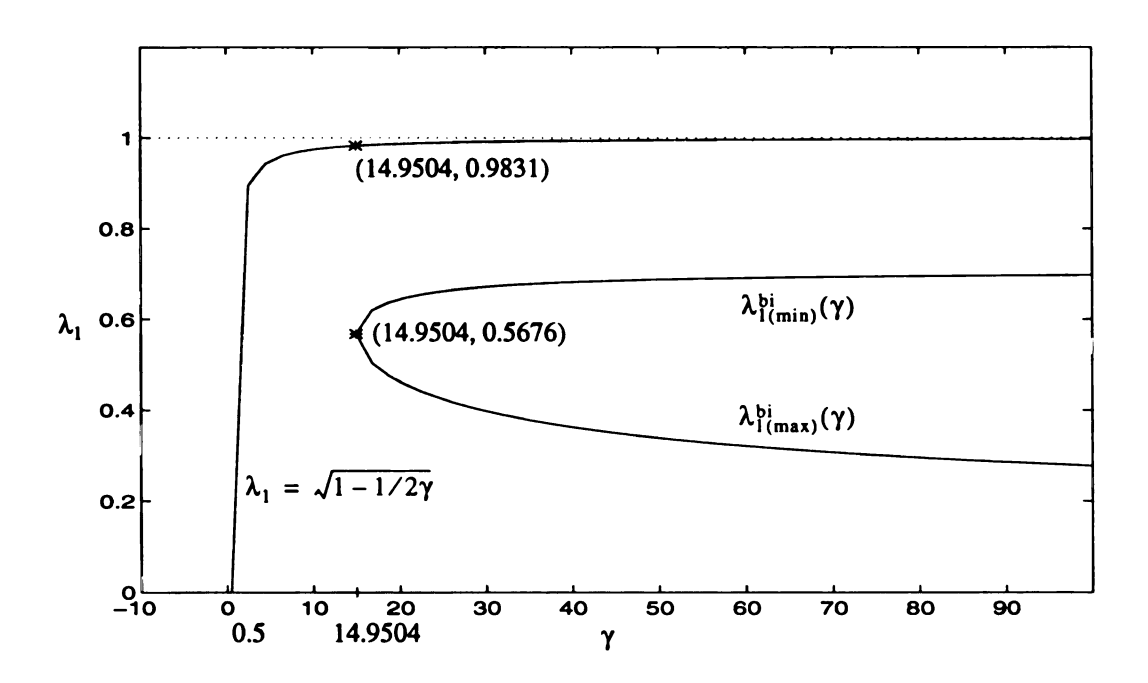


Figure 47. The loss of ellipticity region in biaxial deformation with  $C_{11} < 1$  (where  $C_{11} = \lambda_1^2$  and  $\lambda_1$  is the principal stretch in the fiber direction) is given by  $\lambda_1 < \sqrt{1 - 1/2\gamma}$ . The principal stretches associated with this loss of ellipticity phenomena do not correlate in any obvious way with nonmonotonic stress response for this deformation. The nonmonotonic stress response, in terms of  $\lambda_{1(\max)}^{bi}$  and  $\lambda_{1(\min)}^{bi}$  was used previously in Figure 6.

General simple shear deformation in the  $(X_1, X_2)$ -plane

We now turn to examine the ellipticity under the more general simple shear deformation discussed in section 2.3. It was shown in that section, loss of monotonicity in the shear response curves could be addressed in terms of fiber contraction/relaxation/elongation, as for example shown in Figure 17, which diagramed  $C_{11}$  vs. k, where  $\sqrt{C_{11}}$  gives the fiber stretch and k is the amount of simple shear. To address any relation that this may have with loss of ellipticity it is useful to recast Figure 17 as a diagram of  $C_{11}$  vs.  $C_{12}$ , since this is the deformation space in which we have determined loss of ellipticity phenomena (in terms of  $\gamma$ ). One finds that Figure 17 correlates with Figure 48. In Figure 48, the  $\psi = 0$  curve corresponds to simple shear in the fiber direction and the  $\psi = \pi/2$  curve is the  $k \rightarrow -k$  image of the curve for simple shear perpendicular to the fiber direction as shown previously in Figure 46. As discussed above, neither of these curves involves  $C_{11} < 1$ . Note from Figure 48 that if  $0 < \psi < \pi/4$ , then  $C_{12}$  first increases and then decreases with k, whereas  $C_{12}$  is monotonically decreasing with k if  $\pi/4 < \psi < \pi/2$ . One finds that  $C_{12}$  is again zero for  $k = 2 \cot 2\psi$ , corresponding to fiber rotation  $\phi = -(\pi/2 - 2\psi)$ .

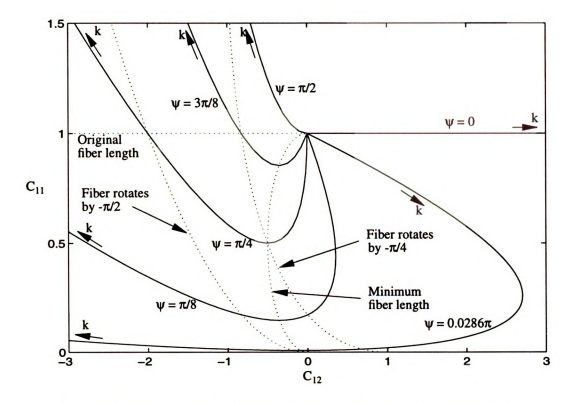


Figure 48. Loading paths for simple shear in various directions with respect to fiber direction ( $\psi$  is in radian). The fiber is rotated by  $\pi t/4$  as  $k = 1/(sin^2\psi + cos\psi sin\psi)$ , and the fiber is rotated by  $\pi t/2$  as  $k = 1/(cos\psi sin\psi)$ . The minimum deformed fiber length occurs at  $k = cot\psi$ , corresponding to  $C_{11} = sin^2\psi$  and  $\phi = -(\pi/2 - \psi)$ . Hence the fiber relaxes back to its original length for  $cot\psi < k < 2cot\psi$  corresponding to  $-(\pi/2 - \psi) < \phi < -\pi + 2\psi$ .

Since the general simple shear curves for  $0 < \psi < \pi/2$  involve a regime of fiber contraction for moderate k, it follows that loss of ellipticity may occur. Figure 49 superposes cross sections of global plane strain ellipticity boundary for various  $\gamma$  in preparation for comparisons with Figure 48. Note in this figure that the cross sections of global plane strain ellipticity boundary are extended into negative values of  $C_{12}$ . Figure 50 then combines general simple shear curves of Figure 48 with the cross section of global plane strain ellipticity boundary for the special value  $\gamma = 10$ . As illustrated in Figure 50, loss of global ellipticity will not occur for  $0.4261\pi < \psi \le \pi/2$  as well as  $\psi = 0$ . Loss of

ellipticity and recovery of ellipticity, in turn, will take place with increasing k for  $0 < \psi \le 0.4261\pi$ . Furthermore, loss of ellipticity-recovery of ellipticity will take place twice for  $0.0168\pi \le \psi < 0.0423\pi$ .

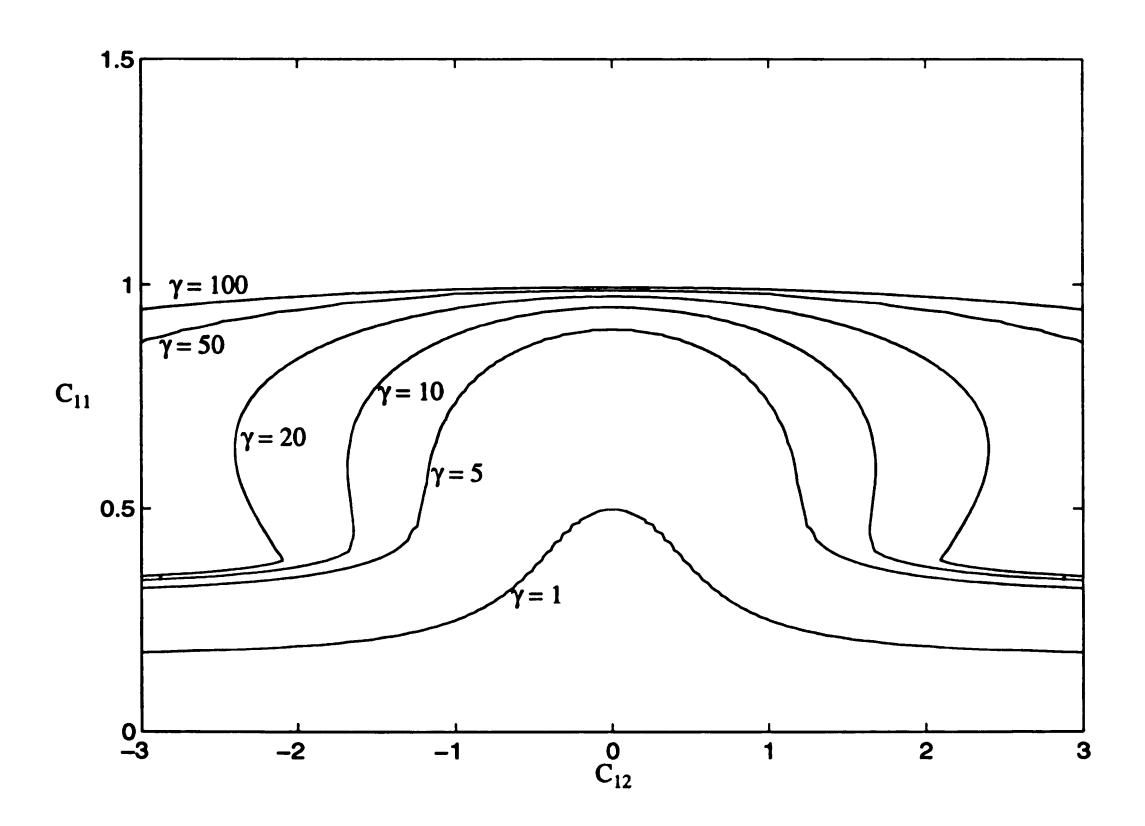


Figure 49. The cross sections of the global plane strain ellipticity boundary for  $\gamma = 1, 5, 10, 20, 50$  and 100. Here, unlike Figure 40-Figure 45, the global plane strain ellipticity boundary is shown for both positive and negative  $C_{12}$  in order to aid comparison with Figure 48.

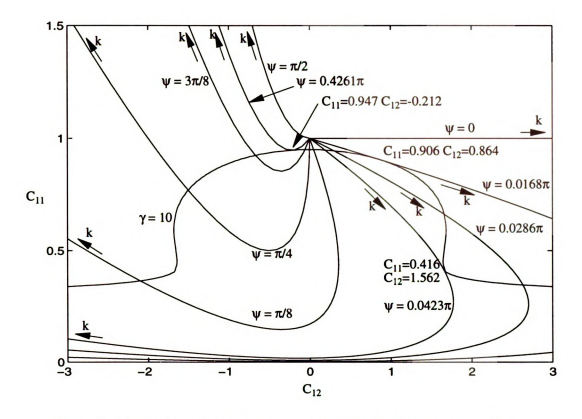


Figure 50. Loading paths for simple shear in various directions with respect to fiber direction ( $\psi$  is in radian). The cross section of  $\mathcal{S}$  for  $\gamma = 10$  is also plotted here. For  $\gamma = 10$  material, simple shear with  $0 < \psi \le 1.3385$  involves loss of global plane strain ellipticity.

For this  $\gamma=10$  material, Figure 51 gives the shear stress response function for some of the original fiber orientation  $\psi$  shown in Figure 50. In this respect the figure is similar to Figure 20 of section 2.4. However, now the loss of ellipticity portions of the response curves are shown in dot lines. It is clear that loss of ellipticity has no explicit correlation with loss of monotonicity of the stress response. Finally, Figure 52 is the counterpart to Figure 21 in that it displays the locations in the (C<sub>11</sub>, C<sub>12</sub>)-plane corresponding to  $k_{max}$  and  $k_{min}$  for the  $\gamma=10$  material, together with the deformation paths and the loss of ellipticity region (in shading).

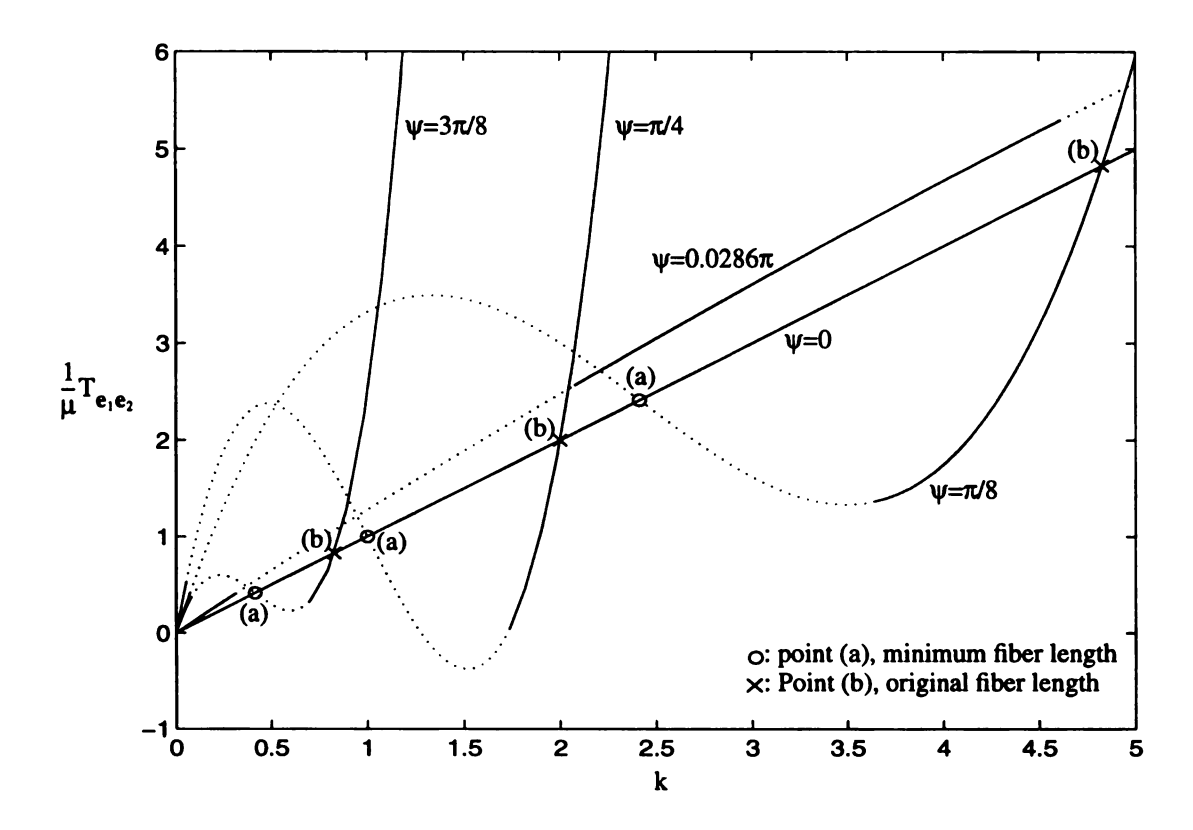


Figure 51. Shear stress  $T_{e_1e_2}/\mu$  in (2.4.51) ((2.4.47)) varies with simple shear k for a material with  $\gamma=10$  and various fiber orientations  $\psi$  with respect to the direction of shearing. As in Figure 20, the fibers contract from the origin to the point marked (a), and then relax back to their original length between points (a) and (b). From point (b) onwards the fibers continue their elongation. In this figure the region of the curve corresponding to loss of ellipticity is shown in dotted line.

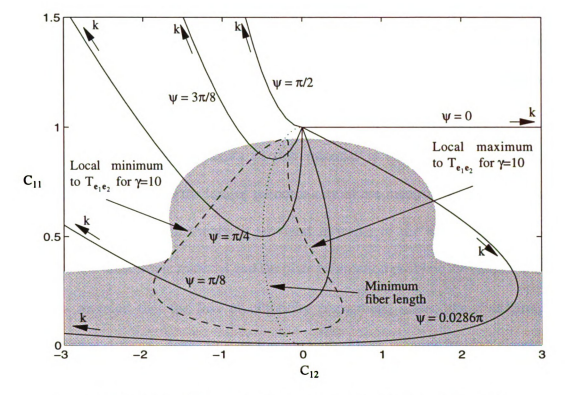


Figure 52. Loading paths for simple shear in various directions with respect to fiber direction ( $\psi$  is in radian). Points on the loading paths associated with  $k_{max}$  and  $k_{min}$  are also plotted (see Figure 21), as is the loss of global plane strain ellipticity region (in shadow).

# 4. Summary and Conclusion

A model for incompressible finitely deformable materials with fiber reinforcements is established. The engineering significance of this material model is verified since it fits well with real material data.

The fully nonlinear responses of this material is discussed for a number of important deformations, and the loss of monotonicity of the material response is studied. The correlation to the linear theory is provided in terms of the elastic constants. The ellipticity of this anisotropic material and the plate bifurcation problem are further studied.

It is revealed that the loss of ellipticity phenomena under planar deformation involve different patterns, depending on loading path. These patterns involve simple loss of ellipticity, loss-recover-loss of ellipticity, and primary loss-secondary loss of ellipticity. The geometry of the ellipticity boundary is made clear. The discussion on the directions of the weak discontinuity surfaces is also presented.

Finally, it is concluded that there is no explicit correlation between loss of ellipticity and loss of monotonicity of the stress response, and no explicit correlation between loss of ellipticity and bifurcation.

The buckling problem presented in Appendix B is, by its own right, an interesting research topic, including the research aspects as: complete buckled solutions for bifurcation conditions (B.1), (B.1) and (B.1), the number of the buckled solutions, the asymptotic behaviors of the buckled solutions for large values of parameters  $\gamma$  and  $\eta$ , as well as the ordering of the buckling loads.

# Appendix A: Algebraic Root Analysis of the Characteristic Polynomial

Since the characteristic polynomial (3.5.1) is of degree 4 in x, it follows that its roots can be expressed in terms of radicals of the polynomial coefficients. In this appendix we present certain aspects behind this process that enable us to determine properties of S, which, we recall, is the locus in the  $(C_{11}, C_{12}, \gamma)$ -space associated with double real roots to the characteristic polynomial.

#### A.1 General Algebraic Procedures upon the Quartic Polynomial

By applying the linear transformation of the independent variables

$$x = y - \frac{1}{4}a_1 = y + \frac{C_{12}}{2C_{11}},$$
 (A.1)

and eliminating the common factor  $C_{11}^2$  ( $C_{11}>0$  (3.2.5)<sub>1</sub>), the polynomial P(x,  $C_{11}$ ,  $C_{12}$ ,  $\gamma$ ) given in (3.5.2), (3.5.3) is written as

$$\bar{P}(y, C_{11}, C_{12}, \gamma) \equiv y^4 + b_2 y^2 + b_3 y + b_4, \tag{A.1}$$

where

$$b_2 \equiv b_2(C_{11}, C_{12}) = -\frac{3}{8}a_1^2 + a_2,$$

$$b_3 \equiv b_3(C_{11}, C_{12}, \gamma) = -\frac{1}{8}a_1^3 + \frac{1}{2}a_1a_2 - a_3,$$

$$b_4 \equiv b_4(C_{11}, C_{12}, \gamma) = -\frac{3}{256}a_1^4 + \frac{1}{16}a_1^2a_2 - \frac{1}{4}a_1a_3 + a_4.$$
(A.1)

This linear transformation will not change the nature of the roots of  $P(x, C_{11}, C_{12}, \gamma)$ . That is, if y is a complex (real) root of equation

$$\bar{P}(y, C_{11}, C_{12}, \gamma) = 0$$
 (A.1)

then x given by (A.1) is a complex (real) root of  $P(x, C_{11}, C_{12}, \gamma)$ , and if y is a double root, then x given by (A.1) is also a double root, etc., and vice versa.

If  $b_3 = 0$ , polynomial (A.1) is factored as

$$\bar{P}(y, C_{11}, C_{12}, \gamma) = \left(y^2 + \frac{1}{2}b_2 - \sqrt{\frac{1}{4}b_2^2 - b_4}\right) \left(y^2 + \frac{1}{2}b_2 + \sqrt{\frac{1}{4}b_2^2 - b_4}\right),$$
for  $b_3 = 0$ . (A.1)

Its four roots are given by

$$y_{1} = \sqrt{-\frac{1}{2}b_{2} + \sqrt{\frac{1}{4}b_{2}^{2} - b_{4}}}, y_{2} = -\sqrt{-\frac{1}{2}b_{2} + \sqrt{\frac{1}{4}b_{2}^{2} - b_{4}}}, (A.1)$$

$$y_{3} = \sqrt{-\frac{1}{2}b_{2} - \sqrt{\frac{1}{4}b_{2}^{2} - b_{4}}}, y_{4} = -\sqrt{-\frac{1}{2}b_{2} - \sqrt{\frac{1}{4}b_{2}^{2} - b_{4}}}.$$

If  $b_3 \neq 0$ , then, following the standard solution procedure (refer to [Kurosh 1980]), the four roots of polynomial (A.1) are given by

$$y_{1} \equiv y_{1}(\tilde{z}) = \frac{1}{\sqrt{2}}(\sqrt{\tilde{z}} + \sqrt{\Delta_{1}}), \qquad y_{2} \equiv y_{2}(\tilde{z}) = \frac{1}{\sqrt{2}}(\sqrt{\tilde{z}} - \sqrt{\Delta_{1}}),$$

$$y_{3} \equiv y_{3}(\tilde{z}) = \frac{1}{\sqrt{2}}(-\sqrt{\tilde{z}} + \sqrt{\Delta_{2}}), \qquad y_{4} \equiv y_{4}(\tilde{z}) = \frac{1}{\sqrt{2}}(-\sqrt{\tilde{z}} - \sqrt{\Delta_{2}}),$$
(A.1)

where

$$\Delta_1(\tilde{z}) = -\tilde{z} - b_2 - \frac{b_3}{\sqrt{2\tilde{z}}}, \qquad \Delta_2(\tilde{z}) = -\tilde{z} - b_2 + \frac{b_3}{\sqrt{2\tilde{z}}}.$$
(A.1)

Here  $\tilde{z}$  is any one root obtained from equation

$$z^{3} + b_{2}z^{2} + \left(\frac{1}{4}b_{2}^{2} - b_{4}\right)z - \frac{1}{8}b_{3}^{2} = 0.$$
 (A.1)

The three roots of equation (A.1), denoted by  $z_1$ ,  $z_2$  and  $z_3$ , can be obtained again by

following a standard procedure for cubic polynomials as discussed in [Kurosh 1980], for example. Equation (A.1) has a root z = 0 if and only if  $b_3 = 0$ , and in this case  $\{y_1, y_2, y_3, y_4\}$  are given by (A.1).

#### A.2 Criteria for Double Real Roots

It follows from the theory of cubic equations [Kurosh 1980 p228] that equation (A.1) has a double (real) root if and only if

$$\vartheta(C_{11}, C_{12}, \gamma) \equiv 27\xi_1^2 + 4\xi_2^3 = 0, \tag{A.1}$$

where

$$\xi_1(C_{11}, C_{12}, \gamma) = -\frac{b_2^3}{108} + \frac{b_2b_4}{3} - \frac{b_3^2}{8}, \qquad \xi_2(C_{11}, C_{12}, \gamma) = -\frac{b_2^2}{12} - b_4.$$
 (A.1)

It is found that equation (A.1) has double real root if and only if equation (A.1) has double root. In fact, if  $z_1$  and  $z_2$  are distinct roots of (A.1), then examination of the expressions for the roots of (A.1) as given by say (A.1), reveals that  $y_i(z_1) \neq y_i(z_2)$ , i = 1,2,3,4. Since  $\{y_1(z_1), y_2(z_1), y_3(z_1), y_4(z_1)\}$  and  $\{y_1(z_2), y_2(z_2), y_3(z_2), y_4(z_2)\}$  give the same set of four roots of (A.1), there must be an 1-1 correspondence between these two sets. Without loss of generality, assume that  $y_1(z_1) = y_3(z_2)$ . Now, consider  $z_1 = z_2$  being double roots of (A.1), then  $y_1(z_1) = y_3(z_1)$  are double roots of (A.1). Furthermore, if the double roots  $y_1(z_1) = y_3(z_1)$  are complex, then it is required that  $y_2(z_1) = y_4(z_1)$  and are the complex conjugate. According to the previous discussion, equation (A.1) can only has two pairs of imaginary double roots, and this case is prohibited by (A.1). Inversely, if  $y_1(z_1) = y_3(z_1)$  are double real roots, then by the 1-1 correspondence we have  $y_1(z_1) = y_3(z_2)$ . It is then follows from (A.1) that  $y_3(z_1) = y_3(z_2)$  requires  $z_1 = z_2$  be double roots of (A.1). this procedure can be

exhausted for all the possibilities of the 1-1 correspondence to prove that equation (A.1) has double real root if and only if equation (A.1) has double root. Consequently, S is completely defined by the triplets that satisfy (A.1) which determines a two-dimensional manifold in the  $(C_{11}, C_{12}, \gamma)$ -space.

#### A.3 Criteria for Two Pairs of Double Real Roots

We now examine the situation at which (A.1) has two pairs of double roots. By expanding  $(y-Y_1)^2(y-Y_2)^2$  and comparing the coefficients of the powers of y in the expansion with that in (A.1), one finds that the following simultaneous equations

$$Y_1 + Y_2 = 0,$$
  $2Y_1Y_2 = b_2,$   
 $b_3 = 0,$   $b_2^2 - 4b_4 = 0,$  (A.1)

must be satisfied. Equation  $(A.1)_1$  shows that  $Y_1$  and  $Y_2$  are either both real or both imaginary. Examination of  $b_2$ , which is real, according to  $(A.1)_2$  under the condition that  $b_3$  = 0 reveals that

$$\begin{vmatrix} b_2 |_{b_3 = 0} > 0 & \text{if } 0 \le C_{12} < 2, \\ b_2 |_{b_3 = 0} \le 0 & \text{if } C_{12} \ge 2. \end{vmatrix}$$
 (A.1)

This result, in conjunction with (A.1), shows that if  $C_{12} \ge 2$ , then a  $(Y_1, Y_2)$  double root pair involves real  $Y_1$  and real  $Y_2$  whereas if  $C_{12} < 2$  then a  $(Y_1, Y_2)$  double root pair involves imaginary  $Y_1$  and imaginary  $Y_2$  and so need not concern us further. Hence for  $C_{12} \ge 2$ , equation  $(A.1)_{3,4}$  gives the subset of S associated with two pairs of real double roots. This one-dimensional manifold, denoted by  $1^{(3)}$ , locates intersection points of S with itself (Figure 29-Figure 33).

# A.4 Criteria for a Triple Roots and a Quadruple Roots

A similar procedure can be execute to prove that equation (A.1) has triple (real) root if and only if equation (A.1) has triple root. Equation (A.1) has triple (real) root if and only if

$$\xi_1(C_{11}, C_{12}, \gamma) = 0$$
 and  $\xi_2(C_{11}, C_{12}, \gamma) = 0$ . (A.1)

The subset of S associated with triple (real) root of (A.1) are given by the simultaneous satisfaction of both of (A.1). Space curves along which (A.1) has triple roots are  $I^{(4)}$  and  $I^{(5)}$  and are the cusp points in Figure 29-Figure 32. All  $I^{(3)}$ ,  $I^{(4)}$  and  $I^{(5)}$  initiate at the unique point where (A.1) has quadruple roots. This requires that  $b_2 = b_3 = b_4 = 0$ . This set of algebra equations can be solved to give  $C_{12} = C_{12}^{(2)} = 2$ , and give the associated  $C_{11}$  and  $\gamma$  by lengthy exact expressions. Together this gives the quadruple root x = 2.57539, at  $(C_{11}, C_{12}, \gamma) = (0.3883, 2, 17.0815) \equiv \mathcal{P}$  as the 0-dimensional intersection of the three 1-dimensional manifolds  $I^{(3)}$ ,  $I^{(4)}$  and  $I^{(5)}$ .

Following the discussion here we know that to find those triplet  $(C_{11}, C_{12}, \gamma)$  at which (3.5.4) has double real roots and root type transition takes place is equivalently to find the triplet  $(C_{11}, C_{12}, \gamma)$  that satisfies equation (A.1).

# Appendix B: Bifurcation from Homogeneous Deformation under End Thrust

Buckling is a major failure mode for load-carrying engineering structure. Mathematically, buckling corresponds to bifurcation from some equilibrium solution. In [Haughton 1987], the co-occurrence of loss of ellipticity and in-plane inhomogeneous bifurcation was observed. This motivate us to seek the correlation between loss of ellipticity and out-of plane bifurcation here. The bifurcation analysis will be carried out in the context of the theory of small deformation superposed onto finite homogeneous deformation [Biot 1965]. The equivalent problem for the neo-Hookean plate (which therefore does not admit loss of ellipticity) was studied by Sawyers and Rivlin [1974]. They found a family of flexural buckled solutions at relatively low end-thrust and a family of barrelling buckled solutions at relatively high end-thrust. The extension to a layered neo-Hookean construction was given by Pence and Song [1991] and Qiu, et. al. [1994]. In particular, the latter work established the extension of additional families of buckled solutions, and the conjecture was put firth that an N-ply construction would admit N + 1 families of plane strain buckled solutions.

Here, the composite construction involves directional reinforcing, rather than multi-layers. For the purpose of comparison, plane deformation inhomogeneous bifurcation onset from the global plane deformation (2.3.10) (or (3.13.3)) of a thick rectangular plate under *end thrust* will be investigated here. This plate is constructed from the material (2.4.1) reinforced with one single family of fibers oriented in  $X_1$ -direction. The associated ellipticity problem was investigated in section 3.7 for  $C_{12} = 0$  and section 3.13. First addressed will be the finite homogeneous deformations, figured out by using

semi-inverse method, of this plate under end thrust. Next, the inhomogeneous bifurcation phenomena studied.

#### **B.1 Homogeneous Plane Deformation**

The thick plate in its original configuration, placed in the 3-dimensional rectangular Cartesian coordinate system, occupies the region  $\mathcal{R}(X_1, X_2, X_3)$ . The region  $\mathcal{R}(X_1, X_2, X_3)$  is confined by

$$\Re: -l_1 \le X_1 \le l_1, -l_2 \le X_2 \le l_2, -l_3 \le X_3 \le l_3,$$
 (B.1)

with  $l_2$  significantly smaller than either  $l_1$  or  $l_3$ . Illustrated earlier in Figure 1 (M = 1) is the original configuration of the plate.

The following traction boundary conditions will be applied on the plate and furnish the so called end thrust condition. We define the *lateral surfaces* as the surfaces originally at  $X_1 = \pm l_1$  and  $X_3 = \pm l_3$ , so that the *top* and *bottom surfaces* of the thick plate are the surfaces originally at  $X_2 = \pm l_2$ . By *thick* we mean that the deformation along the plate thickness need not relate to each other (or to a central neutral surface) by some simple prescribed relation through thickness, so that a fully three dimensional continuum analysis is required through the plate thickness. By *end thrust* we mean a total normal force T in the  $X_1$ -direction will be applied on the pair of lateral surfaces at  $X_1 = \pm l_1$ , and no shear tractions will be applied on this pair of surfaces. The top and bottom surfaces of the plate are kept traction free during deformation. In solving the problem, normal displacements will first be imposed on the pair of lateral surfaces at  $X_1 = \pm l_1$ . The traction required to maintain these displacements will then be calculated following the semi-inverse method. Deformations are assumed to take place in planes

parallel to the  $(X_1, X_2)$ -plane globally. Hence, the surfaces at  $X_3 = \pm l_3$  are kept frictionlessly in their original planes. Thus, and to be more specific, we have the boundary conditions, as

$$x_1 = \pm \lambda_1 l_1,$$
 on  $X_1 = \pm l_1,$   
 $S_{12} = S_{13} = 0,$  on  $X_1 = \pm l_1,$   
 $S_{21} = S_{22} = S_{23} = 0,$  on  $X_2 = \pm l_2,$   
 $S_{31} = S_{32} = 0,$  on  $X_3 = \pm l_3,$   
 $x_3 = \pm l_3,$  on  $X_3 = \pm l_3.$  (B.1)

Here S is the Piola-Kirchhoff stress tensor.

As follows from (2.4.21) and (2.4.22), that the particular biaxial deformation (2.3.10) can be sustained with in-plane tractions on lateral surfaces. Since in the constitutive equation (2.2.1), for the material (2.1.10) considered in the context, the hydrostatic pressure p is arbitrary, is assumed to be constant in position **X** for homogeneous deformations. It is then clear from equation (2.2.1) that the Cauchy stress tensor **T**, and the corresponding Piola-Kirchhoff stress tensor **S**, is independent of position **X** if the deformation is homogeneous. In this case, the equilibrium equation

$$divS^{T} = 0 (B.1)$$

is satisfied. Hence, in all the discussions on homogeneous deformations, equilibrium is ensured.

For the material (2.4.1) reinforced with single fiber family, the Cauchy stress tensor is given by (2.4.2). The in-plane fiber reinforcement is represented by the unit vector field  $\mathbf{A} (= \mathbf{A}^{(1)})$  given by (2.4.3)<sub>1</sub>. The potentially nonzero components of the Cauchy stress tensor  $\mathbf{T}$  are given by (2.4.21). The hydrostatic pressure  $\mathbf{p}$  in equation (2.4.2) has

been eliminated by equating  $T_{22}$  to zero in accordance with the traction free condition  $(B.1)_3$  on the surfaces  $X_2 = \pm l_2$ . The potentially nonzero components of the Piola-kirchhoff stress tensor, calculated from  $S = F^{-1}T$ , are given by

$$S_{11} = \mu(\lambda_1 - \lambda_1^{-3}) + 2\beta(\lambda_1^2 - 1)\lambda_1,$$
  

$$S_{33} = \mu(1 - \lambda_1^{-2}).$$
(B.1)

As required,  $S_{11}=\lambda_2\lambda_3T_{11}=\lambda_1^{-1}T_{11}$  and  $S_{33}=\lambda_1\lambda_2T_{33}=T_{33}$ , where  $T_{11}$  and  $T_{33}$  are given in (2.4.21) and  $\lambda_3=1$ ,  $\lambda_2=\lambda_1^{-1}$ .

It is then evident that the boundary conditions (B.1) can be satisfied by the homogeneous deformation (2.3.10) and the corresponding Piola-kirchhoff stress tensor (B.1). Thus, deformation (2.3.10) with  $\lambda_2 = \lambda_1^{-1}$  is the homogeneous solution to the problem posed by the equilibrium equation (B.1) and the boundary conditions (B.1) for the plate construction with fiber reinforcement oriented in the  $X_1$ -direction.

The end thrust T applied on surfaces originally at  $X_1 = \pm l_1$  can now be figured out as

$$T = 4\mu l_2 l_3 (\lambda_1 - \lambda_1^{-3}) + 8\beta l_2 l_3 (\lambda_1^3 - \lambda_1).$$
 (B.1)

To obtain equation (B.1), the current area,  $A = 4\lambda_1^{-1}l_2l_3$ , of the surfaces on which the end thrust is exerted is applied to (B.1)<sub>1</sub>.

#### **B.2 Incremental Formulation**

We now turn to consider the out-of-plane inhomogeneous bifurcation problem. The homogeneous deformation solution that takes place in planes parallel to the  $(X_1, X_2)$ -plane was given in the previous section. The small incremental deformation to be

superposed onto finite homogeneous deformation is assumed to be a plane deformation that takes place in planes parallel to the  $(X_1, X_2)$ -plane.

Thus, the full deformation, by superposing a small incremental deformation **u** onto the homogeneous deformation described by (2.3.10), can be written as

$$\hat{x}_{1} = \lambda_{1} X_{1} + \varepsilon u_{1}(X_{1}, X_{2}),$$

$$\hat{x}_{2} = \lambda_{1}^{-1} X_{2} + \varepsilon u_{2}(X_{1}, X_{2}),$$

$$\hat{x}_{3} = X_{3},$$
(B.1)

where  $\varepsilon$  is a small parameter that will be used to obtain the linearized formulation that governs bifurcation onset. In the foregoing discussion, quantities associated with the full deformation (B.1) are indicated by a superposed "\(^{\alpha}\)", and linearized quantities associated with the incremental deformation  $u_1(X_1, X_2)$  and  $u_2(X_1, X_2)$  are indicated by a superposed "-". It is only necessary to take into account the linearized quantities, since our interest is bifurcation onset and not the post bifurcation behaviors. Thus, the corresponding incremental quantities, such as deformation gradient tensor  $\hat{\mathbf{F}}$ , hydrostatic pressure  $\hat{\mathbf{p}}$ , the Cauchy stress tensor  $\hat{\mathbf{T}}$  and the Piola-Kirchhoff stress tensor  $\hat{\mathbf{S}}$  can be calculated as

$$\hat{\mathbf{F}} = \begin{bmatrix} \lambda_1 + \varepsilon \mathbf{u}_{1,1} & \varepsilon \mathbf{u}_{1,2} & 0 \\ \varepsilon \mathbf{u}_{2,1} & \lambda_1^{-1} + \varepsilon \mathbf{u}_{2,2} & 0 \\ 0 & 0 & 1 \end{bmatrix},$$
 (B.1)

$$\hat{p}(\mathbf{X}, \varepsilon) = p + \varepsilon \bar{p}(\mathbf{X}) + O(\varepsilon^2),$$
 (B.1)

$$\hat{\mathbf{T}}(\mathbf{X}, \boldsymbol{\varepsilon}) = \mathbf{T} + \boldsymbol{\varepsilon} \overline{\mathbf{T}}(\mathbf{X}) + O(\boldsymbol{\varepsilon}^2), \qquad (B.1)$$

$$\hat{\mathbf{S}}(\mathbf{X}, \varepsilon) = \mathbf{S} + \varepsilon \bar{\mathbf{S}}(\mathbf{X}) + \mathcal{O}(\varepsilon^2), \tag{B.1}$$

respectively. Now, we have the determinant of the deformation gradient tensor  $\hat{\mathbf{F}}$ 

$$\det \hat{\mathbf{F}} = 1 + \varepsilon (\lambda_1 \mathbf{u}_{2,2} + \lambda_1^{-1} \mathbf{u}_{1,1}) + O(\varepsilon^2).$$
 (B.1)

Hence, for the linearized problem, incompressibility requires that

$$\lambda_1 u_{2,2} + \lambda_1^{-1} u_{1,1} = 0. (B.1)$$

According to equation (B.1), the components of linearized incremental Piola-kirchhoff stress tensor are given by

$$\begin{split} \bar{S}_{11} &= \mu(u_{1,1} - \lambda_{1}^{-2}u_{2,2}) - \lambda_{1}^{-1}\bar{p} + 2\beta(3\lambda_{1}^{2} - 1)u_{1,1} \,, \\ \bar{S}_{12} &= \mu(u_{2,1} + \lambda_{1}^{-2}u_{1,2}) + 2\beta(\lambda_{1}^{2} - 1)u_{2,1} \,, \\ \bar{S}_{21} &= \mu(u_{1,2} + \lambda_{1}^{-2}u_{2,1}) \,, \\ \bar{S}_{22} &= -\lambda_{1}\bar{p} + 2\mu u_{2,2} \,, \\ \bar{S}_{33} &= -\bar{p} \,, \\ \bar{S}_{13} &= \bar{S}_{31} = \bar{S}_{23} = \bar{S}_{32} = 0 \,. \end{split}$$

Substituting the linearized incremental Piola-Kirchhoff stress tensor into the equilibrium equation  $div\bar{S} = 0$ , a set of three second order partial differential equations,

$$\begin{split} -\lambda_{1}^{-1}\bar{p}_{,1} + \mu(u_{1,11} + u_{1,22}) + 2\beta(3\lambda_{1}^{2} - 1)u_{1,11} &= 0 ,\\ -\lambda_{1}\bar{p}_{,2} + \mu(u_{2,11} + u_{2,22}) + 2\beta(\lambda_{1}^{2} - 1)u_{2,11} &= 0 ,\\ -\bar{p}_{,3} &= 0 . \end{split} \tag{B.1}$$

for the unknown functions  $u_1$ ,  $u_2$  and  $\overline{p}$ , can be obtained. Equation (B.1)<sub>3</sub> yields

$$\bar{p}(X_1, X_2, X_3) = \bar{p}(X_1, X_2).$$
 (B.1)

That is, the hydrostatic pressure p is a function of  $X_1$  and  $X_2$  only. Equation  $(B.1)_{1,2}$ , together with the constraint of incompressibility (B.1), are a set of differential equations governing the bifurcation onset for the plate with reinforcement oriented in the direction of the end thrust. The boundary conditions are posed in (B.1).

#### **B.3 Inhomogeneous Bifurcation**

In the foregoing analysis, we seek nontrivial solutions (corresponding to bifurcation) for the incremental deformation  $u_1(X_1, X_2)$  and  $u_2(X_1, X_2)$ . By using the method of separation of variables, the set of partial governing differential equations  $(B.1)_{1,2}$  and (B.1) can be turned into

$$\begin{split} \lambda_1^{-1} \Omega P(X_2) + [\mu + 2\beta(3\lambda_1^2 - 1)] \Omega^2 U_1(X_2) - \mu U_1''(X_2) &= 0 \;, \\ \lambda_1 P'(X_2) + [\mu + 2\beta(\lambda_1^2 - 1)] \Omega^2 U_2(X_2) - \mu U_2''(X_2) &= 0 \;, \\ \lambda_1 U_2'(X_2) - \lambda_1^{-1} \Omega U_1(X_2) &= 0 \;. \end{split} \tag{B.1}$$

Here the solution form proposed for the set of partial differential equations  $(B.1)_{1,2}$  and (B.1) is

$$\mathbf{u}_1 = \frac{-\sin\Omega \mathbf{X}_1}{\cos\Omega \mathbf{X}_1} \left\{ \mathbf{U}_1(\mathbf{X}_2), \quad \mathbf{u}_2 = \frac{\cos\Omega \mathbf{X}_1}{\sin\Omega \mathbf{X}_1} \right\} \mathbf{U}_2(\mathbf{X}_2), \quad \bar{\mathbf{p}} = \frac{\cos\Omega \mathbf{X}_1}{\sin\Omega \mathbf{X}_1} \left\{ \mathbf{P}(\mathbf{X}_2), \quad (B.1) \right\}$$

where  $\Omega = j\pi/l_1$  for upper case of (B.1),  $\Omega = (j-1/2)\pi/l_1$  for lower case of (B.1), and j = 1,2,... gives the number of half wavelengths (*mode number*) in the buckled solution. Eliminating  $P(X_2)$  and  $U_1(X_2)$  from equation (B.1), gives the fourth order ordinary differential equation

$$U_2^{(iv)}(X_2) - \Omega^2 h_1(\lambda, \gamma) U_2''(X_2) + \Omega^4 h_2(\lambda, \gamma) U_2(X_2) = 0,$$
 (B.1)

where

$$\lambda = \lambda_1^{-2} > 0, \qquad \lambda > 0 \tag{B.1}$$

is introduced as a *load parameter*. Here, the load parameter  $\lambda$  describes the amount of homogeneous deformation through (2.3.10) and (B.1) under given load T, and the stiffness ratio  $\gamma$  characterizes the increased stiffness in the fiber direction. The two functions,  $h_1(\lambda, \lambda)$ 

 $\gamma$ ) and h<sub>2</sub>( $\lambda$ ,  $\gamma$ ), given by

$$h_1(\lambda, \gamma) = 1 + \lambda^2 + 2\gamma \left(\frac{3}{\lambda} - 1\right)$$
 and  $h_2(\lambda, \gamma) = \lambda^2 \left[1 + 2\gamma \left(\frac{1}{\lambda} - 1\right)\right]$ , (B.1)

are by virtue

$$h_1(\lambda, \gamma) = a_2(\frac{1}{\lambda}, 0, \gamma)$$
 and  $h_2(\lambda, \gamma) = a_4(\frac{1}{\lambda}, 0, \gamma)$  (B.1)

in comparing with  $(3.5.3)_{2.4}$ , by noting that  $\lambda = 1/C_{11}$ .

It is worthwhile noting that the differential system (B.1) (or (B.1) virtually) is a two parameter  $(\lambda, \gamma)$  system. The nature of this system varies with the parameter pair  $(\lambda, \gamma)$  in the domain  $\lambda > 0$ ,  $\gamma \ge 0$ . That is, equation (B.1) will change its type, such as elliptic and nonelliptic, depending on the coefficients  $h_1(\lambda, \gamma)$  and  $h_2(\lambda, \gamma)$ .

The characteristic equation of (B.1) for the proposed solution form  $U_2(X_2) = e^{rX_2}$  for unknown r is

$$r^4 - \Omega^2 h_1(\lambda, \gamma) r^2 + \Omega^4 h_2(\lambda, \gamma) = 0. \tag{B.1}$$

Equation is exactly that given by  $C_{11}^{-2}\Omega^4P(r\Omega^{-1}i, 1/\lambda, 0, \gamma) = 0$  from (3.5.2), where  $i = \sqrt{-1}$ . We shall, here, denote the four roots of the characteristic equation (B.1) by  $\pm r_1$  and  $\pm r_2$ . Thus, we obtain

$$r_1^2 = \Omega^2 f_1^2$$
,  $r_2^2 = \Omega^2 f_2^2$ . (B.1)

Here

$$f_1(\lambda,\gamma) = \frac{1}{\sqrt{2}} [h_1 + (h_1^2 - 4h_2)^{1/2}]^{1/2}, \quad f_2(\lambda,\gamma) = \frac{1}{\sqrt{2}} [h_1 - (h_1^2 - 4h_2)^{1/2}]^{1/2}. \quad (B.1)$$

It can be proved that

$$\begin{split} r_1^2 > 0 \;, & \quad r_2^2 > 0 \qquad & \text{if} \;\; h_2(\lambda,\gamma) > 0 \;, \\ r^2 > 0 \;, & \quad r_2^2 < 0 \qquad & \text{if} \;\; h_2(\lambda,\gamma) < 0 \;, \\ r_1^2 > 0 \;, & \quad r_2^2 = 0 \qquad & \text{if} \;\; h_2(\lambda,\gamma) = 0 \;. \end{split} \tag{B.1}$$

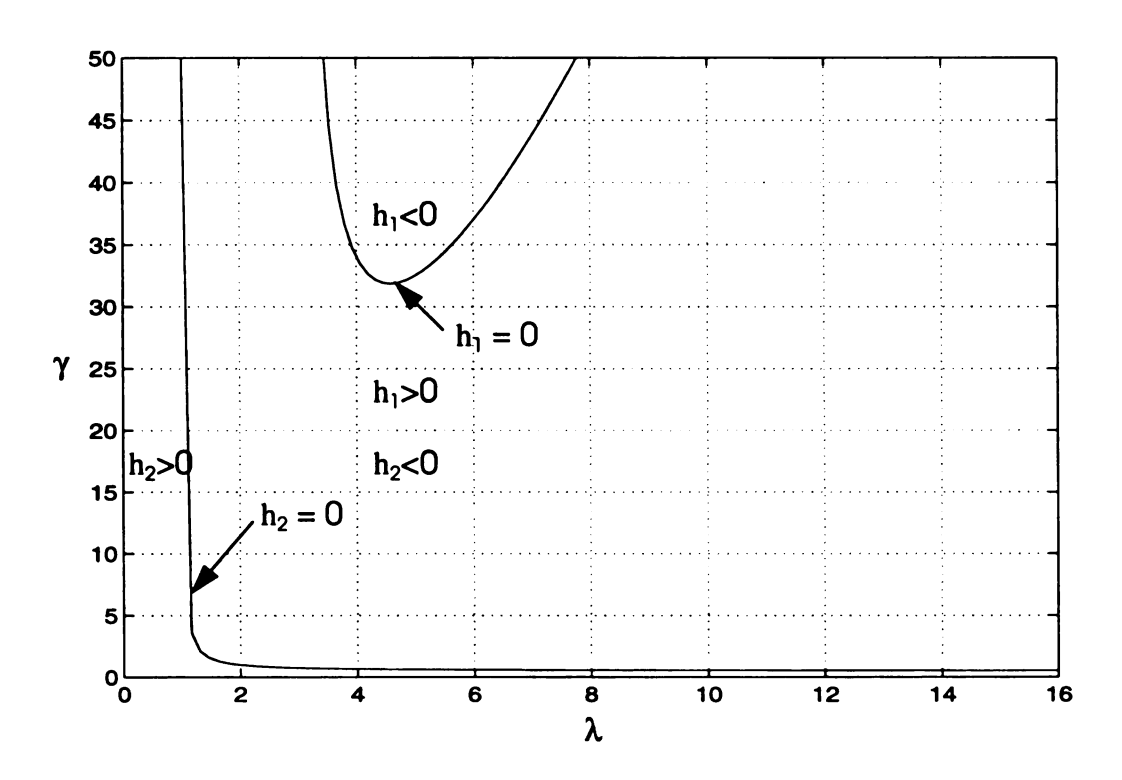


Figure 53. The solution of the fourth order ordinary differential equation (B.1) changes its type with  $(\lambda, \gamma)$  according to the value of  $h_2(\lambda, \gamma)$ . This deformation is biaxial with  $\lambda = 1/C_{11}$ . Ellipticity holds in the region  $h_2 > 0$  and is lost in the region  $h_2 < 0$ .

It is to be noted that  $h_2(\lambda, \gamma) = 0$  yields the same relation as that given by (3.3.4), by noting that  $\lambda = 1/C_{11}$ . The graphs of  $h_1(\lambda, \gamma)$  and  $h_2(\lambda, \gamma)$  are plotted in Figure 53. The curve of  $h_2(\lambda, \gamma) = 0$  becomes the same curve as plotted in Figure 25, if we exchange the ordinate with abscissa and make use of the substitution  $\lambda = 1/C_{11}$ . Hence, for  $h_2(\lambda, \gamma) > 0$ , the differential equation (B.1) is elliptic type, and for  $h_2(\lambda, \gamma) < 0$  or  $h_2(\lambda, \gamma) = 0$ , we shall say that equation (B.1) is non-elliptic type (a parallel discussion is given in Appendix C).

The general solution of the homogeneous equation (B.1) is the linear combination of four linear independent solutions

$$U_2(X_2) = L_1 U_2^{(1)}(X_2) + L_2 U_2^{(2)}(X_2) + M_1 U_2^{(3)}(X_2) + M_2 U_2^{(4)}(X_2),$$
 (B.1)

where  $U_2^{(i)}(X_2)$  (i = 1, 2, 3, 4) are determined by the roots of the corresponding characteristic equation (B.1) and their forms change accordingly.

The solution (B.1) of the fourth order ordinary differential equation (B.1) can be written, according to the value of  $h_2(\lambda, \gamma)$ , as

$$\begin{aligned} U_2(X_2) &= L_1 cosh(r_1 X_2) + L_2 sinh(r_1 X_2) + M_1 cosh(r_2 X_2) + M_2 sinh(r_2 X_2) \;, \\ &\qquad \qquad \text{if } h_2(\lambda, \gamma) > 0, \end{aligned} \tag{B.1}$$

$$U_{2}(X_{2}) = L_{1} cosh(r_{1}X_{2}) + L_{2} sinh(r_{1}X_{2}) + M_{1} cos(Im(r_{2})X_{2}) + M_{2} sin(Im(r_{2})X_{2})$$
if  $h_{2}(\lambda, \gamma) < 0$ , (B.1)

$$\begin{aligned} U_2(X_2) &= L_1 cosh(r_1 X_2) + L_2 sinh(r_1 X_2) + M_1 + M_2 X_2 ,\\ &\quad \text{if } h_2(\lambda, \gamma) = 0. \end{aligned} \tag{B.1}$$

Thus, the existence of the incremental solution  $u_1$ ,  $u_2$  and  $\overline{p}$ , and therefore the existence of buckled solutions, leads to the determination of the set of nonzero coefficients  $\{L_1, L_2, M_1, M_2\}$  of the linear combination.

To obtain this set of  $\{L_1, L_2, M_1, M_2\}$ , the Piola-Kirchhoff stress tensor are then calculated and subjected, with the full deformation (B.1), to the boundary conditions (B.1). This manipulation will yield a linear system, controlled by parameters  $\lambda$ ,  $\gamma$ , and j (mode number), of algebraic equations. The condition for bifurcation to take place is therefore the condition of nontrivial solutions of  $\{L_1, L_2, M_1, M_2\}$  for this linear system of algebraic equations. This virtually is a generalized eigenvalue problem for the triplet  $(\lambda, \gamma, \eta)$ . Here

$$\eta = \Omega l_2 = j\pi l_2/2l_1 \tag{B.1}$$

is defined as the *mode parameter* that is the continuous version of the discrete mode number j, scaled by the length of the plate  $l_1$ . The involvement of  $l_2$  in the definition of  $\eta$  is for the convenience of applying the boundary conditions on top and bottom surfaces. Note here that equation (B.1) can be written in the form of equation (B.1) provided that  $M_2$  is taken as an imaginary number. It can be readily shown that the boundary conditions (B.1), except (B.1)<sub>4,5</sub>, are automatically satisfied by the proposed solution form (B.1) and (B.1). The satisfaction of (B.1)<sub>4,5</sub> gives four relations among these four constants  $L_1$ ,  $L_2$ ,  $M_1$  and  $M_2$ , therefore, gives the following 4 by 4 systems of equations for the four unknown constants  $L_1$ ,  $L_2$ ,  $M_1$  and  $M_2$ ,

$$\mathbf{J1} = \mathbf{0}. \tag{B.1}$$

Here

$$l = (L_1, M_1, L_2, M_2)^T,$$
 (B.1)

and

$$\mathbf{J} \equiv \mathbf{J}^{c} = \begin{bmatrix} A_{1}C_{1} & A_{2}C_{2} & 0 & 0 \\ B_{1}S_{1} & B_{2}S_{2} & 0 & 0 \\ 0 & 0 & A_{1}S_{1} & A_{2}S_{2} \\ 0 & 0 & B_{1}C_{1} & B_{2}C_{2} \end{bmatrix}, \quad \text{for } h_{2}(\lambda, \gamma) \neq 0, \quad (B.1)$$

$$\mathbf{J} \equiv \mathbf{J}^{d} = \begin{bmatrix} DS_{1} & 0 & 0 & 0 \\ EC_{1} & \lambda^{2} & 0 & 0 \\ 0 & 0 & DC_{1} & E \\ 0 & 0 & ES_{1} & \lambda^{2}l_{2} \end{bmatrix}, \quad \text{for } h_{2}(\lambda, \gamma) = 0, \quad (B.1)$$

where

$$\begin{array}{lll} A_1 = r_1^2 + \lambda^2 \Omega^2, & A_2 = r_2^2 + \lambda^2 \Omega^2, \\ B_1 = -r_1(\lambda^2 \Omega^2 + r_2^2), & B_2 = -r_2(\lambda^2 \Omega^2 + r_1^2), \\ C_1 = \cosh(f_1 \eta), & C_2 = \cosh(f_2 \eta), \\ S_1 = \sinh(f_1 \eta), & S_2 = \sinh(f_2 \eta), \\ D = r_1 \lambda^2, & E = h_1 + \lambda^2. \end{array} \tag{B.1}$$

Note that the matrices  $J^c$  and  $J^d$  are functions of load parameter  $\lambda$ , stiffness ratio  $\gamma$  and deformation mode parameter  $\eta$ .

It is clear that the system (B.1) with the matrix  $J^c$  given by (B.1) can be divided into two subsystems as

$$\mathbf{J}^{cF} \begin{pmatrix} \mathbf{L}_1 \\ \mathbf{M}_1 \end{pmatrix} \equiv \begin{bmatrix} \mathbf{A}_1 \mathbf{C}_1 & \mathbf{A}_2 \mathbf{C}_2 \\ \mathbf{B}_1 \mathbf{S}_1 & \mathbf{B}_2 \mathbf{S}_2 \end{bmatrix} \begin{pmatrix} \mathbf{L}_1 \\ \mathbf{M}_1 \end{pmatrix} = \begin{pmatrix} 0 \\ 0 \end{pmatrix}, \tag{B.1}$$

$$\mathbf{J}^{\mathrm{cB}} \begin{pmatrix} \mathbf{L}_2 \\ \mathbf{M}_2 \end{pmatrix} \equiv \begin{bmatrix} \mathbf{A}_1 \mathbf{S}_1 & \mathbf{A}_2 \mathbf{S}_2 \\ \mathbf{B}_1 \mathbf{C}_1 & \mathbf{B}_2 \mathbf{C}_2 \end{bmatrix} \begin{pmatrix} \mathbf{L}_2 \\ \mathbf{M}_2 \end{pmatrix} = \begin{pmatrix} 0 \\ 0 \end{pmatrix}. \tag{B.1}$$

The bifurcation takes place, for  $(\lambda, \gamma)$  obeying  $h_2(\lambda, \gamma) \neq 0$ , if either of the subsystem (B.1) or (B.1) has nontrivial solution. If the nontrivial solution of subsystem (B.1) exists, then  $U_2(X_2)$  is an even function of  $X_2$ . In this case, the thick plate considered here undergoes *flexural* deformation as given by equation (B.1) in connection with equation (B.1). For the subsystem (B.1) to have a nontrivial solution, it is required that the determinant of the 2 by 2 matrix must vanish. We, thus, have the flexural bifurcation condition

$$\Psi^{cF}(\lambda, \gamma, \eta) \equiv \det \mathbf{J}^{cF} = 0, \quad \text{for } h_2(\lambda, \gamma) \neq 0.$$
(B.1)

Similarly, if the subsystem (B.1) has nontrivial solutions, then  $U_2(X_2)$  is an odd function of

 $X_2$ , and  $U_1(X_2)$  is then an even function of  $X_2$ . This type of symmetry corresponds to barrelling deformation. The barrelling bifurcation condition can then be expressed as

$$\Psi^{cB}(\lambda, \gamma, \eta) \equiv \det \mathbf{J}^{cB} = 0, \quad \text{for } h_2(\lambda, \gamma) \neq 0.$$
 (B.1)

Now, we turn to consider the system (B.1) with the matrix  $J^d$  given by (B.1). This system can also be divided into two subsystems as

$$\mathbf{J}^{\mathrm{dF}} \begin{pmatrix} \mathbf{L}_2 \\ \mathbf{M}_2 \end{pmatrix} \equiv \begin{bmatrix} \mathbf{DS}_1 & 0 \\ \mathbf{EC}_1 & \lambda^2 \end{bmatrix} \begin{pmatrix} \mathbf{L}_2 \\ \mathbf{M}_2 \end{pmatrix} = \begin{pmatrix} 0 \\ 0 \end{pmatrix}, \tag{B.1}$$

$$\mathbf{J}^{\mathrm{dB}} \begin{pmatrix} \mathbf{L}_2 \\ \mathbf{M}_2 \end{pmatrix} \equiv \begin{bmatrix} \mathbf{DC}_1 & \mathbf{E} \\ \mathbf{ES}_1 & \lambda^2 \mathbf{l}_2 \end{bmatrix} \begin{pmatrix} \mathbf{L}_2 \\ \mathbf{M}_2 \end{pmatrix} = \begin{pmatrix} 0 \\ 0 \end{pmatrix}. \tag{B.1}$$

Similarly, the bifurcation takes place, for  $(\lambda, \gamma)$  obeying  $h_2(\lambda, \gamma) = 0$ , if either of the subsystem (B.1) or (B.1) has nontrivial solution. It follows directly from (B.1) that

$$\det \mathbf{J}^{\mathrm{dF}} = \mathbf{r}_1 \lambda^4 \sinh(\mathbf{f}_1 \mathbf{\eta}) \neq 0, \qquad \text{for } \mathbf{h}_2(\lambda, \gamma) = 0. \tag{B.1}$$

Thus, the subsystem (B.1) has only the trivial solution, so that flexural buckling is not a possibility for  $(\lambda, \gamma)$  obeying  $h_2(\lambda, \gamma) = 0$ . For subsystem (B.1) to have nontrivial solutions it is required that

$$\Psi^{dB}(\lambda, \gamma, \eta) \equiv \det \mathbf{J}^{dB} = 0, \quad \text{for } h_2(\lambda, \gamma) = 0.$$
(B.1)

This is the barrelling bifurcation condition corresponding to subsystem (B.1), since the solution to subsystem (B.1) will yield  $U_2(X_2)$  as an odd function of  $X_2$ , so that  $U_1(X_2)$  is then an even function of  $X_2$ .

Here, we turn to examine the correlation between loss of ellipticity and bifurcation. A preliminary numerical analysis on the flexural bifurcation condition (B.1)

shows families of buckled solutions for the material with  $\gamma=10$ . The result is plotted in Figure 54 for  $(\lambda, \eta)$  pairs satisfying (B.1). It can be easily figure out from Figure 54 that  $h_2(\lambda, \gamma) < 0$  if it is evaluated with these large  $\lambda$ 's on the solution curves in connection with  $\gamma=10$ . Thus, bifurcations take place with  $(C_{11}, \gamma)$  located in the nonelliptic region. We now examine whether bifurcation will take place for  $(C_{11}, \gamma)$  located in the elliptic region. Solving  $h_2(\lambda, \gamma)=1>0$  we obtain  $\gamma=(1+\lambda)/2\lambda$ . Pairs  $(C_{11}, \gamma)=(1/\lambda, (1+\lambda)/2\lambda)$  are in the elliptic region. Substituting this particular  $\gamma$  values in the flexural bifurcation condition (B.1), we obtain one family of buckled solution, as plotted in Figure 55. It is thus clear that bifurcation can take place for in both elliptic and non-elliptic regions.

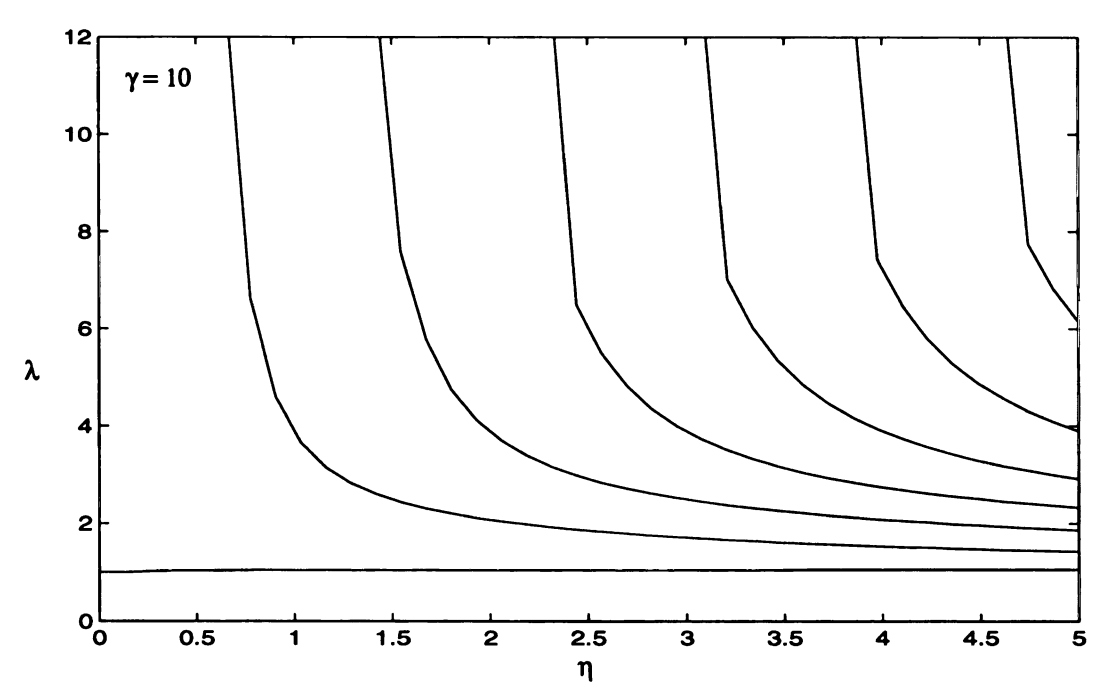


Figure 54. Solution families of the flexural condition (B.1) for the material with  $\gamma = 10$ . These large  $\lambda$ 's in connection with  $\gamma = 10$  are located in the non-elliptic region.

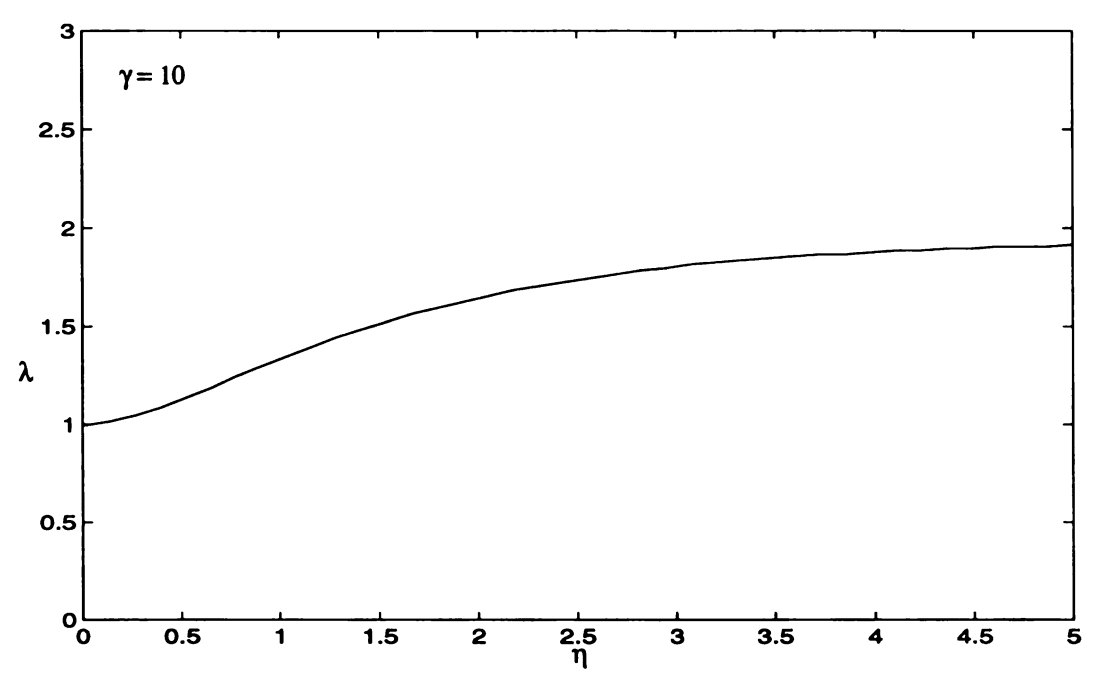


Figure 55. Flexural bifurcation solution for  $(C_{11}, \gamma)$  in the elliptic region.

# Appendix C: An Alternative Way to Obtain the Ellipticity Condition in the Buckling Problem

The set of governing second order partial differential equations  $(B.1)_{1,2}$  and the incompressibility constraint (B.1) are rewritten here as

$$\begin{split} &-\lambda_1^{-1}\bar{p}_{,1} + \mu(u_{1,11} + u_{1,22}) + 2\beta(3\lambda_1^2 - 1)u_{1,11} = 0 ,\\ &-\lambda_1\bar{p}_{,2} + \mu(u_{2,11} + u_{2,22}) + 2\beta(\lambda_1^2 - 1)u_{2,11} = 0 , \end{split}$$
 (C.1)

and

$$\lambda_1 \mathbf{u}_{2,2} + \lambda_1^{-1} \mathbf{u}_{1,1} = 0. \tag{C.1}$$

Let  $u_{1,1} = v_1$ ,  $u_{1,2} = v_2$ ,  $u_{2,1} = w_1$  and  $u_{2,2} = w_2$ , noting that (C.1) yields  $v_1 = -\lambda_1^2 w_1$ , we can obtain from the second order equations (C.1) a set of first order partial differential equations as

$$\begin{split} -\lambda_{1}^{-1}\bar{p}_{,1} + \mu(-\lambda_{1}^{2}w_{2,1} + v_{2,2}) - 2\beta\lambda_{1}^{2}(3\lambda_{1}^{2} - 1)w_{2,1} &= 0, \\ -\lambda_{1}\bar{p}_{,2} + \mu(w_{1,1} + w_{2,2}) + 2\beta(\lambda_{1}^{2} - 1)w_{1,1} &= 0, \\ \lambda_{1}^{2}w_{2,2} + v_{2,1} &= 0, \\ w_{1,2} - w_{2,1} &= 0, \end{split} \tag{C.1}$$

which has the characteristic equation [Whitham 1974]

$$\det(\mathbf{A} - \mathbf{va}) = 0, \tag{C.1}$$

where

$$\mathbf{A} = \begin{bmatrix} -\lambda_1^{-1} & 0 & 0 & -\mu\lambda_1^2 - 2\beta\lambda_1^2(3\lambda_1^2 - 1) \\ 0 & 0 & \mu + 2\beta(\lambda_1^2 - 1) & 0 \\ 0 & 1 & 0 & 0 \\ 0 & 0 & 0 & -1 \end{bmatrix}, \tag{C.1}$$

and

$$\mathbf{a} = 0 \begin{bmatrix} 0 & \mu & 0 & 0 \\ -\lambda_1 & 0 & 0 & \mu \\ 0 & 0 & 0 & \lambda_1^2 \\ 0 & 0 & 1 & 0 \end{bmatrix}. \tag{C.1}$$

Let  $\lambda = \lambda_1^{-2}$  and  $\gamma = \beta/\mu$ , equation (C.1) gives rise to the following equation

$$\lambda^{2} \left[ 1 + 2\gamma \left( \frac{1}{\lambda} - 1 \right) \right] + \left[ 1 + \lambda^{2} + 2\gamma \left( \frac{3}{\lambda} - 1 \right) \right] v^{2} + v^{4} = 0,$$
 (C.1)

which, virtually, is the equation  $P(v, 1/\lambda, 0, \gamma) = 0$  from (3.5.2). Thus, the types of the roots of (C.1) and the type of equations (C.1) (and therefore the equations (C.1)) associated with different values of  $(\lambda, \gamma)$  are as discussed in chapter 3.

# References

- Abeyaratne, R. C., (1980) Discontinuous Deformation Gradients in Plane Finite Elastostatics of Incompressible Materials, J. Elasticity 10 255-293.
- Adkins, J. E. and Rivlin, R. S., (1955) Large Elastic Deformations of Isotropic Material, X. Reinforcement by Inextensible Cords, Phil. Trans. Roy. Soc. Ser. A 248 201-223.
- Ball, J. M. and Schaeffer, D. G., (1983) Bifurcation and Stability of Homogeneous Equilibrium Configurations of an elastic Body under Dead-Load Tractions, Math. Proc. Camb. Phil. Soc. 94 315-339.
- Beatty, M. F., (1987) Topics in Finite Elasticity: Hyperelasticity of Rubber, Elastomers, and Biological Tissues -- with Examples, Appl. Mech. Rev. 40 1699-1734.
- Biot, M. A., (1965) *Mechanics of Incremental Deformations*, John Wiley & Sons, New York.
- Blatz, P. J. and Ko, W. L., (1962) Application of Finite Elasticity to the Deformation of Rubbery Materials, Trans. soc. Rheol. 6 223-251.
- Bradford, I. D. R., England, A. H. and Rogers, T. G., (1992) Finite Deformations of a Fiber-Reinforced Cantilever: Point-Force Solutions, Acta Mechanica 91 77-95.
- 8 Christensen, R. M., (1979) *Mechanics of Composite Materials*, John Wiley & Sons, New York.
- 9 England, A. H., Rogers, T. G. and Bradford, I. D. R., (1992) Finite Deformations of a Fiber-Reinforced Cantilever: Distributed-Load Solution, Q. J. Mech. Appl.

- Math. 45 711-732.
- 10 Ericksen, J. L. and Rivlin, R. S., (1954) Large Elastic Deformation of Homogeneous Anisotropic Materials, J. Rat. Mech. Anal. 3 281-301.
- Green, A. E. and Adkins, J. E., (1960) *Large Elastic Deformations*, Clarendon Press, Oxford.
- Haughton, D. M., (1987) Bifurcation of Plane Incompressible Elastic Membranes

  Subjected to Dead-Load Tractions, Int. J. Solids Structures 23 253-259.
- Hill, R., (1979) On the Theory of Plane Strain in Finitely Deformed CompressibleMaterials, Math. Proc. Camb. Phil. Soc. 86 161-178.
- Hill, R. and Hutchinson, J. W., (1975) Bifurcation Phenomena in the Plane

  Tension test, J. Mech. Phys. Solids 23 239-264.
- Horgan, C. O. and Pence, T. J., (1989) Void Nucleation in Tensile Dead-Loading of a Composite Incompressible Nonlinear Elastic Sphere, J. Elasticity 21 61-82.
- Horgan, C. O., (1996) Remarks on Ellipticity for the Generalized Blatz-Ko

  Constitutive Model for a Compressible Nonlinearly Elastic Solid, J Elasticity 42

  165-176.
- 17 Knowles, J. K. and Sternburg, E., (1975) On the ellipticity of the equations of nonlinear elastostatics for a special material, J. Elasticity 5 341-361.
- 18 Knowles, J. K. and Sternburg, E., (1977) On the Failure of Ellipticity of the Equations of Finite Elastostatic Plane Strain, Arch. Rat. Mech. Anal. 63 321-336.
- 19 Kurashige, M., (1981) Instability of a Transversely Isotropic Elastic Slab

  Subjected to Axial Loads, J. Appl. Mech. 48 351-356.
- 20 Kurosh, A., (1980) Higher Algebra, Mir Publishers, Moscow.

- Ogden, R. W., (1984) Non-linear Elastic Deformations, Ellis Horwood Ltd.
- Ogden, R. W., (1985) Local and Global Bifurcation Phenomena in Plane-Strain

  Finite Elasticity, Int. J. Solids Structures 21 121-132.
- Ogden, R. W., (1987) On the Stability of Asymmetric Deformation of a Symmetrically-Tensioned Elastic Sheet, Int. J. Engng Sci. 25 1305-1314.
- Pence, T. J. and Song, J., (1991) Buckling Instabilities in a Thick Elastic Three-Ply

  Composite Plate under Thrust, Int. J. Solids Structures 27 1809-1828.
- Pipkin, A. C. and Rogers, T. G., (1971) Plane Deformations of Incompressible Fiber-Reinforced Materials, J. Appl. Mech. 38 634-640.
- Polignone, D. A. and Horgan, C. O., (1993) Cavitation for Incompressible

  Anisotropic Nonlinear Elastic Spheres, J. Elasticity 33 27-65.
- Qiu, Y., Kim, S. and Pence, T. J., (1994) Plane Strain Buckling and Wrinkling of Neo-Hookean Laminates, Int. J. Solids Structures 31 1149-1178.
- 28 Rivlin, R. S., (1948a) Large Elastic Deformations of Isotropic Materials, I.

  Fundamental Concepts, Phil. Trans. Roy. Soc. Ser. A 240 459-490.
- 29 Rivlin, R. S., (1948b) Large Elastic Deformations of Isotropic Materials, II. Some Uniqueness Theories for Pure Homogeneous deformations, Phil. Trans. Roy. Soc. Ser. A 240 491-508.
- Rivlin, R. S., (1981) Some Thoughts on Material Stability, in Proc. IUTAM Symp. on Finite Elasticity (eds. Carlson, D. E., et. al.), 105-122, Martinus Nijhoff Pub., The Hague.
- Rogers, T. G., (1975) Finite Deformations of Strongly Anisotropic Materials,
  Chap. 10 of Theoretical Rheology (eds. Hutton, J. F., et. al.), Applied Sciences

- Publishers, London.
- Rogers, T. G. and Pipkin, A. C., (1971a) Small Deflections of Fiber-Reinforced Beams or Slabs, J. Appl. Mech. 38 1047-1048.
- Rogers, T. G. and Pipkin, A. C., (1971b) Finite Lateral Compression of a Fiber-Reinforced Tube, Q. J. Mech. Appl. Math. 24 311-330.
- Rosakis, P., (1990) Ellipticity and Deformations with Discontinuous Gradients in Finite Elastostatics, Arch. Rat. Mech. Anal. 109 1-37.
- Rosakis, P. and Jiang, Q., (1993) Deformations with Discontinuous Gradients in Plane Elastostatics of Compressible Solids, J Elasticity 33 233-257.
- Sawyers, K. N. and Rivlin, R. S., (1974) Bifurcation Conditions for a Thick Elastic

  Plate under Thrust, Int. J. Solids Structures 10 483-501.
- 37 Spencer, A. J. M., (1972) Deformations of Fibre-Reinforced Materials, Oxford University Press, London.
- Triantafyllidis, N. and Abeyaratne, R., (1983) Instability of a Finitely Deformed Fiber-Reinforced Elastic Material, J. Appl. Mech. 50 149-156.
- Truesdell, C. and Noll, W., (1965) The Non-Linear Field Theories of Mechanics,

  Handbook of Physics, Springer-Verlag.
- Whitham, G. B., (1974), Linear and Nonlinear Waves, John Wiley and Sons.
- Zee, L. and Sternberg, E., (1983) Ordinary and Strong Ellipticity in the
   Equilibrium Theory of Incompressible Hyperelastic Solids, Arch. Rat. mech. Anal.
   83 53-90.
- Zheng, Q. S., (1994) Theory of Representations for tensor Functions A Unified

  Invariant Approach to Constitutive Equations, Appl. Mech. Rev. 47 545-587.

Zweben, C., Hahn, H. T. and Chou, T. W., (1989) Mechanical Behavior and Properties of Composite Materials, Vol. 1, Technomic Publishing Co.

